4. SEA ICE AND SNOW

Stefanie Arndt[1], Philipp Anhaus[1], David Clemens-Sewall[2], Steven Fons[3], Jennifer Hutchings[4], Lars Kaleschke[1], Amy Macfarlane[5], Reza Naderpour[5], Alexey Niubom[6], Falk Pätzold[7], Robert Ricker[1], Igor Sheikin[6], Marcel Nicolaus[1] (not on board), Don Perovich[2] (not onboard), Gunnar Spreen[8] (not on board)

[1]DE.AWI
[2]US.Dartmouth
[3]US.NASA
[4]US.Oregon SU
[5]DE.WSL/SLF
[6]RU.AARI
[7]DE.TU Braunschweig
[8]DE.UBremen
[9]DE.UBremen

Grant-No. AWI_PS122_00

A comprehensive summary of the sea ice and snow measurements during all 5 cruise legs can be found in Nicolaus et al., 2022.

Sea ice and snow measurements on Leg 3 have been carried out by a team of 12 scientists, whereas 11 scientists were assigned to team ICE and one scientist (Jennifer Hutchings) to team ATMOS.

The team followed closely the suggested week plan until beginning of April. Due to the extension of the leg into proper spring conditions, the schedule have been adapted afterwards. That included mainly the additional focus on surface optics as well as the set-up of the Laser Strain Observatory. Also, the time for on-site work and deployments of autonomous systems in ridge observatories have been increased.

Despite the numerous challenges of Leg 3, as, e.g., cold temperatures in the beginning, the highly dynamic ice floe causing the need for several rescue and redeployment activities and the final recovery of almost all installations from the ice before leaving the floe, team ICE fulfilled overall the defined key objectives of the team successful (see Table 4.0.1).

In addition to the outlined work in the following chapters, team ICE carried out the daily ice observations from the bridge. Also, they contributed significantly to the regularly updated floe maps as well as the regular updates in the LogBook, i.e. updates on scientific work and prevalent ice conditions as well as photo documentation from the PANOMAX camera and ice observations.

During the transit on Kapitan Dranitsyn from Tromsø to the Central Observatory as well as during the temporary return from Polarstern from the Central Observatory towards Svalbard, the ice observations from the bridge have been carried out hourly supported by different scientists on board.

***Tab. 4.0.1**: Overview on the defined key objectives of Team ICE for MOSAiC and the respective achievements during Leg 3. Each colored column represents achieved 10% per months.*

Key objectives of Team ICE during MOSAiC	**Achieved in March**	**Achieved in April**
Describe **spatial variability** of snow and sea-ice properties		
Gain process level understanding of **seasonal changes** of snow and sea-ice cover		
Determine partitioning of solar radiation in sea ice (**energy budget** of sea ice)		
Determine **mass and fresh water balances**		
Examine sea ice thickness – **dynamics** relationship		
Examine **snow/ice physics-biogeochemistry-ecosystem interaction**		
Measurements for the purpose of developing **remote sensing** methods		

References

Nicolaus, M, Perovich, DK, Spreen, G, Granskog, MA, Albedyll, LV, Angelopoulos, M, Anhaus, P, Arndt, S, Belter, HJ, Bessonov, V, Birnbaum, G, Brauchle, J, Calmer, R, Cardellach, E, Cheng, B, Clemens-Sewall, D, Dadic, R, Damm, E, de Boer, G, Demir, O, Dethloff, K, Divine, DV, Fong, AA, Fons, S, Frey, MM, Fuchs, N, Gabarró, C, Gerland, S, Goessling, HF, Gradinger, R, Haapala, J, Haas, C, Hamilton, J, Hannula, H-R, Hendricks, S, Herber, A, Heuzé, C, Hoppmann, M, Høyland, KV, Huntemann, M, Hutchings, JK, Hwang, B, Itkin, P, Jacobi, H-W, Jaggi, M, Jutila, A, Kaleschke, L, Katlein, C, Kolabutin, N, Krampe, D, Kristensen, SS, Krumpen, T, Kurtz, N, Lampert, A, Lange, BA, Lei, R, Light, B, Linhardt, F, Liston, GE, Loose, B, Macfarlane, AR, Mahmud, M, Matero, IO, Maus, S, Morgenstern, A, Naderpour, R, Nandan, V, Niubom, A, Oggier, M, Oppelt, N, Pätzold, F, Perron, C, Petrovsky, T, Pirazzini, R, Polashenski, C, Rabe, B, Raphael, IA, Regnery, J, Rex, M, Ricker, R, Riemann-Campe, K, Rinke, A, Rohde, J, Salganik, E, Scharien, RK, Schiller, M, Schneebeli, M, Semmling, M, Shimanchuk, E, Shupe, MD, Smith, MM, Smolyanitsky, V, Sokolov, V, Stanton, T, Stroeve, J, Thielke, L, Timofeeva, A, Tonboe, RT, Tavri, A, Tsamados, M, Wagner, DN, Watkins, D, Webster, M, Wendisch, M. 2022. Overview of the MOSAiC expedition: Snow and sea ice. *Elementa: Science of the Anthropocene* 10(1). DOI: https://doi.org/10.1525/elementa.2021.000046

4.1. Ice Coring

Steven Fons[1], Anders Torstensson[2], Jeff Bowman[3], Igor Sheikin[4], Alexey Nuibom[4], Laura Wischnewski[5], Adam Ulfsbo[6], Susanne Spahic[5], Christopher Marsay[7], Annette Rinke[5]

(not onboard) Mats Granskog[8] Sønke Maus[9]

[1]US.UMD/NASA GSFC
[2]SE.SLU
[3]CH.SIO/UCSD
[4]RU.AARI
[5]DE.AWI
[6]SE.GU
[7]EDU.UGA
[8]NO.NPI
[9]NO.NTNU

4.1.1 Objectives

Within the general coring objectives (8.2 Objectives for General Coring), the ICE team is responsible for the ice physics properties analysis (temperature, salinity, density, microstructure).

4.1.2 Work at sea

Each general coring event consisted of two teams with five scientists each, made up of members from the ICE, ECO, and BGC teams. Once per week, when weather and ice conditions allowed, these teams would sample from the remote „Dark Site First Year Ice“ (FYI) and „Dark Site Second Year Ice“ (SYI) Sites. Between 20 and 30 (11 and 19) cores were planned each week from the FYI (SYI) site, depending on processing capability of the different teams each week. Team ICE planned for 8-9 cores each week, with 4 high priority cores (TEMP, SALO18, RHO, CT).

Site maps for the FYI Dark Site and SYI Dark Site can be found below in figures 4.1.1 and 4.1.2, respectively. Throughout leg 3, coring sessions at the FYI Site frequently encountered rafted ice, which necessitated the move to plots across the site on the opposite side of a small ridge (figure 4.1.1). There, thicknesses were closer to expected for FYI at this time of the year (1.65m). At the SYI Site, some weeks saw cores of only 1.7m in length, thinner than expected for SYI at this time of year. Thus, for the last week, the SYI team cored at a plot at the far end of the site, where ice was 2.4m thick (figure 4.1.2).

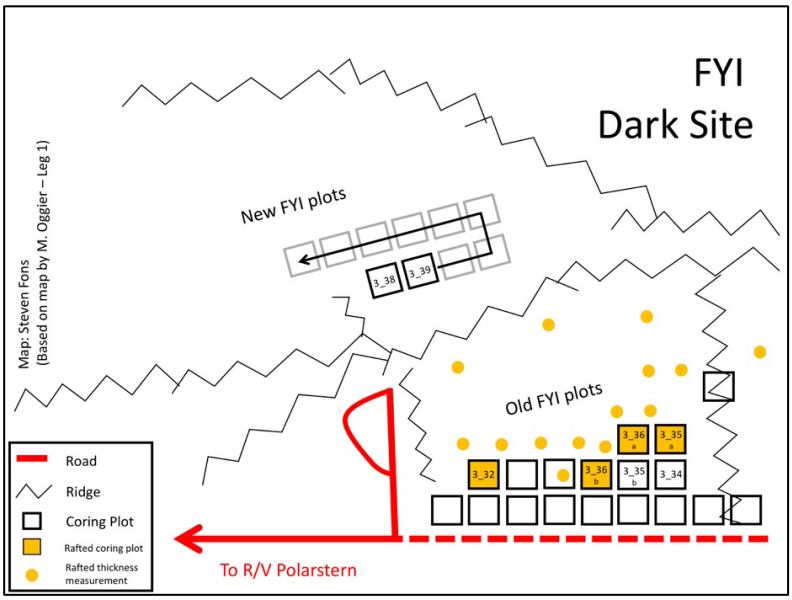

Fig. 4.1.1: *The FYI Dark Site. Coring plots are labelled with the activity week, where '_a' and '_b' indicate weeks where the plot was changed after encountering rafted ice in the first 1-2 cores. Rafted coring plots and thickness measurements are shown in yellow (map: S. Fons).*

Following the general coring event, upon return from the field, the CT samples are centrifuged, and imaged using x-ray computed tomography (CT) technique within 24 hours. Cores for the MOSAiC repository, backup, plastic, optics, and the upper part of the CT core are photographed, sealed in plastic sleeves, and stored at -20 °C. Density is measured at -15 °C by densitometry in paraffin in the freezer lab using a Kern EMB-V scale. Salinity and bulk salinity is then measured on the melted samples and remaining water, respectively, with a conductivity probe Voltcraft LWT-100 from team ICE. After team ECO melted salinity samples (SALO18 core) for nutrient analysis, the samples are measured for salinity using a conductivity probe YSI 30 by team ICE and are bottled for future isotope measurement. According to the initial work plan, texture cores were supposed to be processed into horizontal and vertical thin sections onboard. This was not done due to time and personnel constraints. However, texture cores were taken from both sites each week and stored at -20 °C for future analysis.

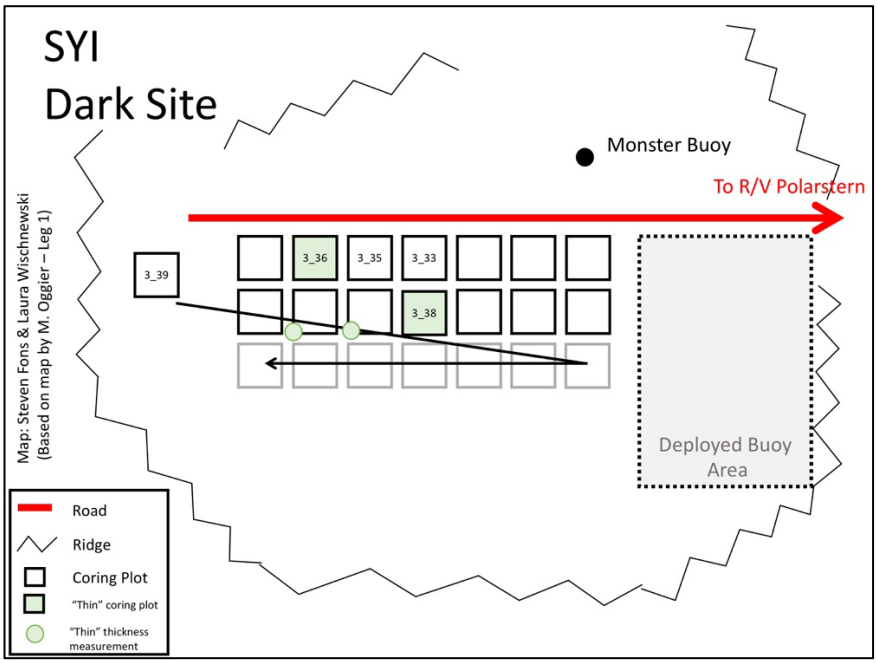

Fig. 4.1.2: *The SYI Dark Site. Coring plots are labelled with the activity week. Weeks with thinner-than-expected ice are shaded in green (map: S. Fons and L. Wischnewski).*

4.1.3 Preliminary (expected) Results

The ice coring team of leg 3 successfully continued – and expanded – the coring activity at the FYI and SYI sites. Due to an increased interest in core samples from the EGO and BGC teams over prior legs, leg 3 had more people available for coring and was able to visit both sites simultaneously each week. However, the frequent ice dynamics throughout the leg often left sites inaccessible. This required flexibility in the day and time of coring as well as transportation to and from the sites. Out of the 10 working weeks of Leg 3 (which do not include handover and pack-up) the Dark Sites were visited on seven occasions: four times to both FYI and SYI sites, two times to just FYI, and once to just SYI. The missed weeks were due to inaccessible sites or poor weather conditions. In addition to the Dark Site coring, team ICE was able to core at other sites in the Central Observatory ("CO", Remote Sensing and BGC1), at the Distributed Network ("DN", L1, L2, L3), and twice at a ridge (ECO Ridge "Ridgey McRidgeFace"). Table

4.1.1 presents a list of cross-disciplinary and ICE team coring sessions together with a total number of recovered ice cores.

Tab. 4.1.1: *Cross-disciplinary and ICE team coring events at Dark Sites, Distributed Network, and other sites around the CO during leg 3.*

Date of Coring	Activity Week	Site	MCS Action # for 9cm Corer (7cm corer)	# of Recovered Cores
9.3.2020	3_31	BGC1	5 (N/A)	2
21.3.2020	3_32	FYI	63 (64)	9
24.3.2020	3_33	SYI	18 (19)	14
30.3.2020	3_34	FYI	4 (N/A)	15
6.4.2020	3_35	FYI	11 (12)	26
6.4.2020	3_35	SYI	4 (73)	12
14.4.2020	3_36	FYI	21 (22)	21
13.4.2020	3_36	SYI	4 (5)	11
17.4.2020	3_36	Remote Sensing	86 (87)	4
22.4.2020	3_37	ECO Ridge (Ridgey McRidgeFace)	32 (34)	4
25.4.2020	3_37	L1	97 (N/A)	2
27.4.2020	3_38	FYI	24 (25)	23
27.4.2020	3_38	SYI	16 (25)	17
30.4.2020	3_38	L2	57 (59)	3
4.5.2020	3_39	FYI	7 (8)	26
4.5.2020	3_39	SYI	18 (19)	15
5.5.2020	3_39	ECO Ridge (Ridgey McRidgeFace)	104 (110)	4
6.5.2020	3_39	L3	107 (108)	3

Basic ice core physical parameters resemble results obtained during legs 1 and 2 with correction for the observed ice growth on both study sites.

At the FYI coring site, over 12 weeks between the last coring of Leg 2 (10.2.2020) and the last coring of leg 3 (4.05.2020), the ice grew from 120 cm to 165cm (depending on the actual core). Much of this growth took place during the weeks of missed coring between legs 2 and 3, as little growth occurred during the course of Leg 3. The FYI site faced frequent rafted ice during Leg 3, leading to longer-than-expected cores (from 2 to 3.3m) and impeding detection of the weekly growth. Nevertheless, the ice structure is similar to the one observed during leg 2 with an upper layer of granular ice, about 15 to 20 cm thick, with columnar growth underneath.

At the SYI coring site, ice consists of a refrozen melt pond about 70 cm to 120 cm thick with a new ice that formed below. With around 60cm of columnar ice at the bottom of the SYI site estimated during Leg 2, preliminary analysis of the retrieved SYI salinity profiles suggest another 40-45 cm growth from the last leg 2 coring (17.02.2020) to the last leg 3 coring (04.05.2020). Once again, much of the growth occurred during the period of missed coring between legs 2 and 3. The longest core recovered on SYI site on 4.05.2020 (activity week 39)

was found to be around 235 cm long. Figure 4.1.3 below shows the evolution of the salinity, temperature, and density profiles acquired for the FYI and SYI sites.

FYI displays the expected C-shape salinity profiles, while the salinity value for SYI profiles mirrors the observed stratigraphy observed during leg 2, with low salinity values (0-1 ppt) in the upper 70 cm, and high salinity values at the bottom (5 ppt) that increase in the lowermost section (8 ppt). High variability in the thickness of remnant ice before the onset of ice growth season is apparent from Figure 4.1.3 with the longest recovered SYI cores exhibiting more than 1.2 m of ice with low salinity values.

The response of the sea ice temperature to warming atmospheric temperatures is apparent at both sites. The first coring sessions (activity weeks 32 and 33) had 1m air temperatures of close to -30°C, while week 39 had 1m air temperatures close to -12°C. This led to ice temperature differences of greater than 10°C between the beginning and end of leg 3, which is can been seen down to 1m depth in the ice.

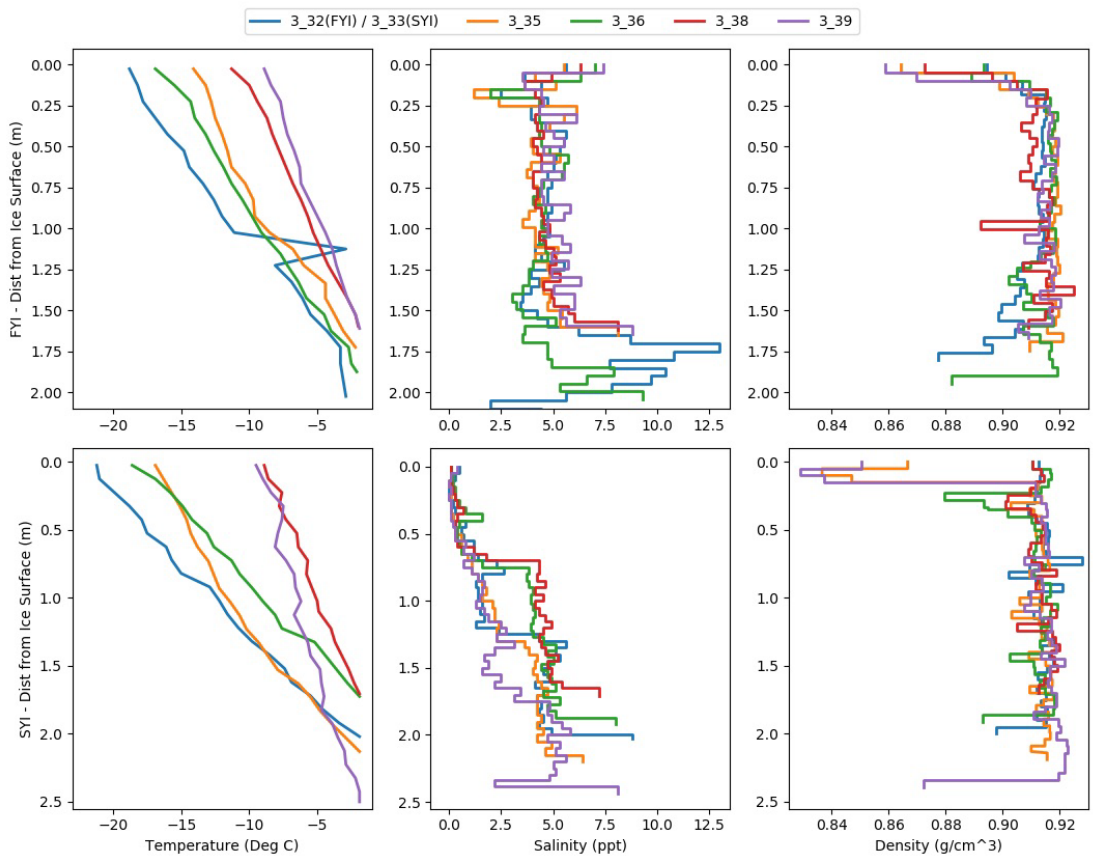

Fig. 4.1.3: *Evolution of salinity, temperature and density profiles over an 8-week (7-week) period of observations during leg 3 for first-year ice (second-year ice). Legend shows DSHIP activity week corresponding to a particular coring session.*

Apart from the Dark Site coring initiative, cores were also taken in the CO and at the DN sites to test the representativeness of the Dark Sites to the surrounding ice cover. Team ICE measured salinity on cores from each of the L-sites (L1, L2, and L3). From Figure 4.1.4, it is clear that the ice types at these DN coring sites range from level SYI (L1, fresh top layer and

2.4m thick) to a SYI re-frozen melt pond (L3, very fresh top layer and 2.0m thick) to FYI (L2, more saline core and 1.6m thick).

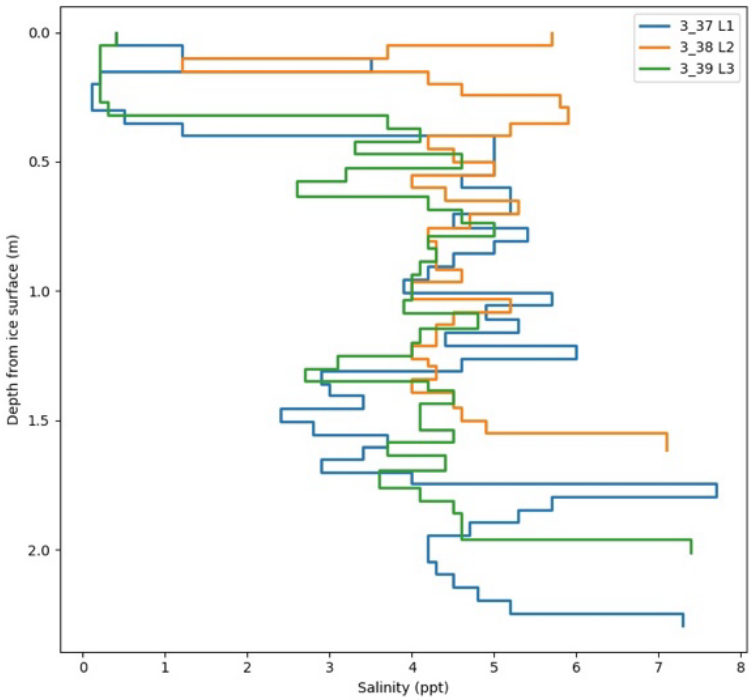

Fig. 4.1.4: *Salinity profiles from the DN L-Site cores taken during leg 3. Legend shows DSHIP activity week and site.*

In the framework of the MOSAiC HAVOC project, ridge coring was conducted twice during Leg 3 on activity weeks 3_37 and 3_39. Given the inaccessibility of the Sea Ice Ridge Observatory (SIRO) Fort Ridge, a new ridge was selected for coring and given the name “Ridgey McRidgeFace”. It was formed in a deformation event in November 2019 between a FYI and SYI floe. The goal for the coring was to locate water-filled gap layers in the ice where seawater could be pumped and later analyzed by the ECO team. The ICE team took cores during both weeks for temperature, salinity/isotope analysis, and density. Further work at ridges in the CO during Leg 3 is given in Section 4.9.

4.1.4 Data Management

All data are handled, documented, archived and published following the MOSAiC data policy (see APPENDIX). All data related to each coring event are located on the MCS within the folder of the device operation corresponding to the deployment of the corer Kovacs Mark II, 9cm. A scanned copy of the field notes and laboratory book have also been included in these folders. The exhaustive list includes:

- Primary data (when available) for each ICE, ECO, and BGC core transcribed into a spreadsheet (section depths, ice thickness, ice draft, weather, date and time, etc.)
- Salinity and density measured on board within 2-5 days of the coring
- Photos of each stored ICE core (BAC, REP, TEX, OPT, PLT, CT) at 10cm intervals
- Tomographic imagery of two bottom-most 5-cm ice sections of microCT cores together with 0-5 cm and 15-20 cm depth sections of density cores are available on the MCS within a separate subfolder contained in the folder of the X-ray tomographer Scanco90.

4.2 Snow

Amy Macfarlane[1], Stefanie Arndt[3], Martin Schneebeli[1] (not onboard), Chris Polashenski[2] (not onboard)

[1]DE.WSL/SLF
[2]USDartmouth
[3]DE.AWI

4.2.1 Objectives

The overarching goal of the snow measurements is to characterize this spatial and temporal varying porous medium. This is conducted with the view of improving snow models and in support of all MOSAiC inquiries from ATMOS, BGC and ECO and Remote Sensing. We refer to the report of leg 1 and 2 for details. Core parameters for snow are divided into physical; depth, temperature, snow water equivalent, density, specific surface area and chemical: see below subheading Chemical sampling.

4.2.2 Work at sea

Conducted snow work can be structured in the following sub-tasks:

1. Snow pits and snow transects
2. Snow sampling
3. Terrestrial Laser Scanning (TLS) of the snow surface
4. Snow lab work

The set-up of the MCS raw data was continued with minimal changes from leg 2. SOPs and field tasks were updated for the handover to leg 4. Protocol sheets for the different snow pits were very useful and used throughout leg 3. All protocols and field note books were scanned and stored on MCS. Detailed documentation is all in the MCS/workspace/snow pits directory.

Snow pits

We continued with the majority of snow sampling sites and pits established during leg 1 and 2. However, the continuation of a large proportion of these became challenging due to the ice dynamics. Details of each individual pit can be found in Table 4.2.1. The location of the sites are shown in Figure 4.2.1. All events are documented in DSHIP as device "snow pit".

In total, 92 snow pit events were realized on leg 3. A pits were most commonly conducted when the snow pit team consisted of two or more people. We found it was most efficient to have one person focusing on the physical measurements and the other on the chemical sampling. As a result of this 34% of pits were A pits. Compared to leg 2, who measured no B-pits, we found that when the snow pit team comprised of one person, they could quickly measure the physical properties but no chemical, thus resulting in a B pit. The outcome of this was 23% of all snow pits conducted were B pits. 3% of snow pits were C pits.

24% transects consisting of SMP measurements over ridges, leads, SYI and FYI. This was a mix of transect timeseries measurements which were repeated sporadically and one-off measurements conducted at a unique opportunity.

16% were unspecified pits, often consisting of just SMP measurements or a mixture of an A/B pit.

Most snow pits were measured weekly, when we had limited accessibility to snow 1 this changed to every fortnight. Each snow pit measures about 1m in width. The spatial variability

of the physical properties within a meter-scale was not too large. However, on a 5 m scale substantial changes were observed, although the surface and relief appeared homogenous. We continued conducting A-pit with 5 additional SMP measurements on each side parallel to the profile with a 1 m-spacing (cf. Logbook A+ snow pit, 2020-02-12), as in leg 2.

We did not use and suggest to skip the following measurements in A-pits: SLF-density and wetness sensor (salinity affects readings), InfraSnow (prototype not available). We suggest that snow wetness (once the snow is melting) is estimated traditionally.

Snow surface SSA is spatially very heterogenous, and NIR-box surface imaging may result in more consistent and relevant results than point sampling. Micro-CT sample in the 44mm diameter sample holder with a resolution of 16 µm of the surface layer were sufficient to resolve most snow types, except very new snow. The snow-surface interface was often sampled using the 88mm diameter and the bulk profile was sampled with 68mm

A warm air intrusion in mid-April was a perfect opportunity to return daily to a site to measure small changes in the snowpack's physical properties over this period of warming and cooling. The chosen site was $Snow2A2$ due to ease of access and homogeneous topography.

The optics transect of both lead ice and SYI was combined with a measurement at the radiation station. The lead transect was measured five times and the SYI was measured three times. Each time albedo measurements were conducted in parallel.

Remote sensing pit ($RS4$) began after the remote sensing relocation, this became a regular B pit with salinity measurements. Due to RS4 being located in close proximity to the logistics area an initial A pit was conducted to act as a 'dirty' reference for chemical samples. In the final week of leg 3, SMP measurements were taken as part of a RS4 displacement experiment.

David's ridge transect was set up to replace the lost Fort Ridge. A SMP transect was measured crossing a SYI ridge and a FYI ridge successively.

The Snow1-transect underwent numerous ice dynamic events, for the majority of leg 3 only the first 'C' of the 'S' shaped transect was accessible and therefore measured.

Tab. 4.2.1: *Details of each unique snowpit ID.*

	Snowpit ID	Comments
1	$BGC1$	Continued from Leg 2. No issues.
2	$BGC2$	Continued from Leg 2. No issues.
3	$DR-transect$	Set-up in leg 3
4	DR	Set-up in leg 3
5	$DS-A7*$	Set-up in leg 3
6	$DS-A7$	Continued from Leg 2. New location ($DS-A7*$) from Apr 30, 2020 due to rafting of FYI coring site see LogBook entry (Week 38 Ice coring)
7	$DS-SYI$	Continued from Leg 2. No issues.
8	$FR-transect$ and FR	Site termination 23.03.2020
9	$L1$	Continued from Leg 2. No issues.
10	$L2$	Continued from Leg 2. No issues.
11	$L3$	Continued from Leg 2. No issues.
12	$lead-flux$	Set-up in leg 3
13	$Met-transect$	Set-up in leg 3
14	$optics-transect-lead$	Set-up in leg 3
15	$optics-transect-SYI$	Set-up in leg 3
16	$radiation-stn$	Set-up in leg 3
17	$random$	Conducted by leg 2
18	$RS3$	Site termination 13.03.2020
19	$RS4-transect$	Set-up in leg 3
20	$RS4$	Set-up in leg 3
21	$snow1-A1$	Continued from Leg 2. Site termination 13.03.2020
22	$snow1-A3$	Continued from Leg 2. Frequent accessibility issues. Possible site termination 17.05.2020
23	$snow1-A5*$	Set-up in leg 3
24	$snow1-A5$	Continued from Leg 2. New location ($snow1-A5*$) from 13.04.2020
25	$snow1-lead$	Set-up in leg 3
26	$snow1-transect$	Continued from Leg 2. Frequent accessibility issues
27	$snow2-A11$	Set-up in leg 3
28	$snow2-A12-transect$	Set-up in leg 3
29	$snow2-A12$	Set-up in leg 3
30	$snow2-A2$	Continued from Leg 2
31	$snow2-A8$	Continued from Leg 2
32	$snow2-lead$	Set-up in leg 3 in parallel to dO18 lead coring
33	$stakes1$	First and last snow measurements conducted 29.03.2020. Site termination 29.03.2020.
34	$snow3-A6$	Site termination 13.03.2020
35	$RS-transect-north$	No remote sensing transect was conducted

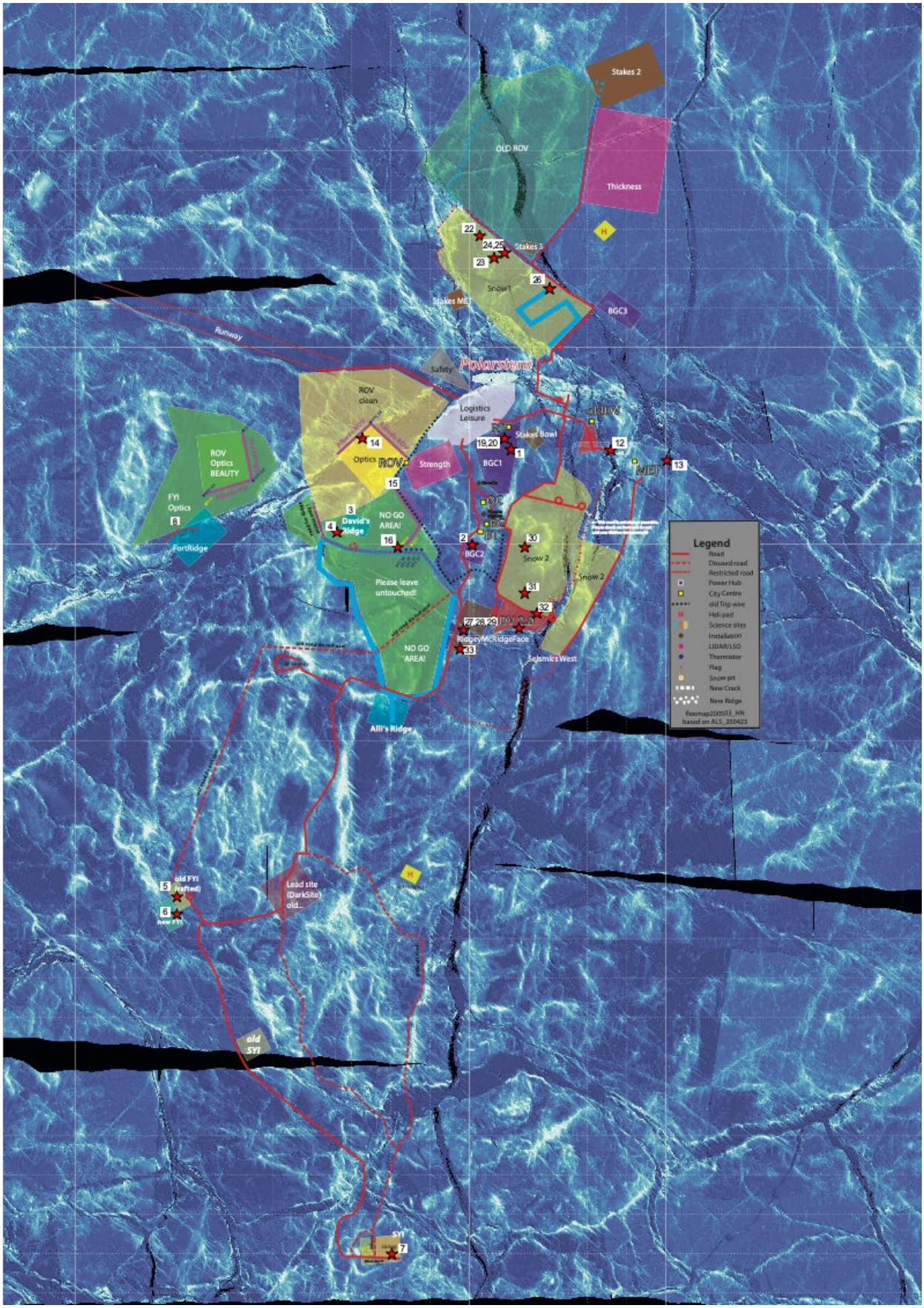

Fig. 4.2.1: *Floe map (state 2020-05-03) with locations of the snow pits and snow transect. See Table 4.2.1 for unique location identifier.*

Chemical Snow Sampling

Each week, at an A-Pit location, we conducted several sampling tasks. Due to time, personnel and weather/ice constraints we could not fulfil all requests as listed. Furthermore, some sampling was requested only for e.g. 2-weekly, monthly ore only after snowfall. However, we took snow samples for the following purposes (in parentheses: sample coordinator)

- Black Carbon (AWI/Daniela Krampe)
- Halocarbons (BGC/Katarina Abrahamsson)
- Ice Nucleating Particles (INPs) (Jessie Creamean)
- Iodide (Uni Grenoble/Hans-Werner Jacobi)
- Major Ions and Water Isotopes (AWI Glaciology/Maria Hörhold)
- Major Ions, Bromide, INPs, 34S (SO4), Salinity, S-Isotopes (BAS/Markus Frey)
- Major Organic Compounds (PSI/Julia Schmale)
- Microplastics (AWI/SLF)
- Salinity (ICE)
- Sugars (TROPOS)
- micro-CT samples
- Beryllium sampling (contact: David Kadko) was mostly conducted by Chris Marsey but was frequently sampled alongside snow pits
- The melted snow for salinity measurements was also used for d18O samples (NPI)
- The rocket traps at MET city for BAS/Markus Frey were checked by Markus (MET group) and samples put into the BAS-storage boxes.
- Tritinate was collected in fresh snowfall at remote locations for Natalia (OCEAN group) for more details see file \scientists\Team_OCEAN\CFC_SF6_He_Ne_Tr_sampling\Tritium_snow_protokoll_all.docx

Unlabelled sample vials were pre-labelled by us before going into the field and for each sample the corresponding snow pit and location within the profile has been documented.

After sampling, the bags and vials were stored either in the -20°C freezer in the F-Deck or in the -20° AWI sea ice physics freezer at the bow - either in prepared boxes by the institutes who conducted the sampling requests or in one of the WSL skufa boxes.

The number of samples collected on leg 3 can be found in Table 4.2.2.

Tab. 4.2.2: *Total number of chemical samples collected over leg 3.*

Sample ID	*Leg3*
BAB	33
BAS	162
BC surface	52
BC profile	150
BER	35
TRI	9
IDA	14
IDB	66
INP	92
ION	81
ORG	22
PLA	6
dO18	188
Rocket traps + BAS (M.Frey)	112
Iodide (H.W.Jacobi)	18
ORG (J.Schmale)	55
Halocarbons (P.Simoes)	34
SUM	1129

Terrestrial LiDAR Surveys (TLS)

TLS snow accumulation maps could not be calculated prior to snow pit measurements, the implementation of the stratigraphy-based directed sampling was not possible. To cover spatial variability, snow specific transects were measured in a relatively open field (Snow1-transect) and across a ridge (David's Ridge and Fort ridge transects). In addition, we continued with the previous 10m transect at each A-profile.

The TLS scans were conducted by David Clemens-Sewall for leg 3. After a brief look at the data, exact snow pit locations appear easy to identify in the scans and can be tracked each week. Scanned areas included Snow 1 (with added difficulties due to ice dynamics), David's ridge, Snow 2, Remote Sensing 4, optics transect (FYI,SYI), radiation station.

This snow-related task is described separately in Section 4.3.

Snow Lab

We processed samples cored in the field for micro-CT analysis, see Figure 4.2.2 as an example profile. 132 snow samples and 40 ice cores were scanned, which correlates to approximately 12m total snow profile length and 2m ice core length. For details on the coring procedure refer to the SOP 'snow coring' and the SOP / cheat sheet for the micro-CT 90 on the MCS. There were no problems with partial reconstruction or missing slices. Scanned snow profiles as seen in Figure 4.2.2 included fresh snow, melt crusts located above a wind-compacted layers and depth hoar. Special attention was taken to scan the interface between snow and ice, this included re-frozen 'snow-ice' interfaces from melt or flooding events and clear snow to ice transitions. The majority of these interface scans were taken using the 88mm diameter holder.

No samples were cast in the field or in the laboratory, as there was no time left for this time-consuming task, and due to the excellent performance of the micro-CT.

Data is stored on MCS semi-automatically in the correct folder using a script developed on Leg 2 (see 4.2.4 Data management).

We measured snow salinity in Trockenlabor 3, with the salinity sensor provided by U. Fairbanks, the same as used for the physical measurements of the ice cores. The 20 ml sample vials for d18O from NPI were suitable for the melted volumes of snow from salinity measurements.

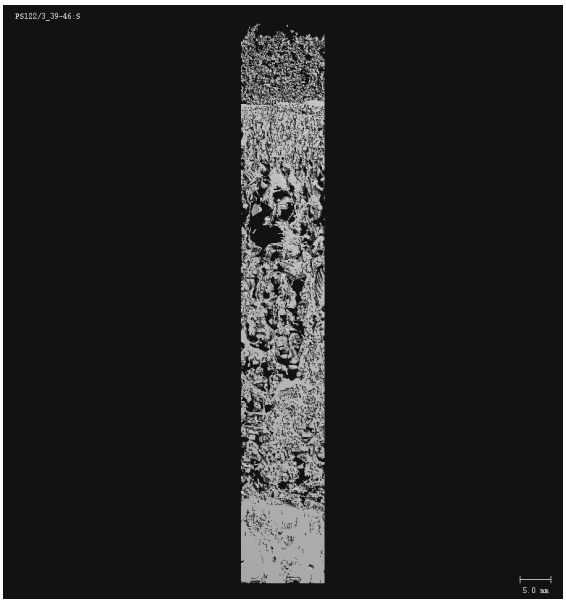

Fig. 4.2.2: *A snow profile scanned using the Micro-Computer Tomograph taken during event PS122/3_39-46 Snow pit A $snow1-A5*$ in a 68mm sample holder.*

4.2.3 Preliminary results

We could measure all core parameters for snow regularly, at least weekly.

All key devices for measurements of snow on the ground such as SMP, NIR worked without major issues. The NIR box was often not taken into the field due to large ridges that had to be crossed and difficulty with transportation, however it worked at temperatures down to -40°C with the additional heating. Thermometers, balances, Garmin GPS and cameras had to be kept above about -25°C to be usable before handling at these very low temperatures. The usually reliable measurement of snow density with the density cutter was difficult or impossible in the thin and very fragile depth hoar layers, and in the very hard (knife) recrystallized "snow-ice" depth hoar.

Preliminary results of the Snow2A2 warm air intrusion event can be seen in Figure 4.2.3. Showing density variability decrease in the snow pit alongside an increase in bulk density. Also, the significant change in the temperature gradient within the warm air phase becomes clear.

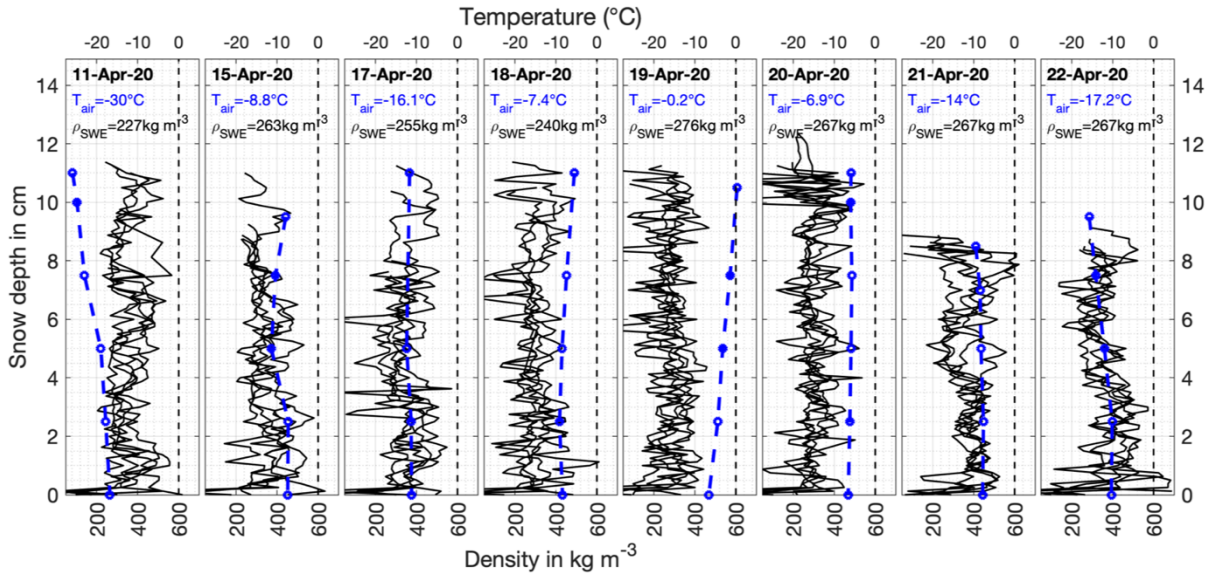

Fig. 4.2.3: *Weekly SnowMicroPen measurements at Snow2A2 at the same time as a warm air intrusion event. Temperature values were measured in the field and density calculated using Proksch et al. (2015) are plotted. Figure by S. Arndt (unpublished).*

Preliminary results for different salinity values for first, second year and lead ice can be seen in Figure 4.2.4. Distinguishing which pits were located on which ice type was done through ice thickness surveys and coring events.

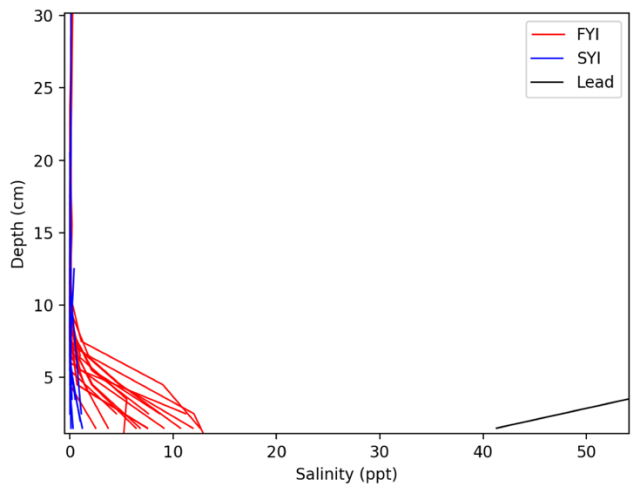

Fig. 4.2.4: *Showing the relation between salinity of the snow above different ice types at the snow-ice interface (0cm).*

4.2.4 Data management

All data are handled, documented, archived and published following the MOSAiC data policy (see APPENDIX). All device operations were logged in DSHIP and all sensor raw data files are stored in platforms/packice/snow pit section of the MCS. Final geophysical parameters will be made available via the workspace section of the MCS and archived in the PANGAEA data repository according the MOSAiC data policy.

Tab. 4.2.3: *Overview on all measured parameters for the three defined snow pit types during leg 3.*

Type A: Parent snow pit	Type B: Quick snow pit	Type C: SnowMicroPen
Complete sampling of physical and chemical properties	Complete physical sampling	Super quick measurements
• 10 m - SMP transect, 1 m spacing • Pictures for snow surface and ice surface roughness (SfM) • MicroCT sampling • Density (volumetric) • Temperature • Salinity • Snow samples for chemical and physical properties **All Type B measurements**	• SnowMicroPen (SMP) • NIR photography (SSA) • SWE (ETH tube) • MicroCT sampling • Site overview photos	• SnowMicroPen (SMP)

See the DSHIP action log extract file for an overview of the snowpits conducted for legs 1, 2, and 3

References

Proksch, M., Lowe, H., and Schneebeli, M.: Density, specific surface area, and correlation length of snow measured by high-resolution penetrometry, J Geophys Res-Earth, 120, 346-362, 10.1002/2014jf003266, 2015.

4.3 Terrestrial LASER scanning

David Clemens-Sewall[1], Amy Macfarlane[2], Steven Fons[4], Saga Svavarsdottir, Ronald Visser, Carl Schonning, Thomas Olufson, Martin Radenz[5], Chris Polashenski[1,3] (not on board), Don Perovich[1] (not on board), Ian Raphael[1] (not on board)

[1]US.Dartmouth
[2]DE.WSL/SLF
[3]US.CRREL
[4]US.UMaryland
[5]DE.TROPOS

4.3.1. Objectives

Quantifying changes in sea ice surface morphology is critical to understanding the thermodynamic and dynamic evolution of the sea ice cover. Because sea ice moves, it is critical to track changes in the surface from an ice-fixed reference frame. We used Terrestrial Laser Scanning (TLS) to track cm-scale changes in the surface due to snow accumulation, snow redistribution, and ice dynamics. Throughout leg 3 our TLS campaign had three major foci: we observed snow redistribution—especially from single storm events—across four dominant ice types—new ridge, old ridges, level ice, and leads. We acquired high temporal and spatial coverage of changes where snow pits and snow transects were conducted. And we coordinated our observations of changes in surface morphology with ROV multibeam

observations of changes in basal morphology at a site that included a new ridge, an old ridge, level ice, and a lead.

These data will be used to build process level understanding of snow redistribution and accumulation. In coordination with the Stakes and Snow datasets, we will quantify the snow budget. And in coordination with the Stakes, Snow, Transect, and ROV datasets we will produce insights into the impact of snow processes on sea ice mass balance and thermodynamics. Additionally, the data document dynamic changes in the ice cover—especially the evolution of new ridges—at high spatial and approximately weekly temporal resolution. Other uses include helping to characterize the impact of surface morphology on the atmospheric boundary layer and assessing how the history of the snow surface morphology impacts the albedo evolution of the snow surface in the spring season.

4.3.2 Work at sea

Legs 1 and 2 established three TLS scan fields: Snow1, Snow2, and ROV. Snow1 was the oldest and most consistently measured scan field, with measurements going back to October. The scanned area included Met City, MET Stakes, Stakes 3, half of the Southern Transect, the snow transect, and three regularly measured type “A” snow pits (A1, A3, and A5). Snow2 was scanned regularly in Leg 1 but only measured twice throughout Leg 2 due to prioritization of the ROV area. The scanned area included a significant second year ridge, flux chamber measurements, and two regularly measured type “A” snow pits (A2 and A8). The ROV scan field was established in early Leg 2 with the relocation of the ROV hut. The TLS scan field included much of the ROV multibeam area, the Ft. Ridge Observatory, half of the Northern Transect, and nine DTC stations. Figure 4.3.1 shows the configuration of the Central Observatory with the TLS scan locations at the start of Leg 3.

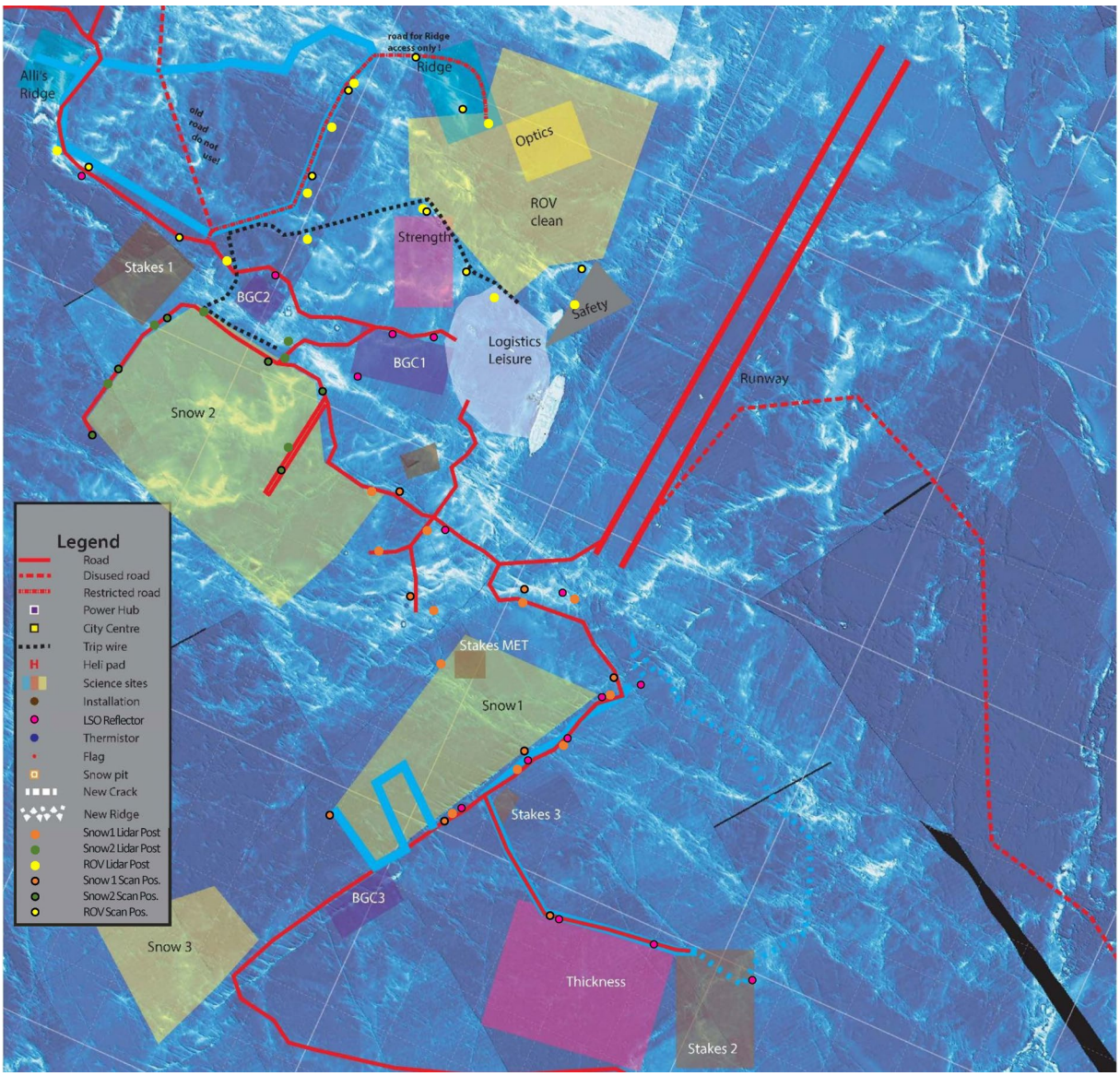

Fig. 4.3.1: *Map of Lidar Fields and Features as of 2020.02.28 against an ALS basemap of the CO. Each Scan Position indicates a single scan in its respective scan field. All of the scans in a scan field are registered together using the fixed reference points (Lidar Posts) to create an integrated scan product.*

March 11 was the first day on Leg 3 that weather and logistics permitted TLS measurements. However, after just a single scan position had been completed (at Ft. Ridge as part of the ROV scan field), the Mosaic floe was cleaved by a series of fractures whose dynamics would become the defining feature of Leg 3. Figure 4.3.2 shows the fractures and the approximate times (to within 20 minutes) they visibly opened on March 11. On March 13, the Lunch Lead crack opened between Met Crack and Ship Crack (running through Stakes 1 and the Northern Transect), further subdividing the ROV scan field. On March 14, we scanned a subset of the ROV scan field from the four accessible scan positions in which the geometry of the cracks in that area can be seen. Between March 15 and 18 (probably on March 15) the Ship Crack underwent shear with the Ft. Ridge portion moving in the direction of the Northern Transect/Dark Site. This motion built the first stage of David's Ridge which we measured in our March 18 TLS scan. During the March 18 scan a fracture opened from the Ship Crack through the secondary ridge on the Northern Transect side of Ft. Ridge. Subsequent motion along this fracture system would demolish Ft. Ridge and ultimately transport the remains of

the Ft. Ridge Observatory and ROV clean area approximately 200 m in the direction of the Dark Site.

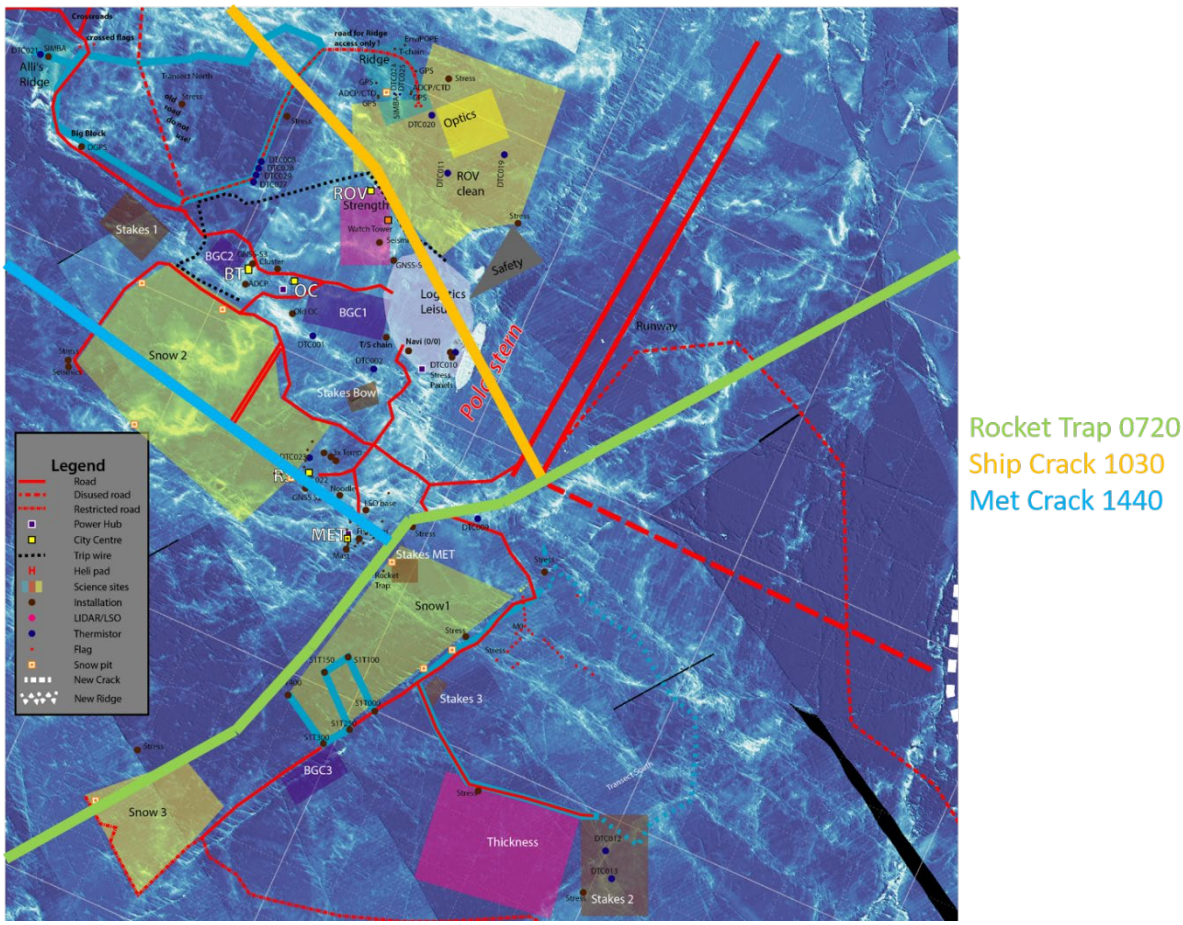

Fig. 4.3.2: *Map of the Central Observatory with annotations for the cracks which opened on March 11 and the times that they visibly opened (UTC).*

Meanwhile, over the course of this week Rocket Trap Lead opened several hundred meters wide, transported Snow 1 and the Southern Transect to the port side of the vessel, and then ridged. The Snow 1 sampling area was relatively undisturbed although two sides of it were now walled in by 1.5 m high ridges and rubble that would persist for the remainder of Leg 3. Figure 4.3.3 shows a TLS scan of Snow 1 from March 22 that illustrates this situation. The cracks and rubble fields between the rest of the Central Observatory and Snow 1 would remain restive throughout the rest of Leg 3 resulting in only intermittent access to Snow 1. The dynamic changes throughout the Central Observatory destroyed many of the TLS reflector posts and so when available other pvc posts (e.g. MET Stakes and Stakes 3) were utilized. When necessary temporary reflector posts were also added for the duration of a scanning day.

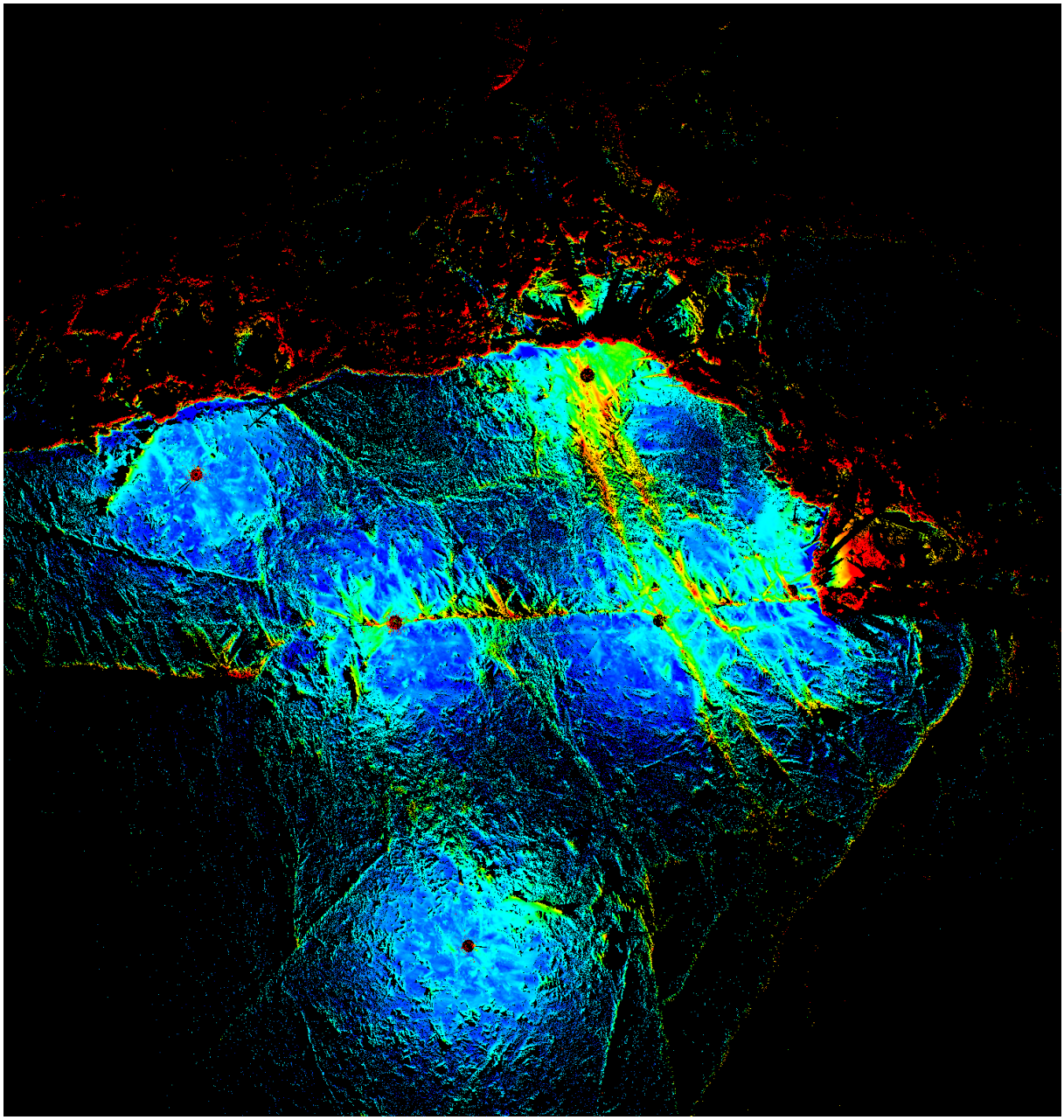

Fig. 4.3.3: *TLS pointcould of Snow 1 scan field from March 22. Note the ship at the top of the figure. The line of ridges running left-right across the image is the road at the bottom of the Snow1 snowfield and the bottom-most scan position is at the bend in the road on the Southern Transect. The coloration is by height (arbitrary reference) with 1 m of relief between deep blue and bright red.*

Dynamic changes continued unabated throughout this period. On March 19 a crack formed through Snow 2 that paralleled the Met Crack (now ridged) across the Snow 1 side and then intersected the Met Crack near the boundary road. Then at 04:20 UTC on March 23 this crack ridged to form the Ridge to Snowhere (RtS). We decided to resume regular measurements of Snow 2, with a particular focus on RtS, in order to examine snow redistribution around a new ridge, old ridge, and level ice. Figure 4.3.4 shows the configuration of Snow 2 on March 26 at the beginning of our regular measurements. Additionally, due to access considerations the snow team reoriented their intensive sampling efforts to the two “A” pits in Snow 2.

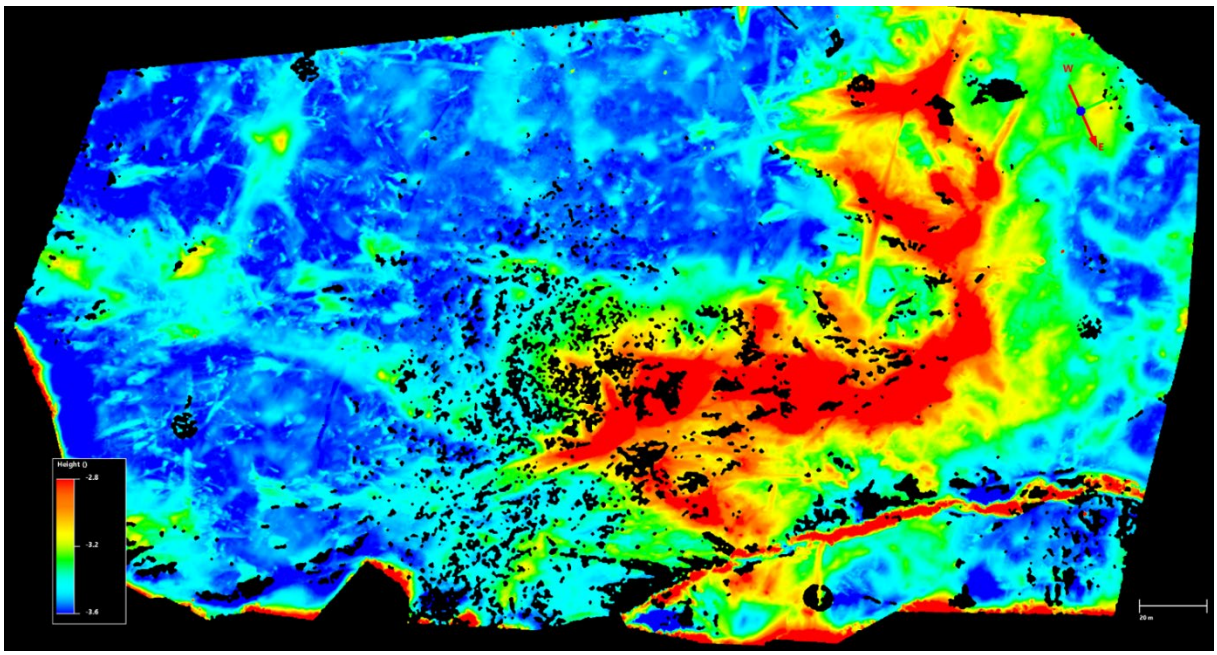

Fig. 4.3.4: *TLS gridded surface of Snow 2 on March 26. Ridge to Snowhere is the narrow ridge in the bottom right. We conducted this scan three days after RtS formed and before it had experienced its first blowing snow event. Ignore the compass arrow. Balloon Town is just above the top of this map. Met City is a bit past the bottom right corner.*

The ROV scan area largely stabilized by the end of March and now contained a large extent of level lead ice which the ROV optics grid and MISS Stakes would be added to. We decided to conduct regular scans of the ROV and Snow 2 scan fields with a particular focus on the two new ridges—David's Ridge and RtS. We continued to scan Snow 1 whenever ice conditions permitted access. The two new ridges experienced similar snow redistribution after blowing snow events—discrete fingers of snow on the lee sides (see Figure 4.3.5). Neither ridge became consolidated, and both ridges developed cracks running down their spines in mid-April. However, RtS was separated into a lead on April 21 and then subsequently modified beyond recognition. Besides these changes the ice at the Snow 2 and ROV scan fields remained fairly constant until the May 12-13 dynamics event. Total we scanned the ROV scan field 10 times and Snow 2 7 times. On two occasions, April 4 and May 9, we linked Snow 2 and the ROV areas into a single scan field. May 9 was the final scan done before the May 12-13 dynamics event that shattered the Central Observatory. On this occasion we made an explicit effort to also cover the Central Observatory so that the relative positions of most installations in the area can be identified.

We scanned the Snow 1 area four times throughout Leg 3. Major dynamics changes occurred within the scan field between each scan. On March 23, one day after the March 22 scan, The "Snow 3 Crack" opened lengthwise through Snow 1, it joined the ridge next to the road to Snow 3 a bit past Stakes 3. Further down the road this crack turned into a fracture system that fragmented the remainder of Snow 3. Then, on April 4 the Stakes 3 crack formed through the middle of Snow 1 and the Southern Transect, running 1 m to the runway side of Stakes 3 (it eventually turns towards Snow 3 and separated CRVW1953 and CRVW1954). The Southern Transect portion of the Stakes 3 crack stayed open as a lead whereas the Snow 1 portion built a ridge on April 5-6. These changes were observed in the April 8 TLS scan. Between April 8 and April 25 additional cracks opened through the Snow Transect. Then on May 1 the Met City fracture system joined the Snow 3 and Stakes 3 cracks to sunder Stakes 3 and open a 90 m wide lead. Throughout Leg 3 we focused on covering the Snow Transect within our TLS scans.

During Leg 3 we also provided five small scans in service of other teams. Three of these were single scan positions of the Remote Sensing site on April 17, 22, and 30. April 17 and 22

bracket the April 19 surface melt event. Through these scans we can precisely identify the surface which each remote sensing instrument is observing and characterize the snow drifts formed by the instruments (see Figure 4.3.5 for example). One single scan was taken at the ROV site on May 1 for the purpose of getting a new transponder position on the optics grid. In general, we used the TLS to support the ROV's transponder repositioning which needed to happen a couple times during Leg 3. Finally, we collected a single scan of Met City on May 4 to support the atmospheric boundary layer measurements and precisely locate the installations. Also, in the Snow 2 scans we can resolve the instruments on the Noodle which may be of use for interpreting their data as well.

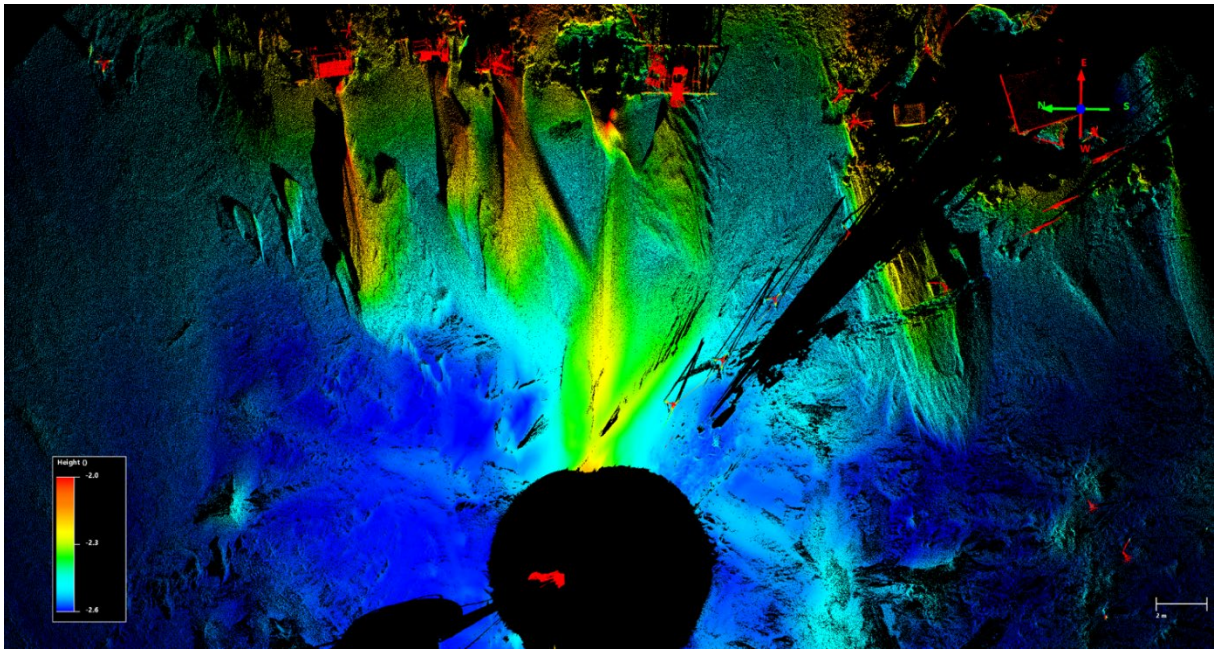

Fig. 4.3.5: *TLS pointcloud of the Remote Sensing site on April 22. Note the snow drifts which formed in front of the instruments. Ignore the compass in the top right. From left to right at the top of the figure the instruments are: HUTRAD, SSMI, GNSS-R, ELBARA, Hyperspectral camera. C-Scat is at the bottom next to where the TLS scanner was positioned.*

4.3.3 Preliminary (expected) results

We observed numerous snow redistribution events and a few accumulation events. Invariably, most snow appeared to be redistributed to drift traps: primarily new ridges, lead edges, and rubble. Old, snow-covered ridges and level ice rarely accumulated fresh snow at the beginning of the leg but may have accumulated more once temperatures warmed. Behind new ridges snow accumulation was not homogeneous but rather exhibited a fingerlike pattern of discrete drifts (Figure 4.3.6). This morphology was observed on most, if not all, new ridges. Some modest erosion of drift features was observed in places, but the weathered, crag and tail snow surfaces stayed largely unchanged throughout Leg 3. Snow pits, albedo/SMP transects and the Snow Transect are all well resolved by the data which will facilitate integration with the snow property datasets.

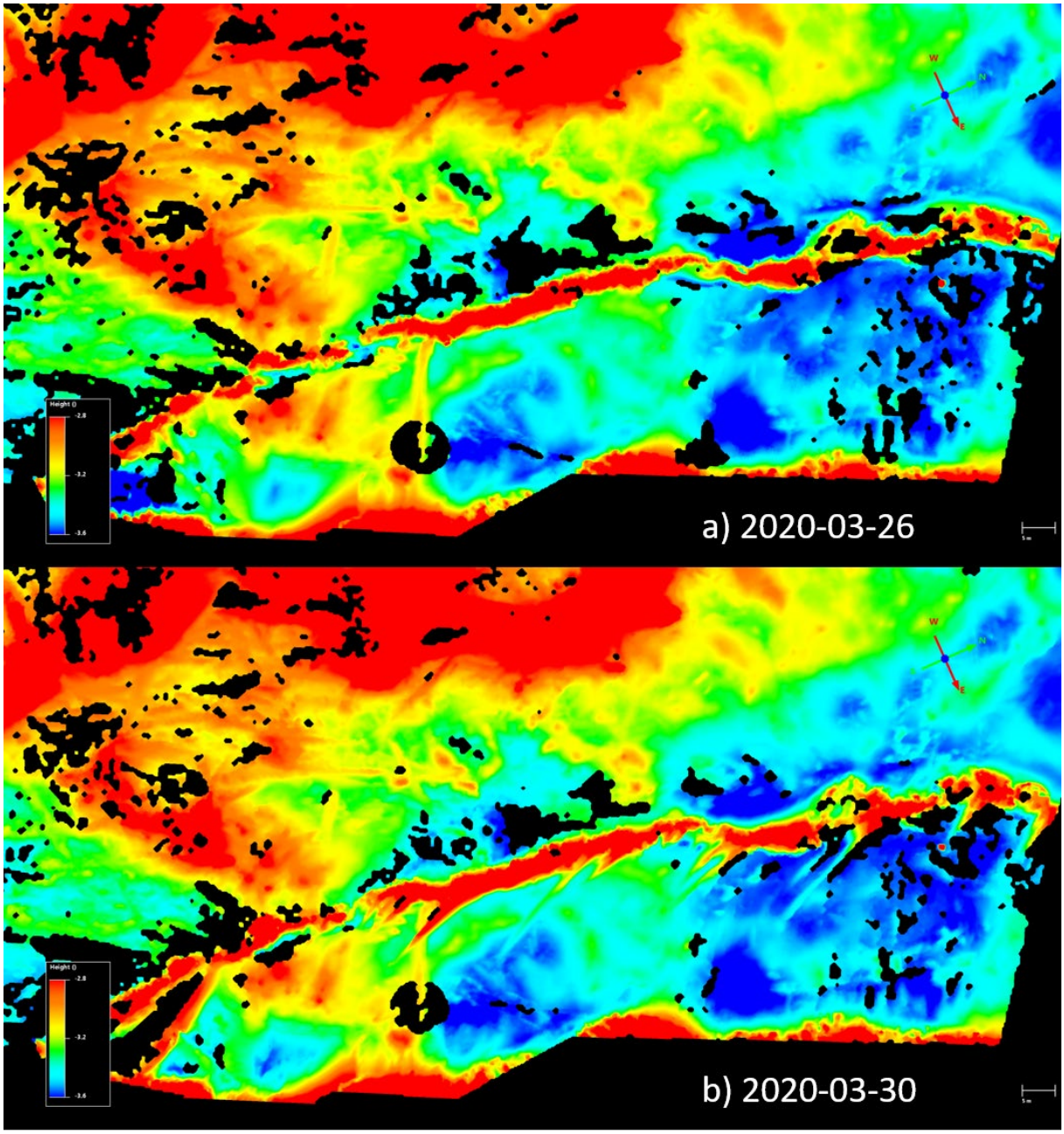

Fig. 4.3.6: *Comparison of surface morphology of Ridge to Snowhere in Snow 2 on March 26 (a) and March 30 (b). Note the fingerlike snow drifts on the lee side of RtS and compare to the lack of change on the second year ridge above it.*

4.3.4 Data management

All data are handled, documented, archived and published following the MOSAiC data policy (see APPENDIX). All device operations were logged in the AWI sensorweb portal and all sensor raw data files are stored in platform section of MCS. Final geophysical parameters will be made available via the workspace section of MCS and archived in the PANGAEA data repository according the MOSAiC data policy.

4.4 Airborne Sea-Ice Surveys (HELI)

R. Ricker, A. Jutila[1], G. Birnbaum[1] (not on board), N. Fuchs[1] (not on board), S. Hendricks[1] (not on board), G. Spreen[2] (not on board), M. Huntemann[1,2] (not on board), F. Pätzold[3], A. Lampert[3] (not on board), T. Sachs[3,4]

[1]DE.AWI
[2]DE.UBremen
[3]DE.TU Braunschweig
[4]DE.GFZ Potsdam

4.4.1 Objectives

The objectives of the helicopter-borne sea-ice surveys during PS122.3 have been described in the Helicopter Observational Plan, the Expedition Programme and the cruise report for PS122.1 and PS122.2. Here we provide a short summary:

1. In the overarching MOSAiC Science Plan question we mainly contribute to: How does sea ice formation, drift, deformation and melting couple to atmospheric, oceanic and ecosystem processes?
2. What is the spatial distribution of snow freeboard and surface roughness within the distributed network (DN)? How does these parameters evolve with the thermodynamic and dynamic forcing in polar winter?
3. What is the surface roughness downwind of the meteorological installation at the central observatory (CO)?
4. How does the sea ice surface deform in response to storms and other dynamic forcing?
5. How does snow precipitation and snow redistribution by wind change the snow freeboard distribution?
6. How does the surface temperature of different ice classes (classified by their snow freeboard) change during the polar winter?
7. How does the lead distribution (open water and thin ice leads) change through polar winter?

The HELiPOD activities during MOSAiC are funded by the DFG-project “ALEXIA - Analysis Linking Arctic Methane, Carbon Release, Heat Fluxes and Sea Ice from Local to Sub-Regional Scales by Airborne Measurements” (LA 2907/11-1). The objectives are:

a) Acquiring and analysing a high-latitude and high-resolution data set of atmospheric and surface properties from a local scale to 100 km range as basis for all planned studies.
b) Linking turbulent sensible and latent heat fluxes to surface temperature variability induced by different sea ice properties and synoptic conditions.
c) Studying methane and carbon dioxide fluxes in the light of atmospheric stratification, conditions of the ice surface and heat fluxes, and identifying the transport pathways vertically from the ocean through sea ice or horizontally by advection from lower latitudes.
d) Exploring the provenance of methane by analysing the isotopic composition signature of methane in air samples at different altitudes.

4.4.2 Work at sea

4.4.2.1 Sensors

The following sensors/instrumentation have been operated during PS122.3 on the D-HARK helicopter (ALS configuration):

- airborne laser scanner (ALS)
- infrared camera (IR)
- 2 RGB cameras: 14 mm wide-angle and fish eye
- DMS including operation of KT-19
- 2 GoPros

The following sensors/instrumentation have been operated during PS122.3 on the D-HAPS helicopter:

- EM-Bird
- HELiPOD

4.4.2.2 Mission types

We have identified 5 different mission types during Leg 3:

- Floe grids – D-HARK (ALS) & D-HAPS (EM-Bird)
- L-Sites – D-HARK (ALS)
- Butterfly pattern – D-HAPS (EM-Bird)
- Triangles – D-HAPS (EM-Bird)
- Combined flight pattern with calibration manoeuvers, out and return transect and vertical profiles (HELiPOD)

With the D-HARK ALS configuration, we carried out all surveys according to the standard flight parameters of 1000 ft altitude above ground level and 90 kn ground speed (see also Leg 1 and 2 cruise reports).

With the D-HAPS EM-Bird configuration, we carried out all surveys on 40 ft operational bird altitude above ground level and 80 kn air speed.

Between 27 February 2020 and 10 May 2020, we accomplished 10 survey flights with the ALS configuration and 6 flights with the EM-Bird (Table 4.4.1). In the following the different mission types are explained in more detail.

With the D-HAPS HELiPOD configuration we carried out a combined flight pattern survey at different altitudes and 75 kn indicated airspeed.

Floe grids

Floe grid surveys following a mow-the-lawn or a double-loop pattern centered over the CO with a target side-length of 5 km (Figure 4.4.2).

L-Site Surveys

Real-time coordinates from the three L-Sites (snow buoys) have been used to span three triangles. The primary objective of this type of mission is to map changes for surface roughness, freeboard and surface temperature in the extended network. As a secondary objective, the survey serves as an opportunity to monitor the ice conditions at the L-Sites. The three L-Sites were chosen as waypoints since these are maintained and have the highest probability for survival rate of near-real time GPS data throughout the entire MOSAiC expedition.

The survey lines contain the spines from Polarstern to all L-Sites as well as the outer triangle between the L-Sites, e.g.:

PS > L3 > L2 > PS > L1 > L3 > PS > L1 > L2 > PS

The total flight time of all legs is approximately 1 hour (excluding turns). All legs have an approximate length of 100 NM combined. Figure 4.4.2 shows an exemplary flight pattern of a L-Site survey.

EM-Bird Butterfly surveys

During Leg 3 the butterfly flight pattern has been introduced. It is defined by Polarstern (PS) as the starting point and 4 iSVP buoys (P90, P217, P92, P124) as corner waypoints (WP). Figure 4.4.3 shows a schematic butterfly pattern. Survey flights are carried out by rotating the pattern by 90° back and force, e.g.:

Survey flight #1: PS > WP1 > WP2 > PS > WP3 > WP4 > PS

Survey flight #2: PS > WP1 > WP3 > PS > WP2 > WP4 > PS

Survey flight #3 = Survey #1, etc.

EM-Bird Triangle surveys

During Leg 3, we have carried out 2 triangle flights, to the North and to the South, in order to cover the largest possible area. This flight pattern is not linked to buoy positions.

HELiPOD calibration pattern

Quadratic wind vector calibration patterns were flown at constant altitude with nominal cruise speed of 75 kn indicated air speed and 1 min base length (wind fixed type).

HELiPOD transect and vertical profile survey

Out-and-return transects of 25 km were flown at constant altitude of 200 ft (60 m). Profiling was limited due to cloud cover to a maximum altitude of 1200 ft above surface.

.

***Fig. 4.4.1**: HELiPOD during outside ground test on 8 May 2020 (photo: F. Pätzold)*

4.4.3 Preliminary (expected) results

Airborne laser scanner

We continued the routine workflow and quick-view processing of the airborne laser scanner data during PS122.3. Using parallel processing that has been established during leg 2, processing the data all the way to the final level-4 gridded product regularly took less than 24 hours. The CO floe grid survey's merged product was the basis and background for the annotated and constantly updated floe map of the CO, but served also as a tool for scouting suitable runway locations (Figure 4.4.4).

RGB 14 mm wide-angle and 8mm fisheye camera

During our ALS helicopter flights, we operated a 14mm nadir camera and a 8mm fisheye camera, collecting high-resolution photos of the ice surface. We are using a processing chain to retrieve ortho-mosaics and eventually a digital elevation model (DEM). Another main goal of this camera will be melt pond detection during the upcoming melt season. Figure 4.4.5 shows an ortho-mosaic of the floe grid flight from 23 April 2020, covering an area of about 6x12 km.

EM-Bird

EM-Bird surveys have been carried out in order map the sea ice thickness distribution on floe size scale and on larger scales beyond the L-sites. Eventually, one goal is to upscale ground-based EM ice thickness measurements from the transects with the GEM-2. Figure 4.4.6 shows the sea ice thickness along the flight track and distributions for the Northern and Southern triangle. The modal thickness for the northern survey is 1.8 m, while for the southern survey it is 1.7 m. On the northern survey, additional modes can be found for very thin ice, since open and refrozen leads have been surveyed. Note that thickness here refers to snow+ice thickness.

Helipod

Technical results: The controlled temperature inside the HELiPOD was very stable within the resolution of the temperature sensors and the overall power consumption of the heaters was 25% below the calculation. The WiFi connection between the HELiPOD and the operator in the helicopter could not be tested beforehand under real conditions and did not work properly. Workarounds are prepared and to be tested on leg 4.

Scientific results: As many of the relevant data must be attitude-corrected and the attitude post-processing cannot be done onboard, no immediate results can be reported at this moment other than exemplary data quick-looks of individual sensors. Figure 4.4.7 for example shows the radiation measurement with the Kipp & Zonen instruments. Figure 4.4.8 shows a screenshot from an onboard video of the surface when the up-welling short wave radiation was reduced and the up-welling long-wave radiation increased in the same short period.

4.4.4 Data management

All data are handled, documented, archived and published following the MOSAiC data policy (see APPENDIX). All device operations were logged in the AWI sensorweb portal and all sensor raw data files are stored in platform section of MCS. Final geophysical parameters will be made available via the workspace section of MCS and archived in the PANGAEA data repository according the MOSAiC data policy. Data from the data acquisition system of Polar Research Aircraft (DMS) can be accessed after registration at https://dship.awi.de/exportdisplay/.

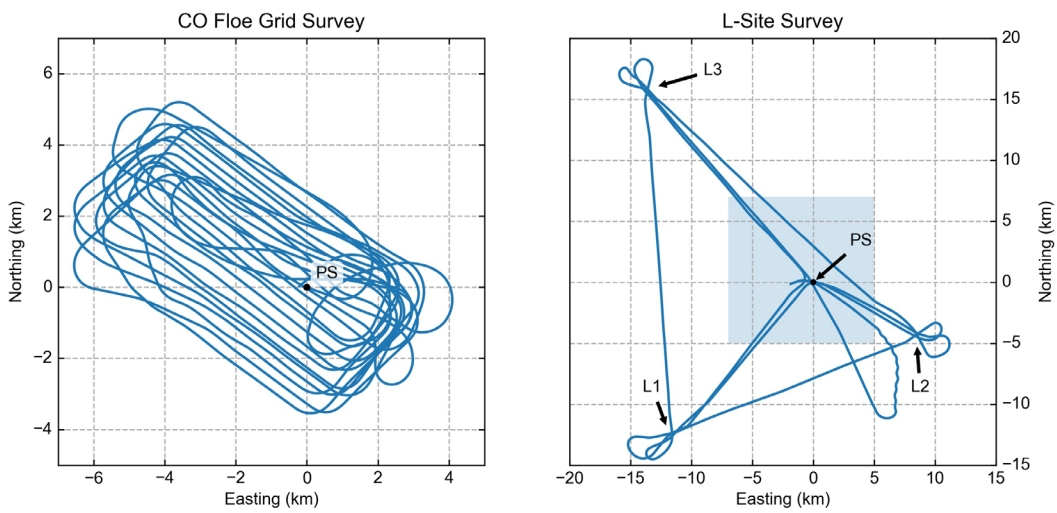

Fig. 4.4.2: *Example flight lines for the two main sea-ice mission types at the end of PS122.2: (left) Grid survey of the CO close to Polarstern and (right) L-Site survey in the DN. The light blue square in right panel marks the spatial extent of the panel on the left. Note that the scale of the axes differ between the panels, but in both the origin (0,0) is set to Polarstern at the start of the survey.*

WP3 **WP4**

***Fig. 4.4.3**: Butterfly EM-Bird survey layout. The corner points of the rectangle are defined by positions of iSVP buoys: P90, P217, P92, P124.*

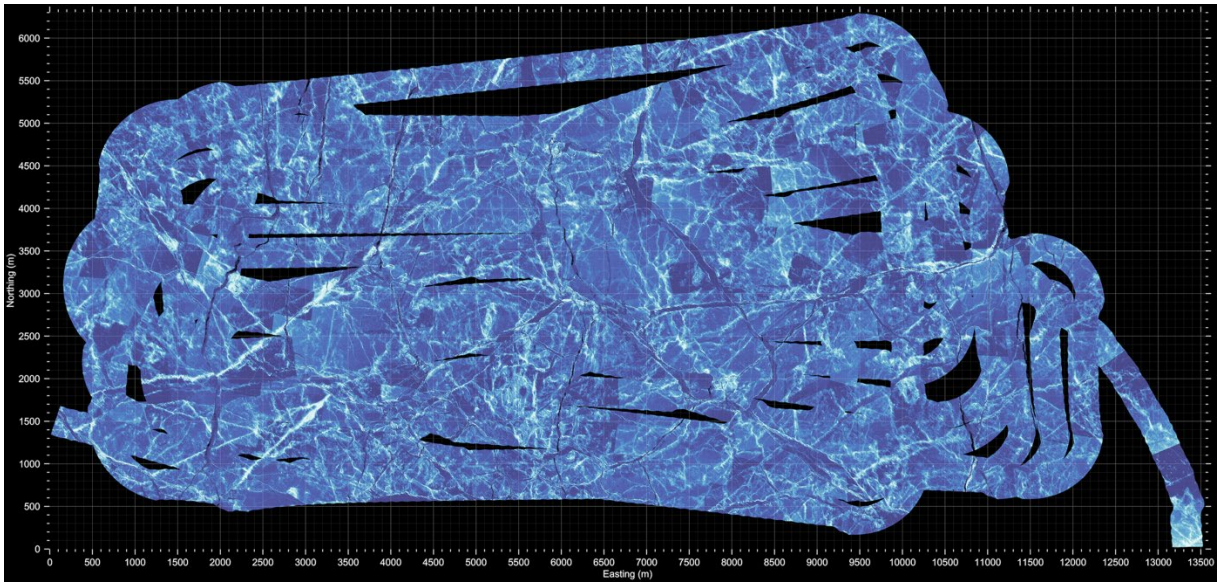

***Fig. 4.4.4:** Example of processed ALS data (23 April 2020) showing gridded ice surface elevations for the central observatory (ALS floe map), retrieved from the floe grid mission type.*

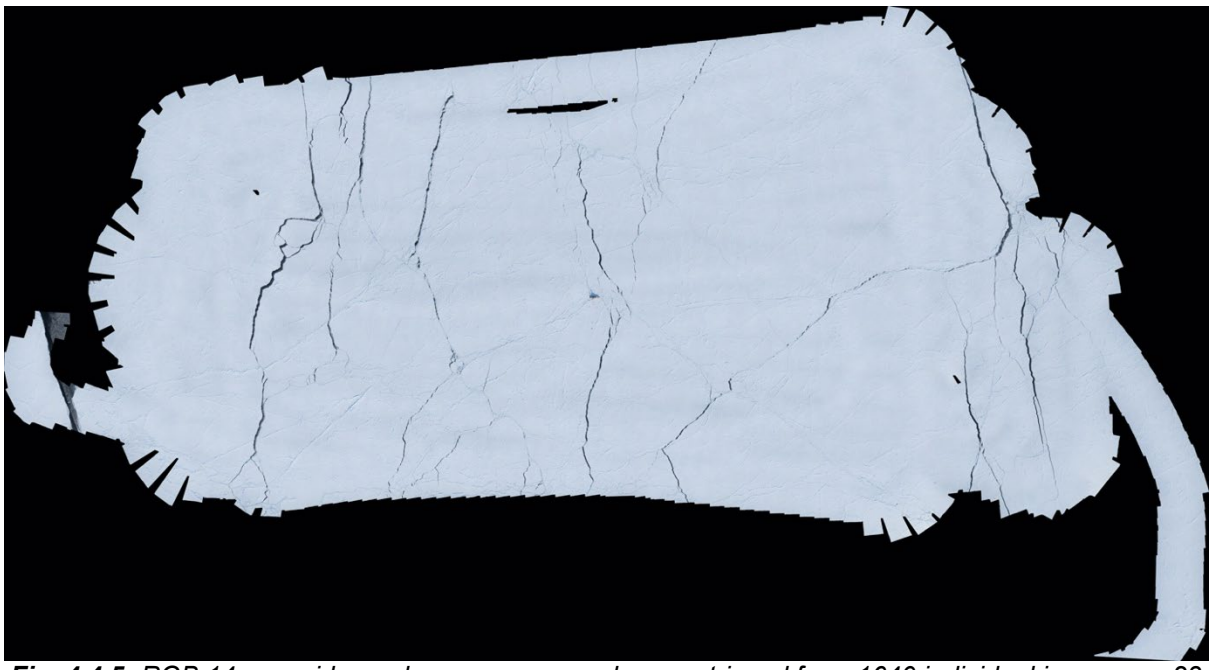

***Fig. 4.4.5:** RGB 14 mm wide-angle camera merged map retrieved from 1640 individual images on 23 April 2020. North is up, Polarstern is in the center, entire patch is about 12x6 km.*

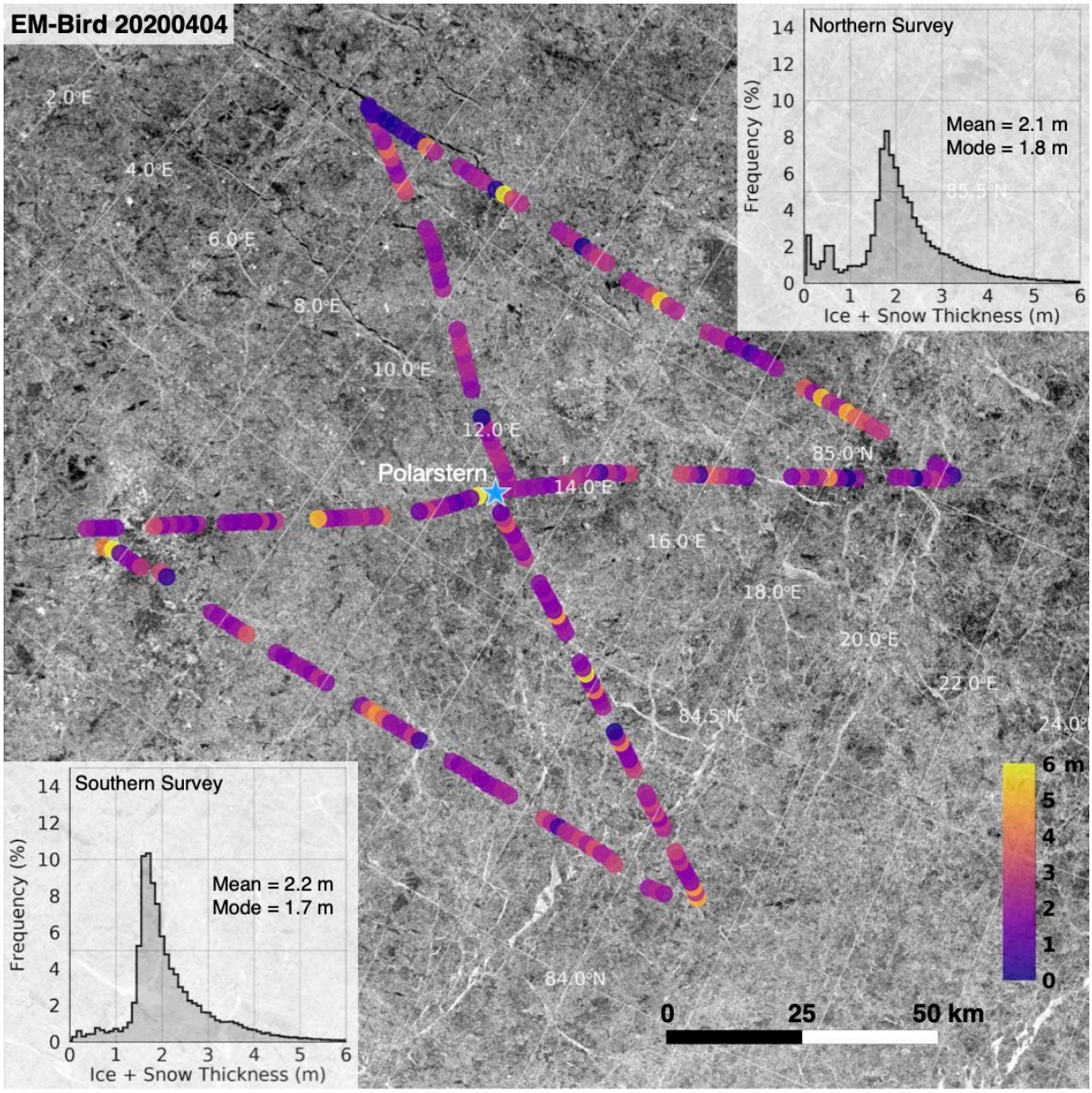

Fig. 4.4.6: *Sea ice thickness retrieved from EM-Bird surveys on 04 April 2020.*

Tab. 4.8.1*: Overview of all helicopter sea ice surveys from Polarstern during PS122/3. TO and LDG designate take-off and landing times in UTC respectively. Grey shades indicate D-HARK surveys with the ALS configuration.*

Flight ID	Device Operation	TO	LDG	Aircraft	Mission Type
20200227_01	PS122/3_29-49	11:43	13:20	D-HARK	CO floe grid
20200318_01	PS122/3_32-42	10:45	11:02	D-HARK	CO floe grid*
20200321_01	PS122/3_32-70	08:08	10:15	D-HARK	CO floe grid
20200321_02	PS122/3_32-71	10:27	11:55	D-HARK	L-Site triangles
20200323_01	PS122/3_33-17	10:37	12:24	D-HARK	ICESat-2 Orbit

20200404_01	PS122/3_34-93	08:12	10:20	D-HAPS	North triangle
20200404_02	PS122/3_34-94	16:21	18:42	D-HAPS	South triangle
20200407_01	PS122/3_35-48	07:51	09:37	D-HARK	L-Site triangles
20200408_01	PS122/3_35-49	08:23	10:25	D-HARK	CO floe grid
20200410_01	PS122/3_35-91	08:12	09:46	D-HAPS	CO floe grid
20200417_01	PS122/3_36-156	09:03	11:11	D-HAPS	Butterfly
20200423_01	PS122/3_37-63	07:39	09:45	D-HARK	CO floe grid
20200423_02	PS122/3_37-66	10:03	11:39	D-HARK	L-Site triangles
20200426_01	PS122/3_37-137	11:13	13:19	D-HAPS	Butterfly
20200430_01	PS122/3_38-112	08:57	11:07	D-HAPS	CO floe grid
20200510_HP01	PS122/3_39-137	11:26	12:41	D-HAPS	mixed pattern
20200510_01	PS122/3_39-109	13:53	15:54	D-HARK	CO floe grid

*aborted

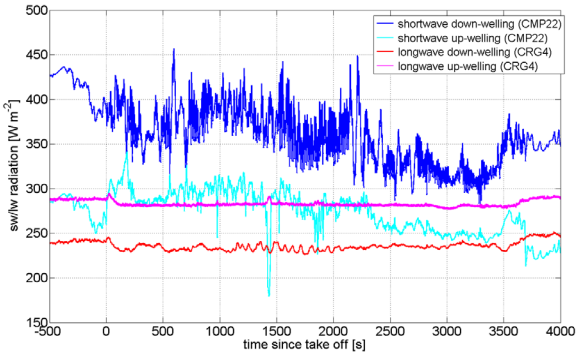

***Fig. 4.4.7**: Radiation measured with Kipp & Zonen instruments at HELiPOD, not attitude corrected.*

***Fig. 4.4.8**: Onboard VIS view on the surface at the significant short-term up-welling shortwave radiation reduction, corresponding to an increased of up-welling longwave radiation, at approx. 1450 sec in Figure 4.4.7.*

4.5 Sea Ice and Water Properties based on ROV Surveys

Philipp Anhaus[1], Stefanie Arndt[1], Serdar Sakinan[2], Susanne Saphic[1], Christian Katlein[1] (not onboard), Marcel Nicolaus[1] (not onboard), Ilkka Matero[1] (not onboard), Julia Regnery[1] (not onboard), Martin Schiller[1] (not onboard)

[1] DE.AWI
[2] DE.WMR

Objectives:

The general objectives for the work with the remotely operated vehicle (ROV) during MOSAiC have been closely described in the ROV Observational Plan, the expedition booklet and the cruise reports for PS122.1 and PS122.2. Here, only a short summary of the scientific background during PS122.3 is presented.

The ROV is the main tool to investigate the spatial variability and the seasonal cycle of ice optical properties, ice bottom topography, bio-physical properties of the uppermost (e.g. 50 m) ocean, organisms living under the sea ice and their variability across / under various surface features and ice types on the scale of the MOSAiC Central Observatory (CO, Figure 4.5.1 a). This includes in particular:

1) High resolution studies of ice bottom topography and roughness achieved by extensive acoustic multibeam sonar surveys (Chapter 4.10 Ridges)
2) Vertical and lateral variability of physical (temperature, salinity) and bio-optical (fluorometry, UV and VIS absorbance spectroscopy) water properties
3) Zooplankton vertical distribution in the direct vicinity of the ice using the ROV towed net (Chapter 6.1 Zooplankton, ecology, and biology)
4) General tasks of ice documentation (photography), as well as under-ice manipulation and installations (e.g. radiation buoys, inspection and recovery of instrumentations)
5) Additional preparations for work related on vertical and horizontal variability of sea ice optical properties and the underwater light field as installations prepared during PS122.2 could not be used most of PS122.3
6) Optical surveys including grids and transects under FYI, SYI, leads and ridges, roll experiments, stable marker positions, depth profiles, upwelling radiation as separate surveys and in co-location with surface optical measurements (Chapter 4.6 Optics)
7) Reading stakes (Chapter 4.7 Stakes)

During PS122.3 sunlight came back and with that optical measurements needed to be collected with the ROV. The overarching objective for the ROV optics is to investigate how the spatial variability of optical properties evolve over the season and how this is linked to physical properties of ice and snow, as well as biological processes. Additional information can be obtained from chapter 4.6 Optics.

Work at sea

During PS122.3 we were able to conduct 20 ROV surveys covering more than 100 hours dive time and a total transect length exceeding 161 km. The dive time was split into the following tasks that were completed according to respective schedules:

- A complete multibeam sonar survey of ice draft in 280 m operation radius around the ROV hole at 20 m depth using a line spacing of 25-30 m was conducted at least every two weeks, but aimed for once a week

- Smaller high resolution studies of the ridge observatories (Fort Ridge and Davids Ridge) as well as refrozen leads and cracks and newly developed ridges using multibeam sonar at 10 m depth and photographic documentation
- Weekly deployment of the towed ROVnet zooplankton net at 10 m depth, slightly below the ice-underside or directly at the ice interface (depending on abundance of plate ice at the ice-underside) as well as at deeper depths between 60 m and 95 m depending on the echosounder analyses by team ECO. During one week this could not be performed and once the operation needed to be aborted due to strong drift. Details can be found in chapter 6.1 Zooplankton, ecology, and biology
- Vertical profiles of water properties and optics in the upper 100 m
- Photographic and video documentation of the ice-ocean interface, as well as installations at the various deployment sites
- Additional deployment and preparation for the optical transect and grid work on newly formed lead due to changes of the floe triggered by severe ice dynamic events (Figure 4.5.2 a and b)

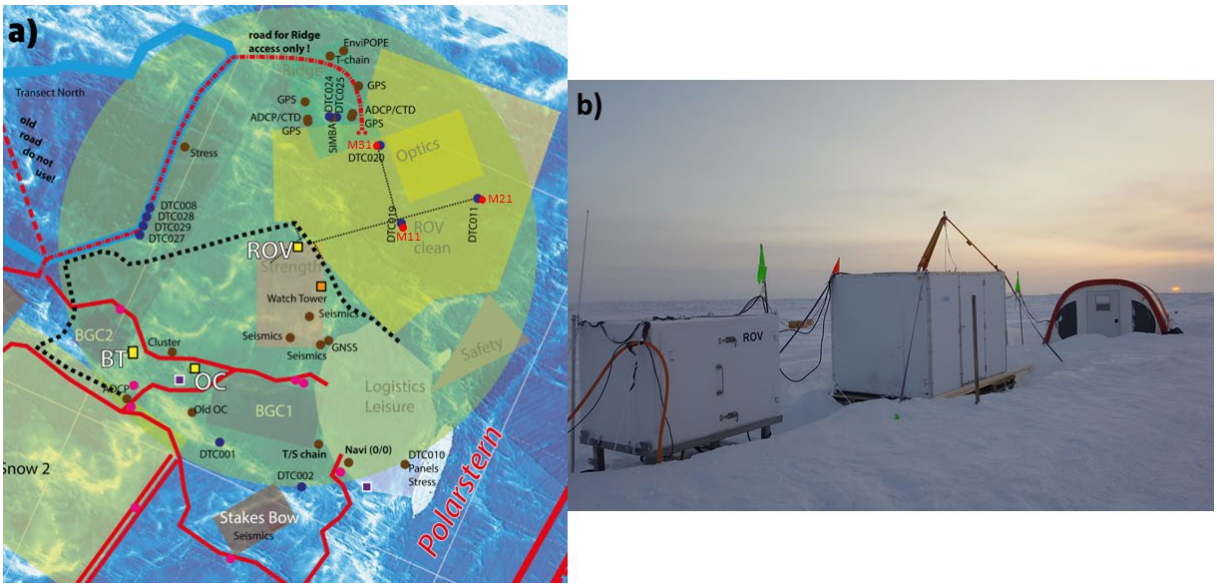

***Fig 4.5.1**: (a) Overview of the ROV operation radius at site 3.0 (green shaded area) established during PS122.2. The map includes the ROV FYI optic grid, installations at the ridge observatory Fort Ridge, the northern transect loop as well as Ocean City (OC) (map: Benjamin Rabe). (b) ROV site 3.0 on March 14 as set-up during PS122.2: (from left to right) Power distribution hub, ROV control hut with surface radiometer on the roof, and ROV tent covering the deployment hole. (photo: Philipp Anhaus).*

Acquisition of optical data was problematic during PS122.3 due to severe ice dynamic events throughout the entire period. Shortly before the sunlight came back and optic surveys were envisioned a major lead opened close to the ROV site on March 11. This led to a displacement of the ROV FYI optic grid prepared during PS122.2 (Figure 4.5.1 a, 4.5.2 a). Since then, the grid was only partly in operational reach of the ROV until March 17 and then not anymore at all.

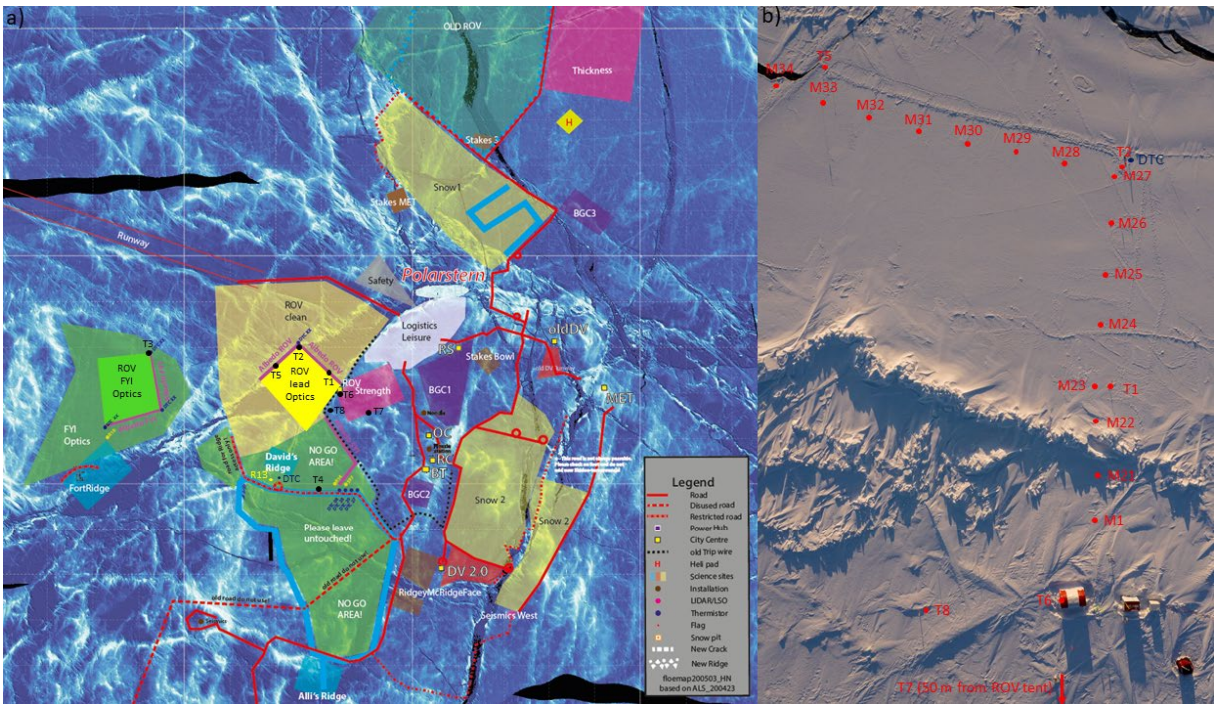

Fig. 4.5.2: *a) Overview of the MOSAiC CO as of May 03 (map: Manuel Ernst). b) Drone picture of the ROV optic lead grid as of April 17 (photo: Manuel Ernst). The grid was established on April 06. An appropriate transponder configuration on the lead (T1, T2, T5) was installed on April 16.*

Further detailed records of all conducted ROV operations can be found in the DSHIP event log, table 4.5.1, and the MOSAiC Logbook. Information about the ROV system can be found in *Katlein et al., 2017*.

ROV City including the power distribution hub, ROV hut, ROV, tether, and all equipment (tool boxes, cables, heater etc.) were brought back onboard Polarstern within three days between May 10 and 12. In the evening of May 12 after the ROV hut was safely back onboard, a crack across the logistics area re-opened. Since then more open water areas appeared and ice deformation destroyed the optics lead grid and buried the ROV tent and transponder 1 in a ridge. Transponder 2 and 8 are since then missing. A drone picture taken on May 16 shortly before Polarstern left shows the most updated MOSAiC floe(s) and its remaining installations (Chapter 1).

Preliminary results

Calibrated transponder positions were measured using the terrestrial lidar (Chapter 4.3 TLS) to achieve the maximum accuracy in under-ice position of the ROV. Absolute position accuracy depends on location and vehicle attitude ranging between 0.1 to 5 m.

Visibility under water was limited by ROV lighting due to the polar night / twilight in the beginning of PS122.3. Once the sunlight came back obviously the visibility would increase. Secchi-depths of more than 20 m were measured during PS122.3 indicating extremely clear waters.

A main preliminary-result of the under-ice ROV work on PS122.2 included ROV footage revealing a significant and widespread cover of locally formed platelet ice at the ice bottom which has not been reported before. Platelet ice was also observed during the first weeks of PS122.3 but vanished around end of March / beginning of April.

ROV based multibeam surveys provide a unique view of the underside of the study subject that is the MOSAiC ice floe and photographic surveys improve the understanding of sea-ice as a non-plane-parallel medium.

ROVs allow to see a great deal of things that would stay occluded without them, clearly justifying the logistical challenges of ROV operations in the harsh Arctic.

Multibeam

Extensive ROV multibeam surveys were performed in order to map the ice draft of the MOSAiC CO. With a tether length of approx. 280 m the ROV could cover the entire CO (Figure 4.5.3 a). The main objective is to investigate bottom melting of the same floe during one year. Due to many severe ice dynamic events during PS122.3 this could not be completely performed as envisioned.

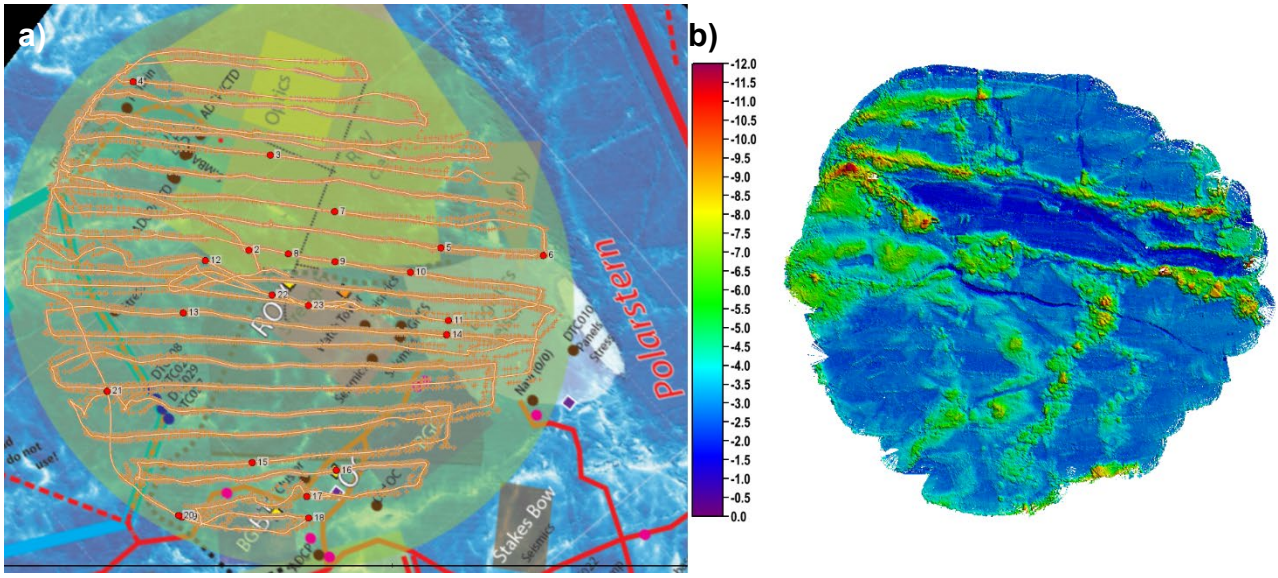

Fig. 4.5.3: *Results from the multibeam survey on April 28: a) Filtered dive track (orange line) overlaid above ALS surface elevation map (by Robert Ricker) and accepted (orange + signs). Polarstern can be seen at the right edge of the image for scale. b) Quicklook processing of the respective multibeam sonar derived ice draft map.*

In the ice draft map from April 28 (Figure 4.5.3 b) many leads, minor and major, cracks and ridges with drafts up to 12 m are visible (Figure 4.5.2 b). Note that due to the major lead formed just off the ROV site (roughly located in the middle of the ice draft map) the ROV could not reach the areas shown in the top of Figure 4.5.3 a where no ROV track is visible.

Leads are mostly very hard to access and to investigate, especially when the ice is still too thin to walk on. With the ROV we are able to access this impressive environment and to measure sea ice related properties under the lead. Consequently, the data that were collected are very valuable and unique, also because of this location in the Arctic Ocean and during this time of the season.

The ice underside of the ridge observatory Fort Ridge was scanned during all multibeam surveys at 20 m depth before it started to disintegrate and flatten on March 18 (Chapter 4.10 Ridges). Since Fort Ridge was not available anymore, Davids Ridge together with Allis ridge was used for the measurement program of the HAVOC (Safe **HAV**ens for ice-associated flora and fauna in a seasonally ice-covered Arctic **OC**ean, http://www.npolar.no/havoc) project led by the Norwegian Polar Institute in Tromsø and the MOSAiC Ridge Observatory work. For a detailed description of the formation and development of David´s Ridge it is referred to chapter 10 Ridges.
In addition to the full CO multibeam surveys high resolution scans at 10 m depth of various leads, cracks, and ridges were performed. David´s ridge was investigated twice (May 02 and 09) through along and across multibeam transects. The high-resolution ice draft map is available in chapter 10 Ridges under Figure 4.10.2. On the surface co-located snow depth and total ice thickness transects were performed (Chapter 8 Transect and Chapter 10 Ridges).

In general, the ROV multibeam work was mostly coordinated in such that co-located terrestrial lidar scans on the surface were conducted.

Optic

Two times, on March 14 (Figure 4.5.6) and 28 (not shown), across lead transects there and back at 10 m, 5 m depth and as close as possible to the under-ice surface were performed when the lead that opened on March 11 was in its very early stage of development. During that mission the focus was to collect, first, oceanographic data such as salinity and temperature in regard of flux measurements through the lead, and second, optical data recorded by the radiance and irradiance radiometers mounted on the ROV. Those measurements were the first reasonable ROV optics data collected during MOSAiC. Obviously, under the leads the transmittance and the transflectance are elevated (Figure 4.5.6 b, c). The transmittance and the transflectance are the transmitted irradiance and radiance normalized by the incoming irradiance (a), respectively, to account for atmospheric variability.

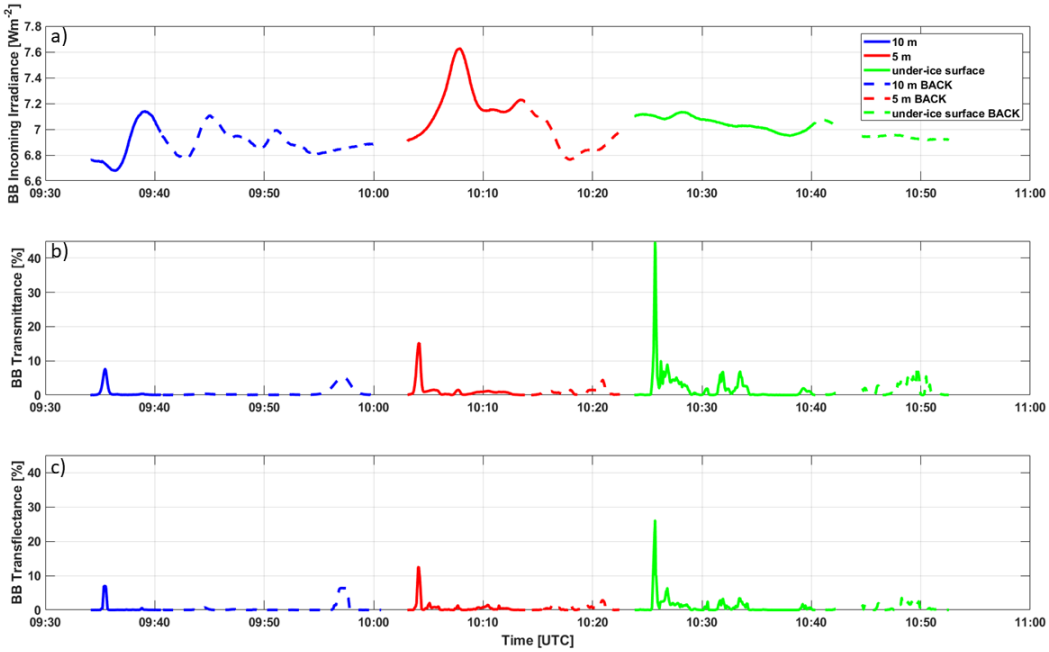

Fig. 4.5.4: *Pre-processed broadband (BB) a) incoming irradiance measured from the radiometer mounted on top of the ROV hut (Figure 4.5.1 b), b) transmittance, and c) transflectance at different depths on March 14 across the two leads that formed on March 11.*

On March 17 it was still possible to reach parts of the FYI ROV optic grid established during PS122.2 (Figure 4.5.1 a). Under-ice irradiance and radiance measurements were collected at 1.5 m depth along the transects starting at M31 towards M11 and continuing across a lead towards the ROV hole (Figure 4.5.7). The peaks in transmitted irradiance and radiance at around 14:11 UTC are due to the elevated solar radiation transmitted through the thinner ice on the lead 20 m off the ROV tent. Due to shadowing of the newly formed ridges at the edges of the lead, the position of the ROV was mostly not available during this transect.

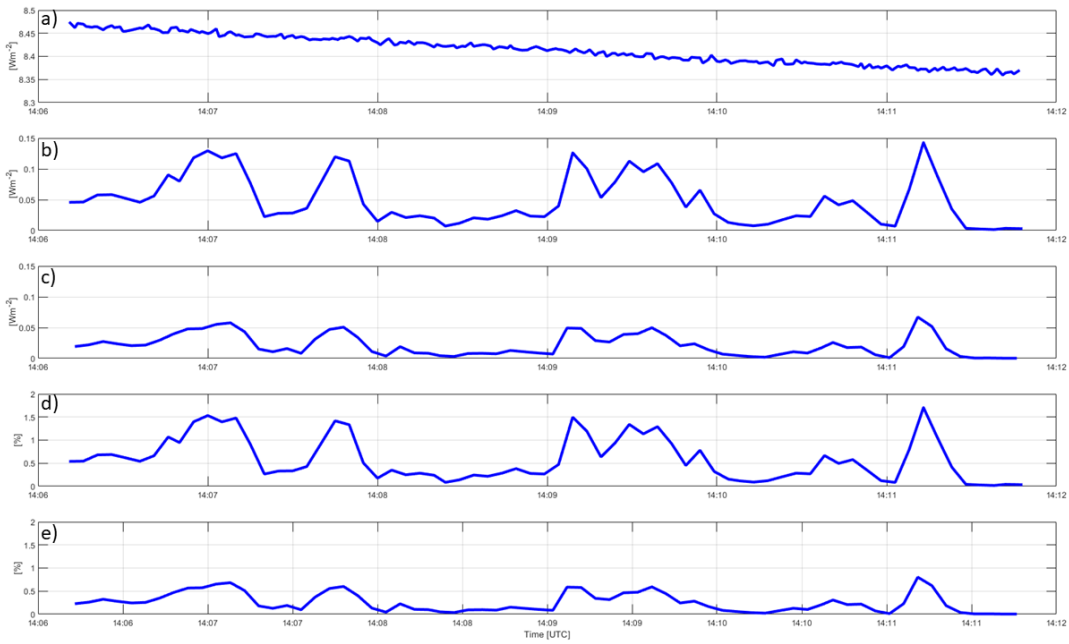

Fig. 4.5.5: *Optical measurements collected at 1.5 m depth along the ROV FYI optics transects starting at M31 towards M11 and continuing across a lead towards the ROV hole collected on March 17: Broadband (BB) a) incoming irradiance, b) transmitted irradiance, c) transmitted radiance, d) transmittance, and e) transflectance. The peaks in transmitted radiation at around 14:11 UTC are due to the lead 20 m off the ROV tent.*

Once the ROV FYI optic grid drifted away and was no longer in the operational reach of the ROV, an optic grid survey were performed underneath undulating SYI between the ROV hole and the four DTC sensors at the northern transect road on March 22 (Figure 4.5.1 a). This area was assumed to be not destructed. Ridges in this area led to shadowing of the acoustic signals between the ROV and the transponders. To improve this T4 was deployed approx. 30 m from the four DTCs and the radiation buoy R14 at the northern transect road on April 02 (Figure 4.5.2 a). It was planned to use this area for further ROV optic grid surveys. Accurate position was also necessary as it was planned (and later performed) to install a 200 m albedo line on this part of SYI and to collect ROV under-ice optics co-located to the surface albedo measurements. However, a co-located data set was not collected during PS122.3.

Once the lead just off the ROV site froze and remained stable optic grid surveys were performed there instead under the SYI area where some issues with the position and undulating surface remained. The grid was established on April 06 using marker poles frozen into the ice (Figure 4.5.2 b). Three transponders (T1, T2, T5) were installed on April 16 to achieve position. The ROV was operated at 2 m depth in such that the dive tracks are straight and separated by 10 m. Roll and pitch are kept close to 0°. In total six ROV optic lead grid surveys were performed on April 07 and 11 (without position), April 18, April 25, May 02 and 09. On May 01 the two transects forming the grid were surveyed (Figure 4.5.2 b). Optic grid and transect surveys were conducted at 2 m depth.

Albedo measurements with the Kipp and Zonen albedometer were performed along the ROV optics lead transects at every ROV marker ideally on the same day and similar time (e.g., solar noon) (Chapter 4.6 Optics).

The broadband transflectance between M1 close to the ROV hole (Figure 4.5.2 b, 4.5.6 a) and the beginning of the lead (M23) is between 0 and 0.3% due to the thick ridges that formed at the edges of the lead. Under the lead the transflectance ranges from 0.4% to 0.8%. At this stage of analyses, it is assumed that the spatial variability of the transflectance under the lead is due snow depth rather due to ice thickness, which is assumed to be very uniformed. In the upper left corner of the grid more ridges are present reducing the transflectance. The elevated transflectance of more than 1% is due to the crack on the lead.

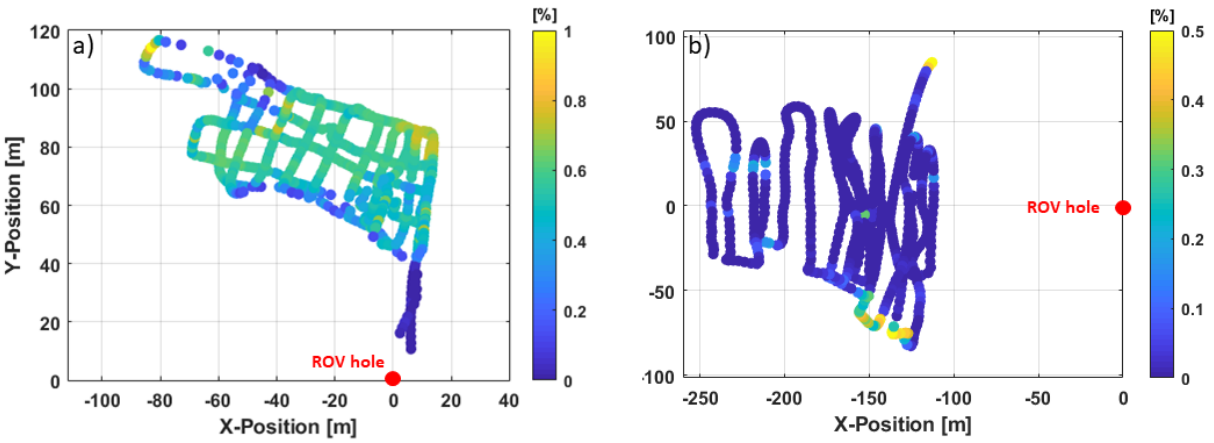

Fig. 4.5.6: *a) Spatial variability of broadband transflectance under the ROV optics lead grid and beyond on May 02 and b) under David´s Ridge on May 09. The position under David´s Ridge is not always available.*

Extensive optic surveys under David´s Ridge were performed twice, on May 02 and 09. This includes along and across transects. Transflectance under the ridge ranges from 0 to 0.2% with the elevated values due to the crack that separates David´s Ridge into two pieces (Figure 4.5.6 b). Transflectance values higher than 0.3% are due to thinner level ice and leads which are present on both sides of the ridge. The surveys were conducted between 5 and 6 m depth, as close as possible to the ice-underside. Due to the ridges shadowing the acoustic signals of the ROV positioning system the position is not always available.

In addition to grids and transects the following optical surveys were performed:

- Depth profiles at several locations (under lead, crack, ridge, FYI, SYI) down to 50 to 100 m in order to measure the decrease of light availability in the water column (Figure 4.5.7 a) performed on March 22 and 28, April 07, 11, 18, 25, May 02 and 09
- Within the roll experiment the ROV is put in a rolled position starting at 0° towards 180° by increments of 20° (Figure 4.5.7 b). Each position is hold for about 10 to 20 s. Thereby, the angle distribution (geometry) of the under-ice light field is investigated. Conducted on April 07 and May 09.
- Upside down dives (180° roll) along the optic lead transects in order to measure the upwelling radiation from the ocean (Figure 4.5.7 c) were carried out on April 07 and May 09
- The ROV is placed directly under the ice at each marker position and put in a stable position (roll and pitch close to 0°) and hold for about 10 to 20 s (Figure 4.5.7 d) which was done on May 02 and 09. This is done to measure irradiance and radiance directly underneath the ice to have as less influence by the water column and the biomass within as possible.

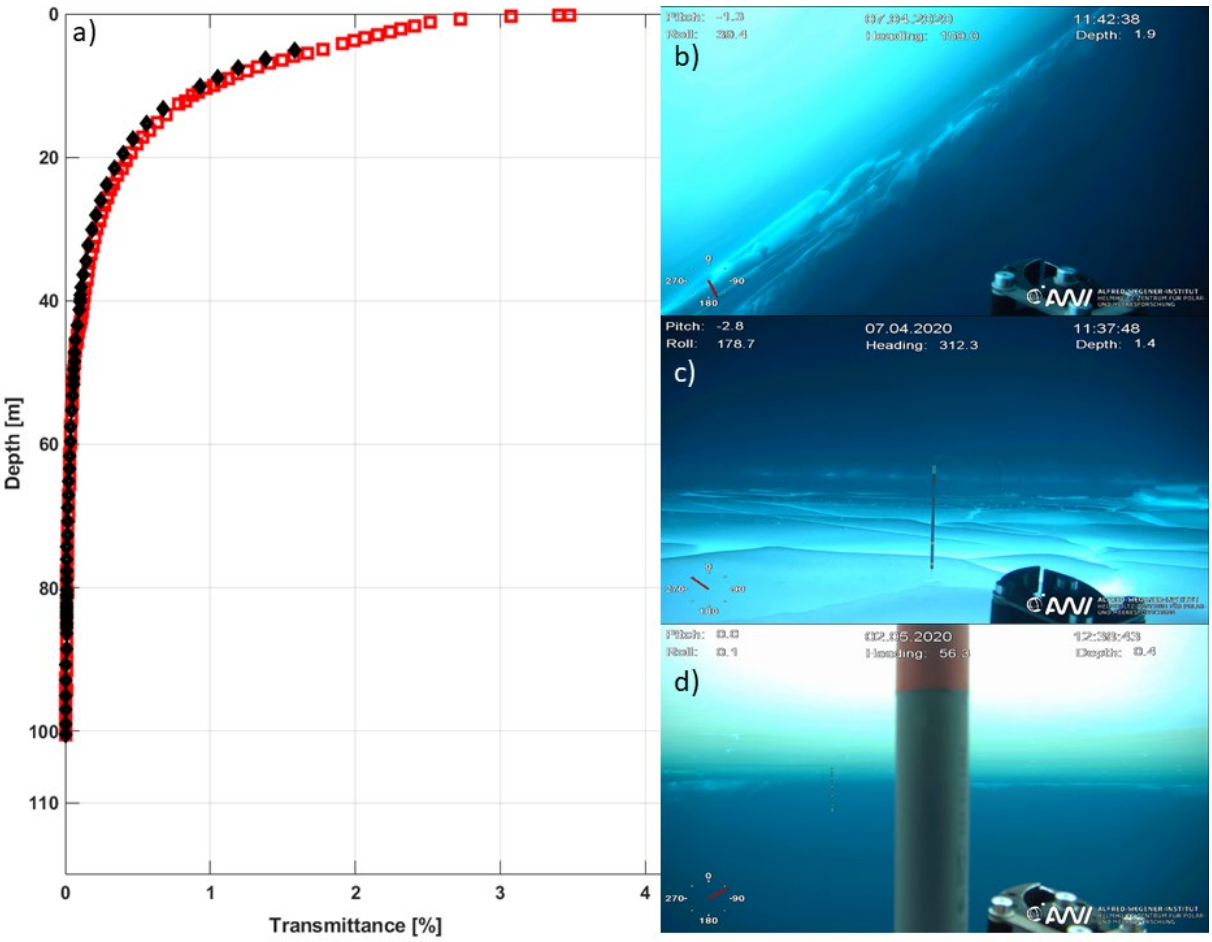

Fig. 4.5.7: *a) Depth profile of light transmittance through about 40 cm thick sea ice under the refrozen lead on April 07. Red indicates the down-cast and black the up-cast. b) roll experiment, c) upwelling radiation on April 07 and d) stable marker positions May 02.*

<u>Stakes</u>

The nine stakes at Fort Ridge deployed during PS122.1 in a cross arrangement were read once on March 07. A second visit could not be accomplished due to the disintegration of Fort Ridge and its movement away from the ROV site.

Five new stakes were installed during PS122.3 on April 28 on the stern lead neighboring the ROV lead. Only one could be read on May 02. One was not found at all, from another one only the wire was still there, and the last two were damaged by rafted ice blocks. Details are available in chapter 4.7 Stakes.

<u>Platelet ice</u>

The presence and distribution of platelet ice was extensively surveyed during PS122.2. It was observed and documented using video footage and photographs from the ROV, oceanographic data from the GPCTD mounted on the ROV, from the MSS and the CTD lowered into the water column at Ocean City, distributed CTDs around the MOSAiC ice floe within 10 to 40 km, and ice core analyses from several locations. This is described in *Katlein et al., 2020 (submitted to GRL)*. During PS122.3 more platelet ice was overserved using the ROV (Figure 4.5.8) before it vanished between end of March and beginning of April.

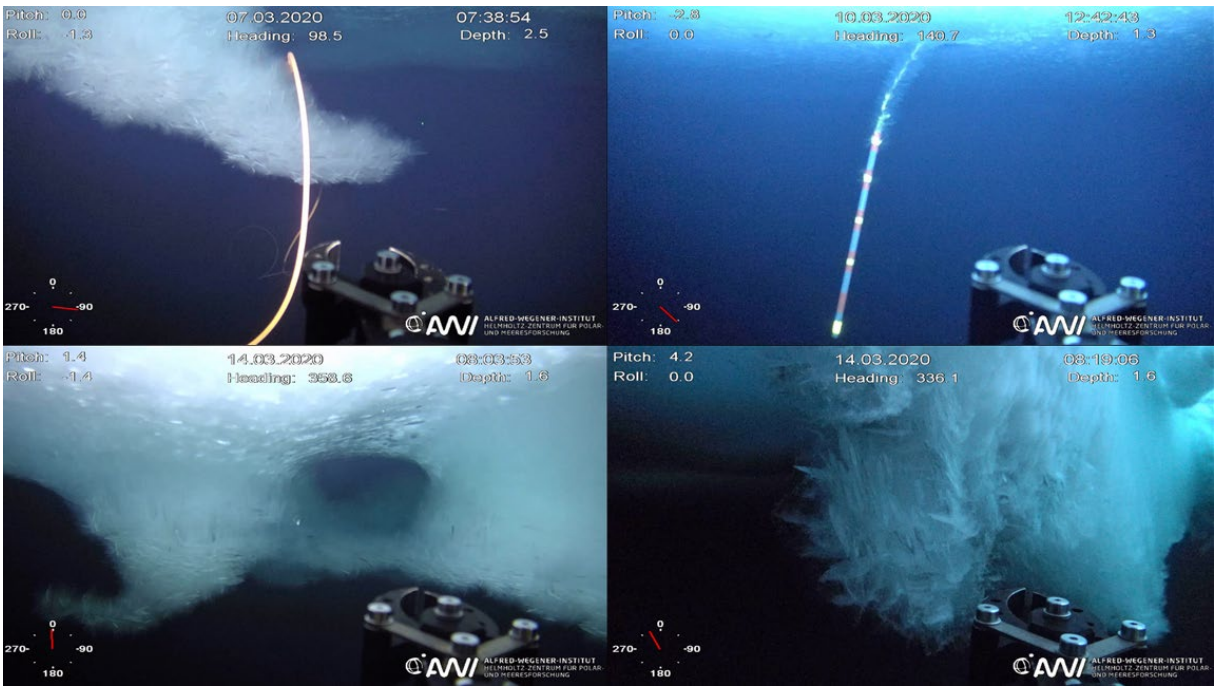

Fig. 4.5.8: *Close-up pictures of platelet ice from the ROV high definition zoom video front camera (Surveyor HD, Teledyne Bowtech, Aberdeen, UK).*

Data management

All data are handled, documented, archived and published following the MOSAiC data policy (see APPENDIX). ROV data is stored in the Mosaic Central Storage under mcs\platforms\vehicle\beast\exdata\ in separate folders for each device operation (Table 4.5.1). Easy data access has been described in the MOSAiC Logbook.

Tab. 4.5.1: *Overview ROV surveys. See also D:\Documentation\ROV-Dives_BEAST on ROV processing PC in log office at A-deck for more details.*

DSHIP_ID	**Dive mission**
20200225 **PS122/3_29_14**	Traps recovery, rope moving from optics transect to trap hook, stakes, small multibeam
20200229 **PS122/3_29_65**	Handover, grid transect dive, ridge optical transect inspection, stake inspection, short multibeam @20m, recover rope from hook
20200307 **PS122/3_30_69**	nets @10m, surface, Fort Ridge stakes,
20200310 **PS122/3_31_75**	multibeam, try to find radiation buoy R10 (not found)
20200314 **PS122/3_31_75**	CTD/optic transects across lead @10m ,5m ,surface, multibeam across lead + other areas, footage of lead
20200317 **PS122/3_32_11**	High resolution multibeam along ridge @10m, FYI optic transects, found radiation buoy R10, footage of ridges and leads
20200318 **PS122/3_32_33**	full CO multibeam survey
20200318 **PS122/3_32_34**	full CO multibeam survey
20200322 **PS122/3_32_78**	nets @60m, 10m, surface, optic lead grid underneath undulating SYI surface between ROV site and 4 DTC sensors, short multibeam lead survey @20m, depth profiles @nets transect and @lead

20200324 **PS122/3_33_27**	multibeam
20200328 **PS122/3_33_83**	multibeam, nets @10m, depth profile, CTD/optic transects across lead @10m,5m,surface
20200331 **PS122/3_34_20**	multibeam
20200407 **PS122/3_35_32**	nets @72m, 10m, surface, optic lead grid (mostly no position), optic marker transect, upwelling radiation, roll experiments, depth profiles, searching and checking under-water deployments
20200411 **PS122/3_35_95**	nets @72m, 10m, surface, optic lead grid (no position), depth profile, crack optic, searching lost under-water deployments
20200414 **PS122/3_36_24**	CO multibeam survey
20200418 **PS122/3_36_112**	nets @75m, 10m, surface
20200418 **PS122/3_36_125**	partly nets @surface, short lead & crack multibeam, optic lead grid, depth profile 50m, video footage, transponder/position checks
20200421 **PS122/3_37_19**	check transponder 5
20200421 **PS122/3_37_20**	full CO multibeam
20200425 **PS122/3_37_108**	nets @95m,10m,surface, optic lead grid, crack optics, depth profile 50m, video footage, transponder/position checks
20200428 **PS122/3_38_50**	full CO multibeam, crack optics, crack video footage/pictures
20200501 **PS122/3_38_85**	optic lead transetcs, recover and re-deploy transponder 5
20200502 **PS122/3_38_91**	nets @75m, 10m, surface, optic lead grid, lead stable marker, David´s Ridge optic transect, read stakes stern lead
20200505 **PS122/3_39_20**	full CO multibeam
20200509 **PS122/3_39_77**	nets @95m, 10m, surface, optic lead grid, depth profile 100m, stable marker, roll experiment, upwelling radiation, optics transect and multibeam David´s Ridge
20200510 **PS122/3_39_111**	Packing up, flatten out tether to get rid of loops
20200510 **PS122/3_39_152**	Packing up, flatten out tether to get rid of loops

References

Katlein, C., M. Schiller, H. J. Belter, V. Coppolaro, D. Wenslandt, and M. Nicolaus (2017), A

New Remotely Operated Sensor Platform for Interdisciplinary Observations under Sea Ice, *Frontiers in Marine Science*, *4*(281), doi:10.3389/fmars.2017.00281.

Katlein, C., Mohrholz, V., Sheikin I., Itkin, P., Divine, D. V., Stroeve, J., Jutila, A., Krampe, D., Shimanchuk, E., Raphael, I., Rabe, B., Kuznetov, I., Mallet, M., Liu, H., Hoppmann, M., Fang, Y.-C., Dumitrascu, A., Arndt, S., Anhaus, P., Nicolaus, M., Matero, I., Haas, C. (2020), Platelet Ice under Arctic Pack Ice in Winter, submitted to *Geophysical Research Letters*

4.6 Optics

Philipp Anhaus[1], Steven Fons[2], Igor Sheikin[3], Alexey Niubom[3], David Clemens-Sewall[4], Falk Pätzold[5], Jenny Hutchings[6], Marcel Nicolaus[1] (not onboard), Christian Katlein[1] (not onboard), Mario Hoppmann[1] (not onboard), Lovro Valcic[7] (not onboard), Don Perovich[4] (not onboard), Bonnie Light[8] (not onboard), Chris Polashenski[4,9] (not onboard), Ben Lange[10] (not onboard), Mats Granskog[10] (not onboard), Dirk Notz[11] (not onboard)

[1]DE.AWI
[2]US.NASA
[3]RU.AARI
[4]US.Dartmouth
[5]DE.TU Braunschweig
[6]US.Oregon SU
[7]CR.IODE (Bruncin)
[8] S.UW Seattle
[9]US.USACE/CRREL
[10]NO.NPI
[11]DE.UHamburg

Objectives

The driving science question of the MOSAiC observational plan for the task optics investigates how the sunlight is partitioned by the sea ice cover and the upper ocean over the course of the sunlit season.

The specific science questions are addressed starting with PS122.3 and are as follows:

- What is the seasonal evolution of apparent optical properties (albedo, transmittance) for representative snow and ice cover (transect) and for representative ice types (study sites)
- Is the SHEBA albedo transect time series still relevant?
- How do optical properties of FY and MY ice types evolve under identical large scale forcing?
- What are the time-dependent AOPs (e.g., albedo, transmittance) for a variety of observed ice types ("AOP library")?
- What are the time-dependent IOPs (e.g., scattering properties mainly) for a variety of observed ice types ("IOP library")?
- Over what spatial scales are ground measurements representative of the broader area (link back to model grid cell and satellite footprint scales)

The optics tasks presented in here have strong linkages to many interdisciplinary science questions within the MOSAiC frame work:

- Sea ice mass balance - both surface and bottom ablation are strongly driven by absorption of sunlight
- Melt pond observations - pond depth, number driven by sunlight and then strongly govern partitioning
- Snow metamorphism- the changing of physical and optical properties of the snow due to incoming radiation
- Ocean - mixed layer dynamics strongly affected by ice cover partitioning of sunlight
- BGC - photosynthetic and photolysis processes
- ECO - primary productivity, photophysiology
- Remote Sensing - hyperspectral and ICESat-2 photon data are strongly affected by surface optical/physical conditions.

The following approaches are envisioned to investigate and to try to answer the above mentioned science questions:

- Optics surveys (linear / grid survey; time series survey)
- Individual study site characterizations (some time series with longevity, some 'destructive'?)
- Fixed radiation stations
- Goniometer
- Drone
- Laboratory optics
- Other laboratory characterization work

In this chapter mainly the work on optical surveys, individual study site characteristics, and fixed radiation buoys is presented.

Work at sea

ROV optics

The entire ROV work package is dedicated the separate chapter 4.5 ROV including the optical measurements collected.

Fixed radiation and ice-mass-balance buoys

Six radiation buoys were deployed during PS122.3 (Table 4.6.1). Details on the deployment and ice conditions can be viewed in chapter 4.12 Buoy Deployments in the Distributed Network.

Two out of four AWI radiation buoys consisting each of three RAMSES radiometers and a solar panel (Figure 4.6.1) were deployed. The radiometers record the incoming, reflected, and trough snow and sea ice transmitted irradiance. R14 (a) was deployed on level SYI next to four DTC sensors on the road that is included in the northern transect road and once led to Fort Ridge on April 03. A weekly snowpit was conducted next to the radiation buoy to understand physical changes in the snowpack between April 10 and May 09 (Chapter 4.2 Snow). R13 (b) was deployed on the ridge observatory David´s Ridge which partly replaced the by ice dynamics destructed Fort Ridge on May 06. For a detailed description of the formation and status of David´s Ridge it is referred to chapter 10 Ridges.

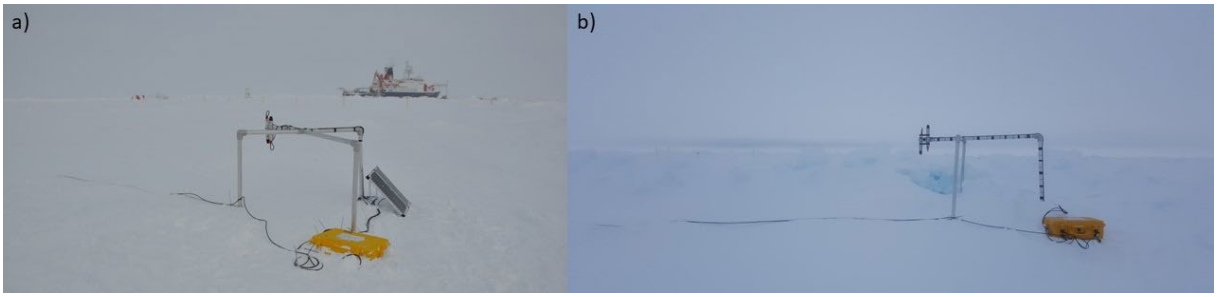

Fig. 4.6.1: *AWI radiation buoy a) R14 deployed close to four DTC sensors, snow buoy S97, SYI albedo line position 20 at the northern transect loop/road which leads towards David´s Ridge (photo: Steven Fons) and b) R13 at David´s Ridge (photo: Philipp Anhaus).*

Three ice-mass-balance (IMB) buoys consisting additionally to three radiometers same as the AWI radiation buoys of each one light chain that is frozen into the ice to monitor long-term in-ice light field. It is 3.2 m long and has 64 multispectral (RGB+PAR) sideward looking irradiance (scalar irradiance) sensors each separated by 5 cm. Apparent extinction coefficient can be derived. Moreover, a snow pinger and a tiltmeter are attached. The snow pinger records changes in snow accumulation and drift. The tiltmeter is useful to correct radiation measurements and monitor the stability of the station. A camera is installed in the electronics peli case which takes a picture every 4 hours. With that the station and the close vicinity are documented in order to get an impression of the weather around and identify possible causes of failure, e.g. if a polar bear plays with the instruments or if a polar fox

chews on the cables. R10 was deployed on relatively level First-Year-Ice (FYI) between the end of the ROV optics grid (transponder 2) and the Fort Ridge on March 08. R11 was deployed on the Second-Year-Ice (SYI) dark site site / LM site next to the snow buoy S96 on March 29. R12 was deployed on the L3 site on April 24 (Figure 4.6.2).

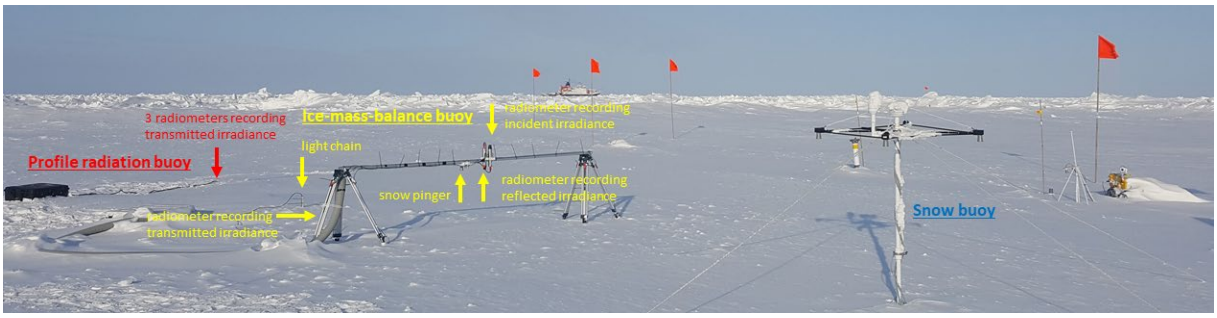

Fig. 4.6.2: *SYI dark site / LM site set-up including the profile radiation buoy R20 (red), the ice-mass-balance buoy R11 (yellow), and the snow buoy S96 (blue) (photo: Philipp Anhaus).*

The profile radiation buoy R20 (Figure 4.6.3) which is part of the HAVOC (Safe **HAV**ens for ice-associated flora and fauna in a seasonally ice-covered Arctic **OC**ean, http://www.npolar.no/havoc) project led by the Norwegian Polar Institute in Tromsø was deployed on the SYI site / LM site next to the IMB R11 and the snow buoy S96 on April 10. Three radiometers hanging at 5 m, 15 m, and 30 m depth referenced to the water level are recording the through snow and sea ice spectral transmitted irradiance for wavelengths 320-900 nm. The buoy was deployed next to R11 that measures incident, reflected and transmitted irradiance, the light field within the sea ice and the upper water column, and changes in snow accumulation and drift. Also next by is snow buoy S96. Combining those measurements results in a very valuable data set.

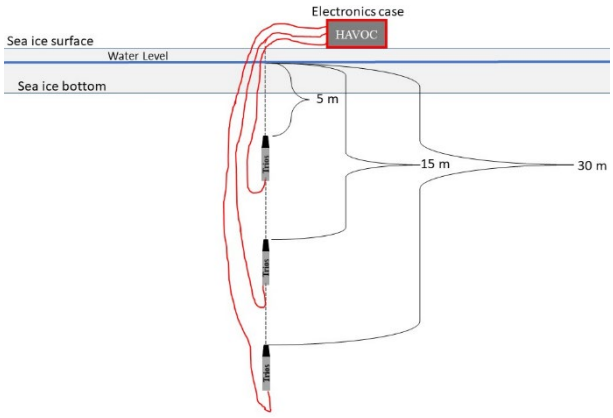

Fig. 4.6.3: *Deployment diagram radiation buoy R20 on SYI dark site / LM site (figure: Ben Lange).*

Surface albedo

Albedo measurements were performed with a Kipp and Zonen albedometer (Figure 4.6.4). It consists of two pyranometers recording the incoming radiation and the reflected radiation in form of an electrical signal that is measured with a multimeter. This device was already used during SHEBA. 230 albedo recordings were collected on four different repeatedly visited sites in the CO (Table 4.6.2) in parallel to SnowMicroPen measurements to capture the snow density and specific surface area changes at the same measurement locations (Chapter 4.2 Snow). The two transects, ROV optics lead transects and SYI albedo line transects, are marked in the floe map as of May 03 (Figure 4.5.2 a in Chapter 4.5 ROV). The ROV optic lead transects consist of (Figure 4.5.2 b in Chapter 4.5 ROV)

15 measurement positions (M0, M21-M34) of which two (M33, M34) were not existing anymore after 4 measurement repetition cycles due to crack openings and rafting.

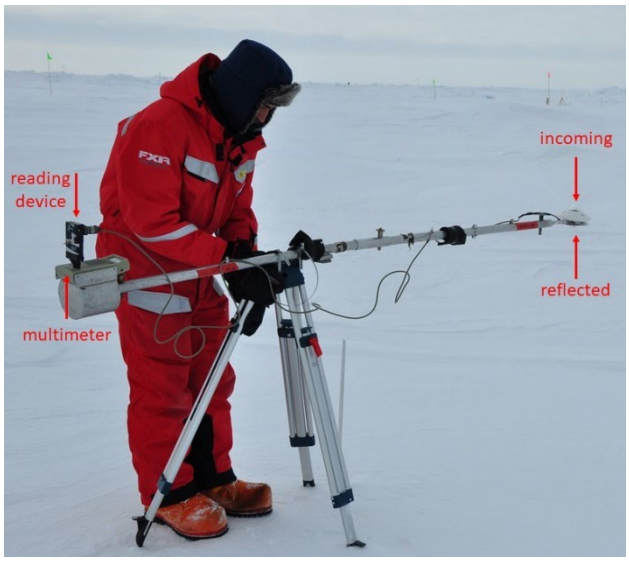

Fig. 4.6.4: *Taking albedo measurements at one of the positions of the SYI line (photo: David Clemens-Sewall).*

Along the SYI albedo line 20 measurements were performed (Figure 4.6.5). After an ice dynamic event a crack opened running through the measurement position 3 and 4. Since then 1-3 albedo recordings were performed above the crack and referred to as position 3a, 3b, and 3c, respectively.

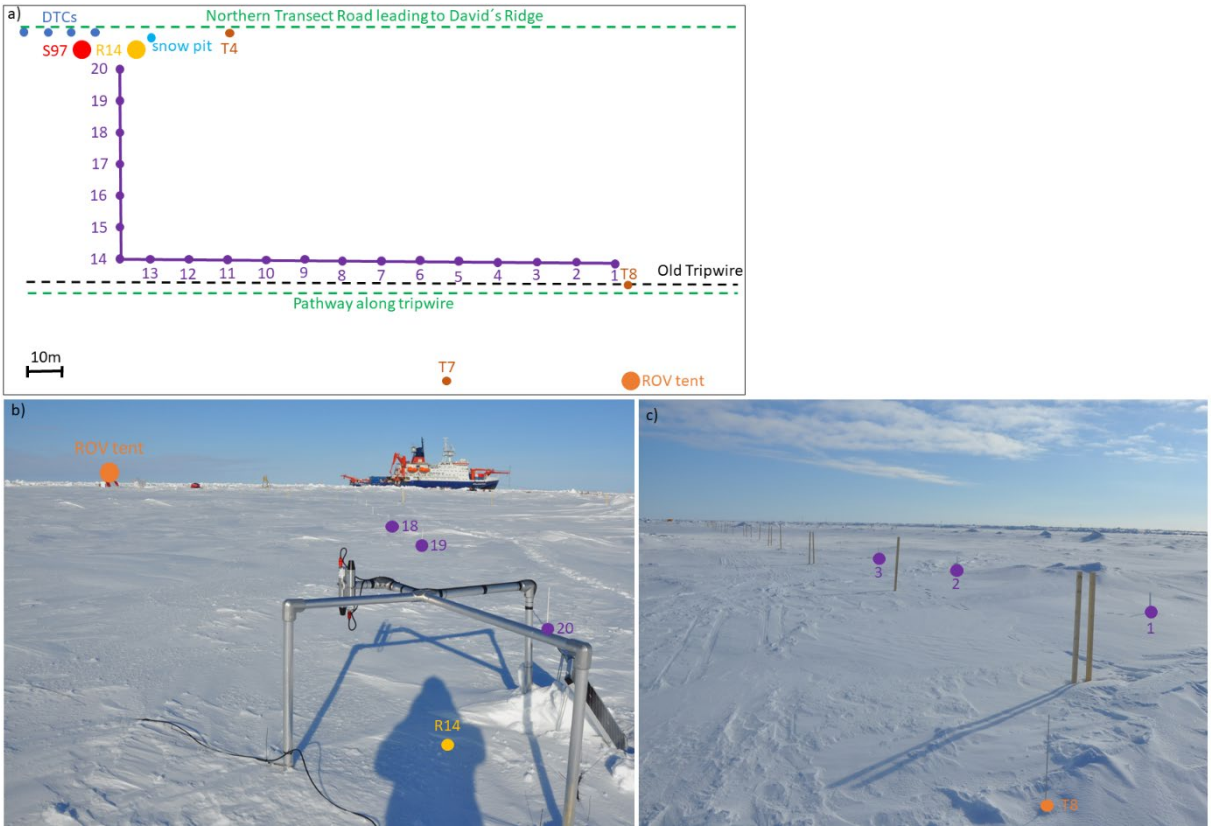

Fig. 4.6.5: *a) Schematic of the SYI albedo line establish on April 27. b) and c) photos of parts of the SYI albedo line (photos: David Clemens-Sewall).*

The recordings performed on the four different sites cover the major surface types (crag and tail, wind packed, new ice/leads, fresh snow). Thus, it is expected that the data collected can be used as a baseline for the albedo at the end of the accumulation season. Measurements of exposed ice in ridges (e.g., David´s Ridge) were not captured at all. For the temporal evolution of the albedo it is referred to the data set collected by the pyranometers mounted on the ASFS stations (Chapter 3.4).

Shortly before Polarstern and the team of PS122.3 left the MOSAiC ice floe a major storm event caused severe ice dynamics which led to many breaks and ridge forming. The most recent photo of the floe including the positions till then of the remaining instruments including the albedo transects and line can be viewed in the introduction chapter 1 of the cruise report.

Light harp

An optical harp was deployed during PS122.2 on the SYI dark site / LM site on January 15 and is since then recording data without any known interruptions. It measures vertical profiles of upwelling and downwelling radiation including low-light period/moon light, four bands, with and without IR filter and temperature at approx. 25 cm spatial resolution. Data is transmitted directly via satellite. Sensors are looking upwards and downwards. The ice-mass-balance buoy R11 with the sideward looking irradiance sensors of its light chain was deployed close by in order to allow comparison of the two approaches.

Optics and sea ice texture cores

The work related to sea ice cores extracted for optical and texture studies are described in chapter 4.1 Ice Coring. Ice cores were regularly taken at the SYI coring site close to the radiation buoys R11 and R20 and to the light and salt harps. Information about the ice core texture is in particular useful in combination with the light chain data from R11 and the data collected by the light and salt harps. The core extracted from the deployment hole of the under-ice RAMSES of radiation buoy R14 was photographed for further optics studies (Figure 4.6.6).
Optical cores will be further analyses during laboratory work after the cruise.

Fig. 4.6.6: *Ice core from the hole for the under-ice sensor of radiation buoy R14 (photo: David Clemens-Sewall).*

Preliminary results

Fixed radiation and ice-mass-balance buoys

The incoming irradiance recorded by the radiometer of R12 deployed on the L3 site shows a diurnal cycle (Figure 4.6.7 a). This is transferred to the measurements of reflected and through snow and ice transmitted irradiances (b, c). Small variations in the respective magnitudes are visible. Since May 12 the incoming irradiance seems to increase. From the incoming and the reflected and the transmitted irradiance the albedo (d) and the transmittance (e) are calculated, respectively.

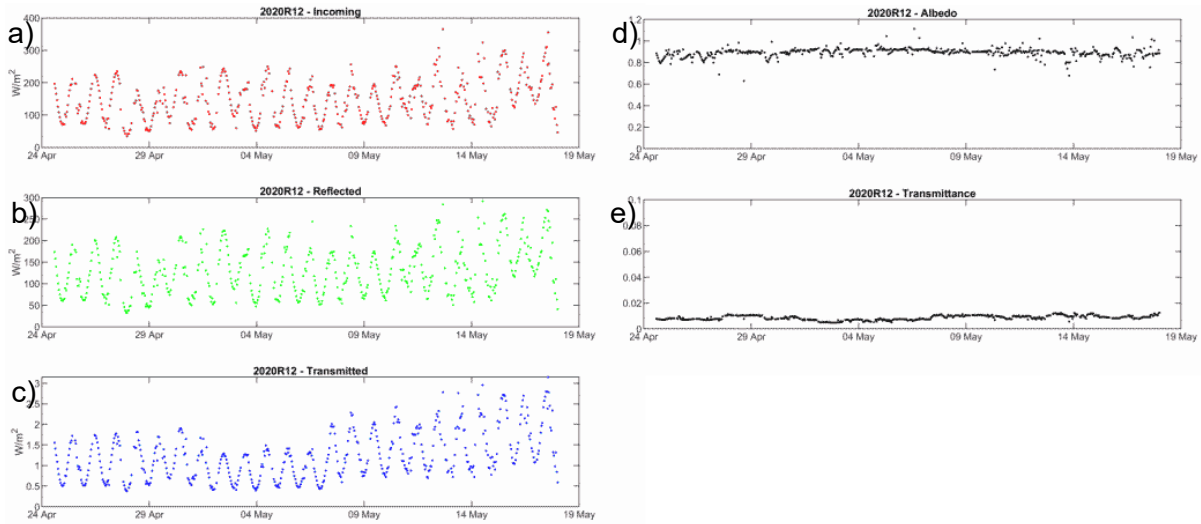

Fig. 4.6.7: *Quicklook plots from the ice-mass-balance buoy R12 on L3 showing a) incoming irradiance, b) reflected irradiance, c) transmitted irradiance in W/m², d) albedo, and e) transmittance as a fraction for the period April 24 to May 19. Figure from meereisportal.de / seaiceportal.de.*

The light chain provides insight into the in-ice light field as well as into the light availability and partitioning within the upper water column. The intensity of the available green light relative to Red+Green+Blue and depending on light chain length / depth for R10, R11, and R12 is displayed in Figure 4.6.8 (a, b, c), respectively. The ice-ocean interfaces of the light chain set-ups were placed at 1.56 m (a), 1.86 m (b), and 1.75 m (c) on deployment day.

Many sensors of the light chain of R10 seemed not to work during different stages after deployment (Figure 4.6.8 a, white areas). Moreover, the under-ice deployments were inspected using the ROV on April 17 and it was discovered that the second half of the light chain was horizontally frozen to the under-ice surface instead of hanging vertically and freely in the water column. With that configuration the measurements that were aimed for could not be retrieved. Instead, the light chain recorded backscatter measurements from the ice underside which is also nice to have. Although, the light chain is completely broken since April 01. A ridge developed very close to R10 as a result of ice dynamics events at the area around Fort Ridge (Chapter 4.10 Ridges). As a consequence, snow piled up trapped by the ridge covering the station set-up including the RAMSES recording reflected irradiance. This most likely started in early April because suddenly very low values of transmitted irradiance were observed (not shown).

8 (33 – 40) sensors of the light chain from R11 which cover the depths 1.65 m to 2 m are damaged from the beginning of the deployment (Figure 4.6.8 b, white area). Light extinction within the ice is not homogeneous (not shown) which is also confirmed by a quick texture analysis from a photography of a core taken in close vicinity (not shown).

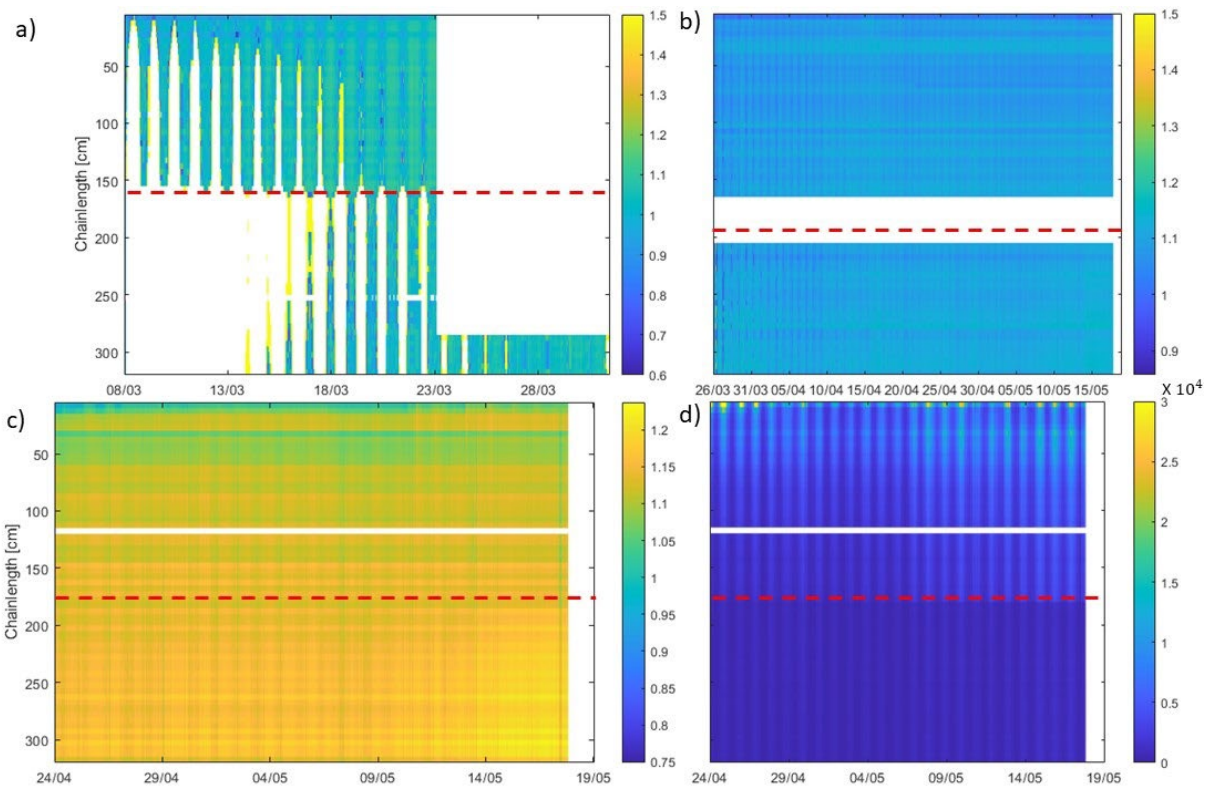

Fig. 4.6.8: *Quicklook plot of the light chain data from the ice-mass-balance buoys R10 (a), R11 (b), and R12 (c,d). a, b, and c show the intensity of the available green light relative to Red+Green+Blue depending on light chain length / depth. d) displays the available PAR in counts. The red dashed lines indicate the position of the ice-ocean interface. Figures provided by Christian Katlein.*

A shift towards the greenish light and its elevated intensity relative to Red+Green+Blue for R12 can be observed in the water column starting at May 13 (Figure 4.6.8 c). This indicates the start of the spring bloom. The upper most 2 sensors are placed in the air as indicated by the high light availability in PAR (Figure 4.6.8 d).

<u>Surface albedo</u>

Albedo was measured above a crack during different steps in its development which made it possible to observe the temporal evolution of albedo for different ice types (Figure 4.6.9). A crack opened at the stern lead where shortly after a thin ice (nilas) layer formed (Figure 4.6.9 a). The albedo was 0.17 (Figure 4.6.9 f) and with that close to the albedo for open water. The following albedo recordings were collected above a crack on the ROV optics lead grid. The evolution of the crack represents the consecutive development of ice. In b) frost flowers have formed on the crack which is followed by more frost flowers in c). The albedos are 0.66 and 0.62, respectively. The lower albedo over more frost flowers (c) compared to over less frost flowers (b) might be explained by the higher temperatures in c) due to the cloud cover. Drifting and partly falling snow covering the crack (d, e) lead to a further increase in albedo (f). By May 12 (e) the albedo approached the back-scatter level due to topography. This example demonstrates how quickly the albedo evolves from low to high values within only 12 days.
Along the SYI albedo line (Figure 4.6.5 a) recordings were collected alongside SMP measurements. This transect included over relatively cold snow with some areas of fresh wind-packed snow (albedo 0.83) and otherwise icy crag and tail (albedo 0.80) (Figure 4.6.10 d). A highlight is the crack that formed between position 3 and 4 (Figure 4.6.5 a) from which the evolution of the albedo from thin ice to snow accumulation could be observed (Figure 4.6.10 a-d) similar to the example in Figure 4.6.9.

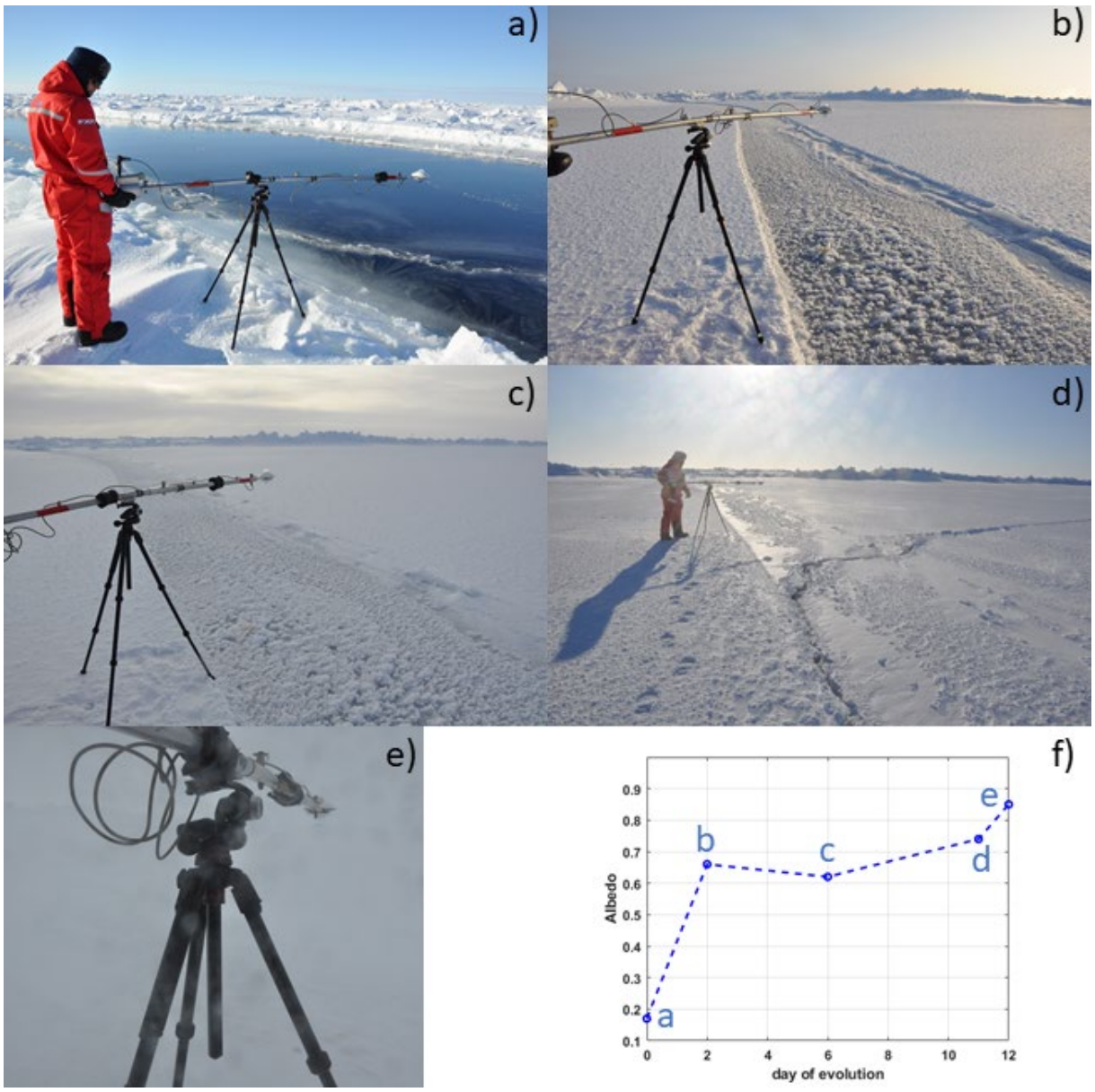

Fig. 4.6.9: *Results from the Kipp and Zonen albedometer. Measuring albedo over a) a thin ice layer (nilas) on the stern lead (photo: David Clemens-Sewall), b) newly formed frost flowers on a crack on the ROV optics lead (photo: David Clemens-Sewall), c) more frost flowers on the same crack (photo: Jennifer Hutchings), d) snow cover (photo: David Clemens-Sewall), e) thicker snow cover (photo: David Clemens-Sewall). f) Temporal evolution of the albedo for the sites a) – e).*

Note the different vertical tripod position between a) and b). In b) the lowest tripod position was selected. The influence of the this is still to be investigated.

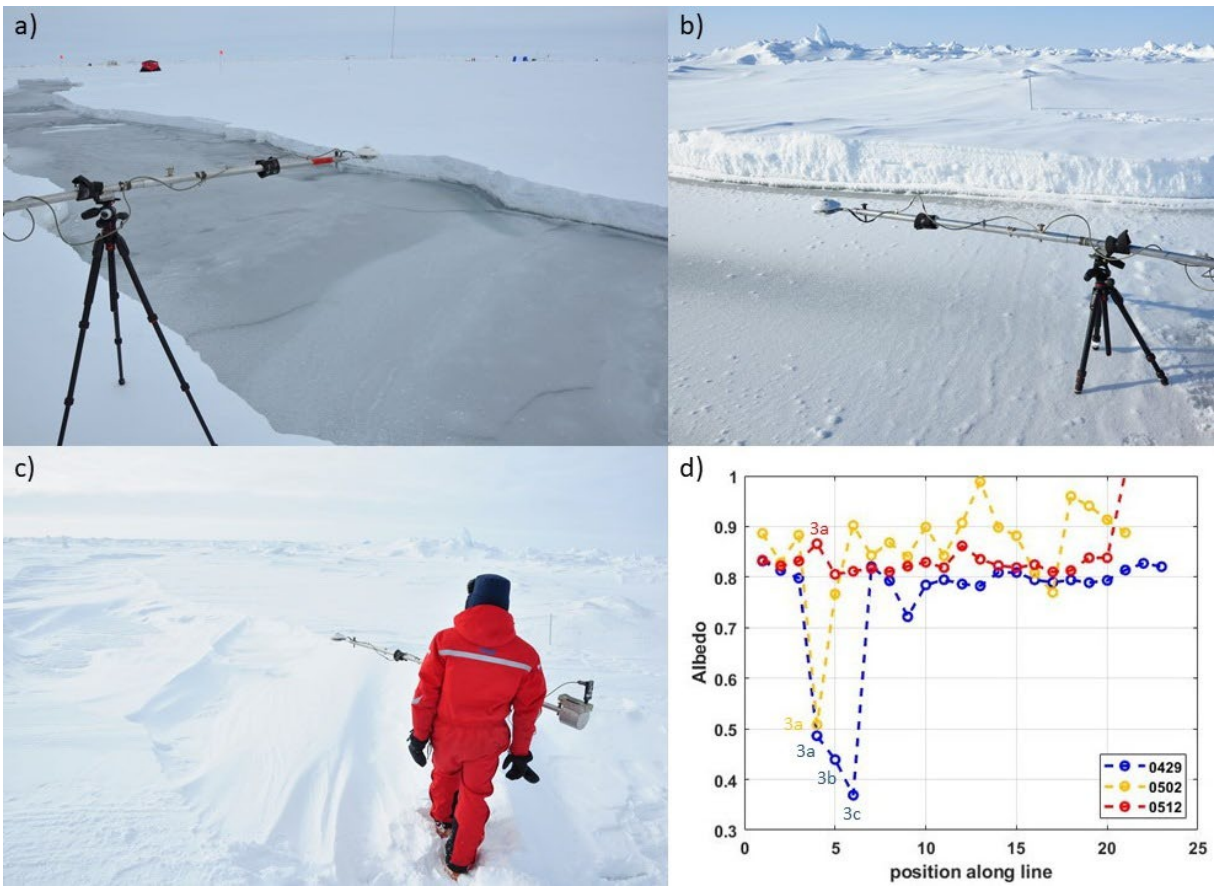

Fig. 4.6.10: *Results from the Kipp and Zonen albedometer measurements along the SYI line. Measuring albedo over a) a thin ice layer (nilas) on the crack (photo: Steven Fons), b) a thin snow cover on the crack (photo: unknown), c) a thick snow cover, partly snow dune (photo: David Clemens-Sewall). d) Albedo recordings along the SYI line.*

Data management

All data are handled, documented, archived and published following the MOSAiC data policy (see APPENDIX). Data from the radiation buoys is stored in the Mosaic Central Storage under mcs\platforms\buoy\"buoyname"\exdata\ in separate folders for each device operation (Table 4.6.1). Easy data access has been described in the MOSAiC Logbook.

Albedo data is stored in the Mosaic Central Storage under mcs\platforms\pack_ice\ice_ps\dart_kipps\exdata\mosaic_albedo_kipps_data.xlsx. Corresponding pictures are stored in separate folders for each device operation (Table 4.6.2). Easy data access has also been described in the MOSAiC Logbook.

In case photos marked "unknown" for the author information refer to the cruise report and this chapter or the data set following the MOSAiC data policy (DSHIP and MSC).

Tab. 4.6.1: *Overview of deployed radiation and ice-mass-balance buoys during PS122.3.*

DSHIP_ID	**Buoy name**
20200308 PS122/3_28-46	2020**R10**
20200326 PS122/3_28-55	2020**R11**
20200403 PS122/3_28-74	2020**R14**
20200410 PS122/3_28-78	2020**R20**
20200424 PS122/3_28-108	2020**R12**
20200506 PS122/3_28-113	2020**R13**

Tab. 4.6.2: *Overview of Kipp and Zonen albedo measurements during PS122.3.*

DSHIP_ID	**Research Site**	**# measurements**
20200407 PS122/3_35-139	rov_optics_lead_transects	15
20200411 PS122/3_35-140	rov_optics_lead_transects	15
20200417 PS122/3_36-171	rov_optics_lead_transects	16
20200418 PS122/3_36-172	rov_optics_lead_transects	16
20200422 PS122/3_37-44	rov_optics_lead_transects	15
20200425 PS122/3_37-98	rov_optics_lead_transects	16
20200425 PS122/3_37-143	stern_lead	11
20200427 PS122/3_38-3	stern_lead	7
20200429 PS122/3_38-39	rov_optics_lead_transects	14
20200429 PS122/3_38-40	SYI_albedo_line	23
20200429 PS122/3_38-60	stern_lead_stakes	5
20200502 PS122/3_38-111	rov_optics_lead_transects	16
20200502 PS122/3_38-122	SYI_albedo_line	21
20200502 PS122/3_38-129	BGC_1	4
20200512 PS122/3_40-20	rov_optics_lead_transects	15
20200512 PS122/3_40-21	SYI_albedo_line	21

4.7 Stakes

David Clemens-Sewall[1], Stefanie Arndt[4], Jennifer Hutchings[2], Steven Fons[5], Amy Macfarlane[3], Philipp Anhaus[4], Eric Brossier, Ian Raphael[1] (not on board), Mario Hoppmann[4] (not on board), Don Perovich[1] (not on board)

[1]US.Dartmouth
[2]US.Oregon SU
[3]DE.WLS/SLF
[4]DE.AWI
[5]US.UMaryland

4.7.1 Objectives

The point measurements of ice and snow mass balance (IMB) encompassing a full seasonal cycle from freeze-up to the melt are very rare. Likewise, despite large horizontal variability of the snow and ice cover such observations are rarely collected in clusters (more than one observation point). The MOSAiC IMB observations are designed in way to address these challenges. The IMB measurements are also necessary for interpretation of ice dynamics (Section 4.8), ROV (Section 4.5) and others, including cross-disciplinary topics (e.g. heat fluxes between ocean-ice and atmosphere). The devices used for the point IMB observations on MOSAiC are shortly referred to as 'stakes' and include:

- IMB buoys
- digital thermistor chains (DTC)
- ablation stakes and hot wires

Additionally, to complement our studies of the snow budget we cored transects of lead ice since snow incorporated in lead ice would not be accounted for by the other IMB measurements.

4.7.2 Work at sea

4.7.2.1 IMB buoys

On Leg 3 we deployed two additional SIMBA type Ice Mass Balance buoys in the Central Observatory: at the Noodle and ASFS station in BGC 1 and next to the FMI stress sensor on the old helipad. See section 4.12 for additional information on these SIMBA deployments. The temperature chain for the SIMBA at Ft. Ridge stopped working sometime during Leg 3, likely during the Ft. Ridge dynamics events in late March. We installed a new temperature chain on May 10. This SIMBA was likely destroyed in the May 12-13 dynamics event.

4.7.2.2 DTC network

Leg 3 took over a DTC network of xx deployed DTC within the Central Observatory. We extended the network by three additional units: DTC44 at the new Remote Sensing Site 4, DTC45 on the new optics grid on the lead, and DTC40 at David's Ridge.

Over the course of Leg 3, seven DTCs had to be recovered or were destroyed by the formation of ridges or due to the movement of the ship (see table 4.7.1). Table 4.7.2 summarizes the remaining 14 DTCs in the Central Observatory before Polarstern left.

Tab. 4.7.1: *List of DTC units that were operational at the beginning of Leg 3 but died for several reasons over the course of the leg*

MCS/DSHIP name	Unit name, map name	Nick name	Deployment date	Deployment site	Reason for the recovery/dead of the system
DTC15_416	RS009	Rob	7-Nov-19	Along the road from MET city to S transect loop	Not working since Jan 07; finally unmounted due to break-up on March 25.
DTC22_416	RS022	Sandro	8-Dec-19	Remote Sensing site 2	Unmounted due to planned ship's track through that spot on May 12.
DTC23_416	RS023	Olaf	10-Dec-19	Remote Sensing site 2	Unmounted due to heavy ridging on April 13.
DTC24_416	RS024	Audun	8-Jan-20	Fort Ridge	Unmounted due to heavy ridging on March 23.
DTC25_416	RS025	Egon	8-Jan-20	Fort Ridge	Unmounted due to heavy ridging on March 23.
DTC45_416	RS016	Trude	11-Apr-20	Optics grid 2 (on lead)	Installed during Leg 3. Dead by heavy ridging on May 13 without data recovery.
DTC44_416	RS018	Hans	10-Apr-20	Remote Sensing City 4	installed during Leg 3; data download on 02.05.2020. Dead by ship's icebreaking on May 14.

Tab. 4.7.2: List of DTC units that were operational at the end of Leg 3

MCS/DSHIP name	Unit name, map name	Nick name	Deployment date	Deployment site	Status
DTC05_256	RS012	Alli	11-Nov-19	Stakes 2 (close to S transect loop)	Data downloaded on 7.1.2020 and 26.2.2020; no data since last download. Unit still in place.
DTC06_256	RS013	Katharina	11-Nov-19	Stakes 2 (close to S transect loop)	data downloaded on 7.1.2020 and 26.2.2020 and 07.05.2020
DTC08_256	RS011	Ruibo	28-Jan-20	ROV site at the Fort Ridge T1	deployed by leg 2, power connector broken during transport to deployment site, fixed and clock re-set on 4.2.2020; data downloaded on 23.03.2020 and 06.05.2020
DTC09_256	RS019	Stefan	28-Jan-20	ROV site at the Fort Ridge T3	data downloaded on 4.2.2020 and 23.03.2020 and 06.05.2020

DTC10_256	RS020	Christian	28-Jan-20	ROV site at the Fort Ridge T2	data downloaded on 4.2.2020 and 27.2.2020 and 23.03.2020 and 06.05.2020
DTC11_416	RS001	Jessie	5-Nov-19	Old remote sensing site, on a ridge between ocean, city bow stakes and BGC1	data downloaded on 26.2.2020 and 07.05.2020
DTC12_416	RS002	Marc	5-Nov-19	Old remote sensing site, on a ridge between bow stakes and BGC1 (close to the road)	data downloaded on 21.1.2020 and 26.2.2020 and 07.05.2020
DTC16_416	RS010	Matt	7-Nov-19	Stress panes close to ship	data downloaded on 7.1.2020 and 26.2.2020 and 29.03.2020 and 27.04.2020; was not connected between April 27 and May 08 due to moving ship; re-deployed on May 08 09:00 UTC
DTC20_416	RS008	Ian B	22-Nov-19	Transect North (4 deployed together)	data downloaded on 4.2.2020 and 27.2.2020; stopped recording on 27.02.2020; detected only on 15.05.2020 (empty battery); new battery and continuation of measurements from 16.05.2020 onwards
DTC26_416	RS021	Ruibo	5-Feb-20	Alli's Ridge	power connector broken during transport to deployment, fixed and clock reset on 7.2.2020; data download on 15.05.2020
DTC31_512	RS027		22-Nov-19	Transect North	data downloaded on 7.1.2019 (in this spreadsheet it was put as unit RS007, fixed to RS027) and 15.05.2020
DTC32_512	RS029	Jian	22-Nov-19	Transect North	data downloaded on 7.1.2020; ripped out battery cable since April 17 but only spotted on April 22 (data downloaded by that time); up and running since April 24 10:00 UTC; data downloaded

					on 24.04.2020 and 15.05.2020
DTC33_512	RS028	Ola	22-Nov-19	Transect North	data downloaded on 4.2.2020; stopped recording on 27.02.2020; detected only on 15.05.2020 (empty battery); new battery and continuation of measurements from 16.05.2020 onwards
DTC40_512	RS040	Egor	6-May-20	David's Ridge	installed during Leg 3; data download on 15.05.2020

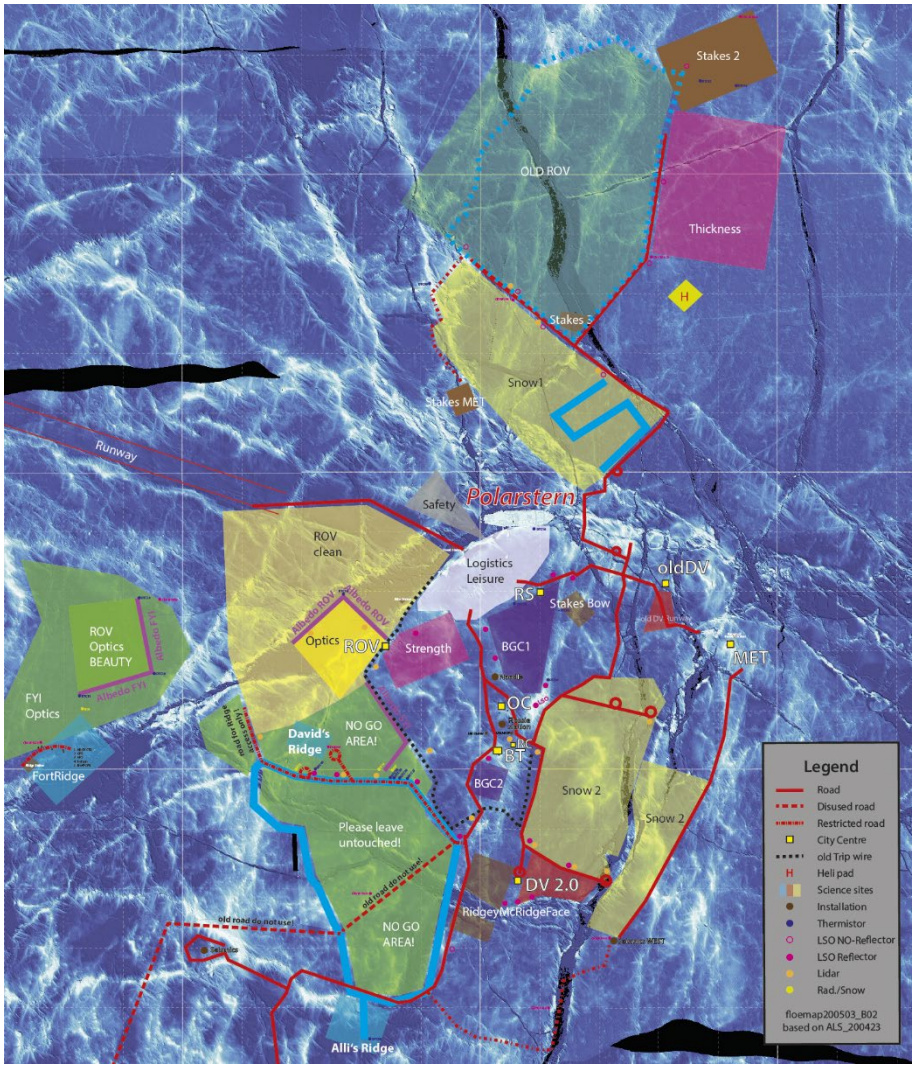

Fig 4.7.1: *Map of CO with locations of DTC units and ablation stakes fields from May 3, 2020.*

4.7.2.3 Ablation Stakes and Hot Wires

The stakes sites are manual ice mass-balance measurement sites. A 'stake' is actually a paired ablation stake and hotwire thickness gauge. The ablation stake gives the position of the ice and snow surfaces, while the thickness gauge indicates the position of the ice bottom. From these measurements we can determine total change in ice and snow thickness. At each site, we installed several stakes as either transects or grids, measuring local spacial variability of ice thickness over time.

We installed 11 stakes sites over Leg 1, Leg 2, and Leg 3 with a total of ~100 individual stakes in order to capture the floe's diverse ice types, as well as take advantage of collocated measurements, e.g. the Transect, ROV, and MET observations:

- Stakes 1
- Stakes 2
- Stakes 3
- ROV stakes
- Bow Stakes
- MET Stakes

- Ridge Ranch Stakes
- Runaway Stakes
- MISS Stakes
- STEAK Stakes
- Return of the Met Stakes

All stakes sites except for Ridge Ranch have been fully or partially destroyed by ice deformation or Polarstern. Most of the destruction was associated with the May 12-13 dynamics event. Many individual stakes are still present and additional hot wires could be added to them to study the melt season. A number of the hotwires at Bow Stakes, Met Stakes and Runaway Stakes were nonexistent at the beginning of Leg 3. We added new hotwires to the stakes at Bow Stakes and Met Stakes. On Leg 3 we attempted to study the growth rates of new lead ice with MISS Stakes and STEAK stakes.

4.7.2.3.1 Stakes 1

Established on leg 1, Stakes 1 was originally installed on second year ice in a refrozen melt pond. During the mid-November shearing event, most of the original stakes were destroyed. The rest were translated several-hundred meters to the East, stopping directly in front of Polarstern. The transported stakes became the basis for Bow Stakes. None of the original stakes remain at Stakes 1. The site was reestablished late in leg 1, now on a refrozen lead which had formed right next to the original Stakes 1 location. The site continued to experience deformation after installation, and several of the reinstalled stakes were destroyed. There were 7 operational stakes at the site on Leg 2, which span the marginal zone from SYI to FYI into the middle of the refrozen lead.

Stakes 1 was split in two and two of the stakes were destroyed by the formation of Lunch Lead on March 13. The cruise leadership decided to reposition Polarstern onto Stakes 1. So on March 29 the remaining stakes were decommissioned and snow out to a meter away from each stake was dug out in an attempt to find the IButton temperature sensors buried at the snow-ice interface. Changing ice conditions then led the leadership to decide not to reposition Polarstern.

4.7.2.3.2 Stakes 2

Stakes 2 was established on leg 1 on SYI. It originally crossed a small ridge, and additionally covered level ice and ponded ice. This site was destroyed during the mid-November deformation event, and is no longer operational.

4.7.2.3.3 Stakes 3

Stakes 3 was established on leg 1 on SYI, and is collocated with the Southern Transect loop. The site crosses a ridge and otherwise densely covers level SYI. Most hot wires at Stakes 3 were frozen in by the beginning of Leg 3. On May 1 the Stakes 3 crack and the Snow 3 crack reactivated to ridge and fragment the Stakes 3 site (Figure 4.7.2). We drilled all of the stakes that had not been destroyed by ridges for thickness to get a final ice thickness for the site. The rest of the site was destroyed by ice dynamics thereafter.

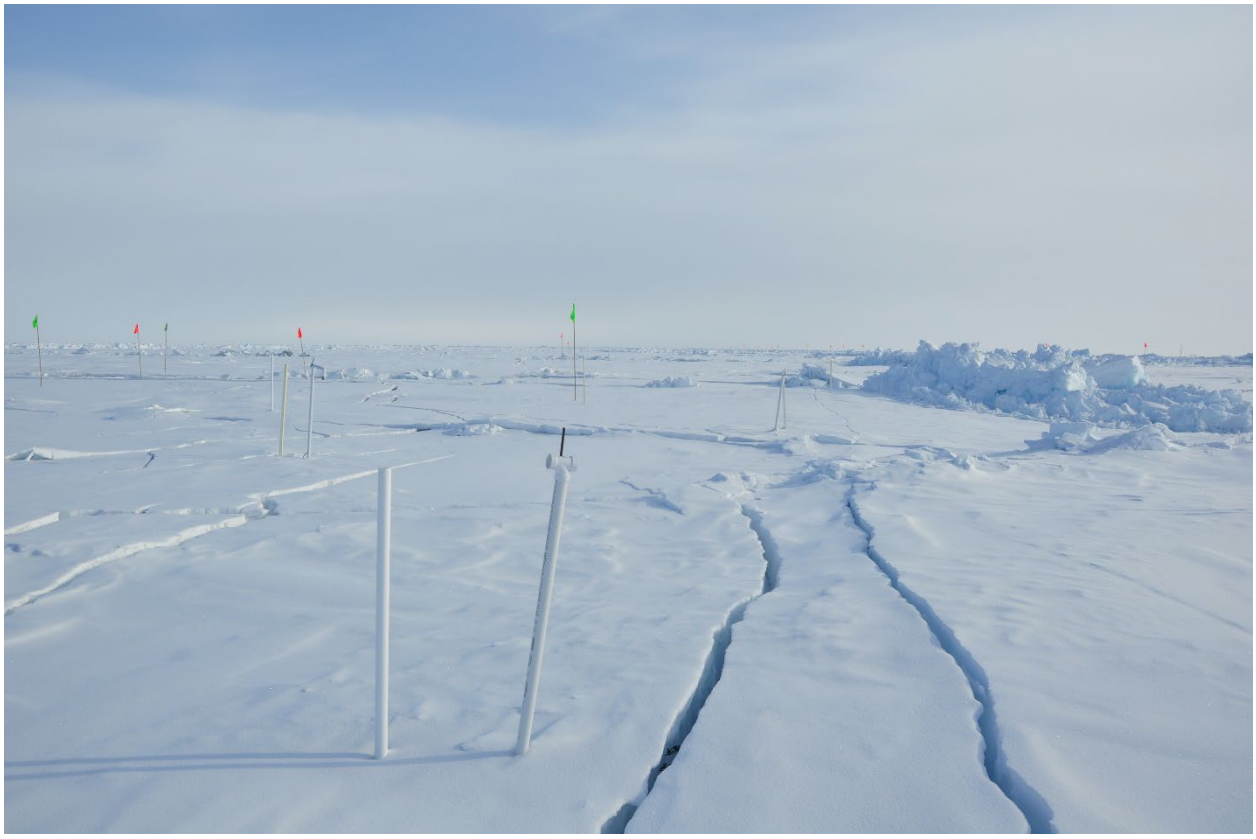

Fig. 4.7.2: *Photo of cracks running through Stakes 3 and ridges encroaching on May 1. Photo: David Clemens-Sewall.*

4.7.2.3.4 ROV Stakes

ROV Stakes was established on Leg 1 on SYI, and was intended to be collocated with the Southern Transect Loop and the ROV survey area. This site was destroyed during the mid-November deformation event, and is no longer operational.

4.7.2.3.5 Bow Stakes

Bow Stakes was established on Leg 1, incorporating the surviving stakes from Stakes1, which were transported several-hundred meters towards Polarstern during the mid-November deformation event. The site transitioned from a large ridge into a level SYI area and a ponded SYI area. The site was bordered by medium and large ridges. Several stakes did not have hot wires at the start of Leg 3 and we added new ones in late April. In the May 12-13 dynamics event cracks formed near Bow Stakes. Then, on May 14, Polarstern drove through the edge of Bow Stakes destroying some stakes and fragmenting the site. Bow Stakes is no longer operational.

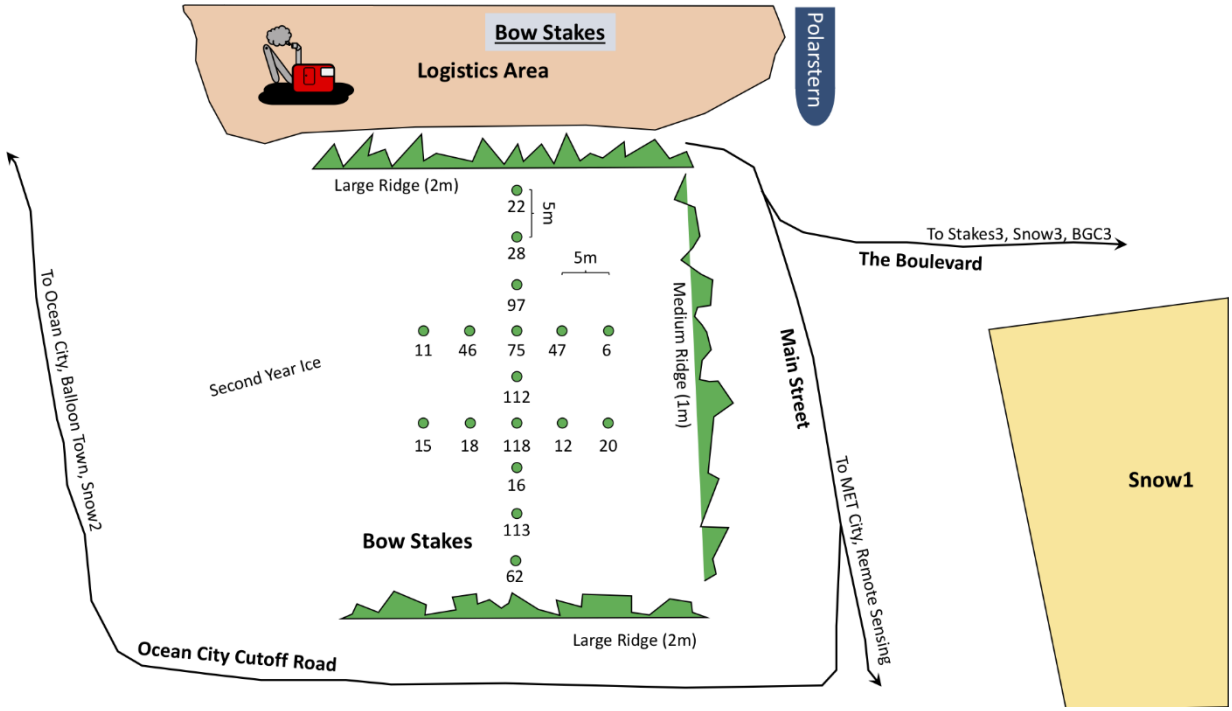

Fig. 4.7.3: *Diagram of Bow stakes and relevant features as of 20.02.2020. This plot was initially installed on undeformed second year ice and refrozen melt pond. It was then mostly destroyed in mid-November, and reinstalled at the end of Leg1. Stakes 22, 28, and 97, 75, 112, and 118 are part of the original installation, while the rest were installed later. The site experienced significant deformation, and is now bordered closely by medium-large ridges on three sides. This map from Leg 2 was largely still accurate (excluding Snow 1) until May 12. Not to scale.*

4.7.2.3.6 MET Stakes

MET Stakes was originally installed late in leg 1, directly underneath the 30m flux mast, 'The Noodle.' It was destroyed during the late December deformation event, with none of the original stakes remaining. We reestablished the site at the beginning of leg 2. The site covers an area of level second year ice, crosses small ridge, and reaches the margin of a large, multiyear rubble field. The site was collocated with the MET observations as well as an A-type snow pit in Snow1.

On March 11 Rocket Trap Crack opened between MET Stakes and Met City. The deformation destroyed the rocket traps and the type A snow pit but left all stakes intact (Figure 4.7.4). However, subsequent rafting beneath the ice (Figure 4.7.5) pinned the hotwires for four of the nine stakes shortly thereafter. Movement in Rocket Trap Lead separated MET Stakes and Snow 1 from the rest of the Central Observatory by several hundred meters. Two of the stakes did not have hot wires at the beginning of Leg 3 and so we added new ones in April. This site was most likely destroyed in the May 12-13 dynamics event although that region of the Central Observatory was not accessed after the event.

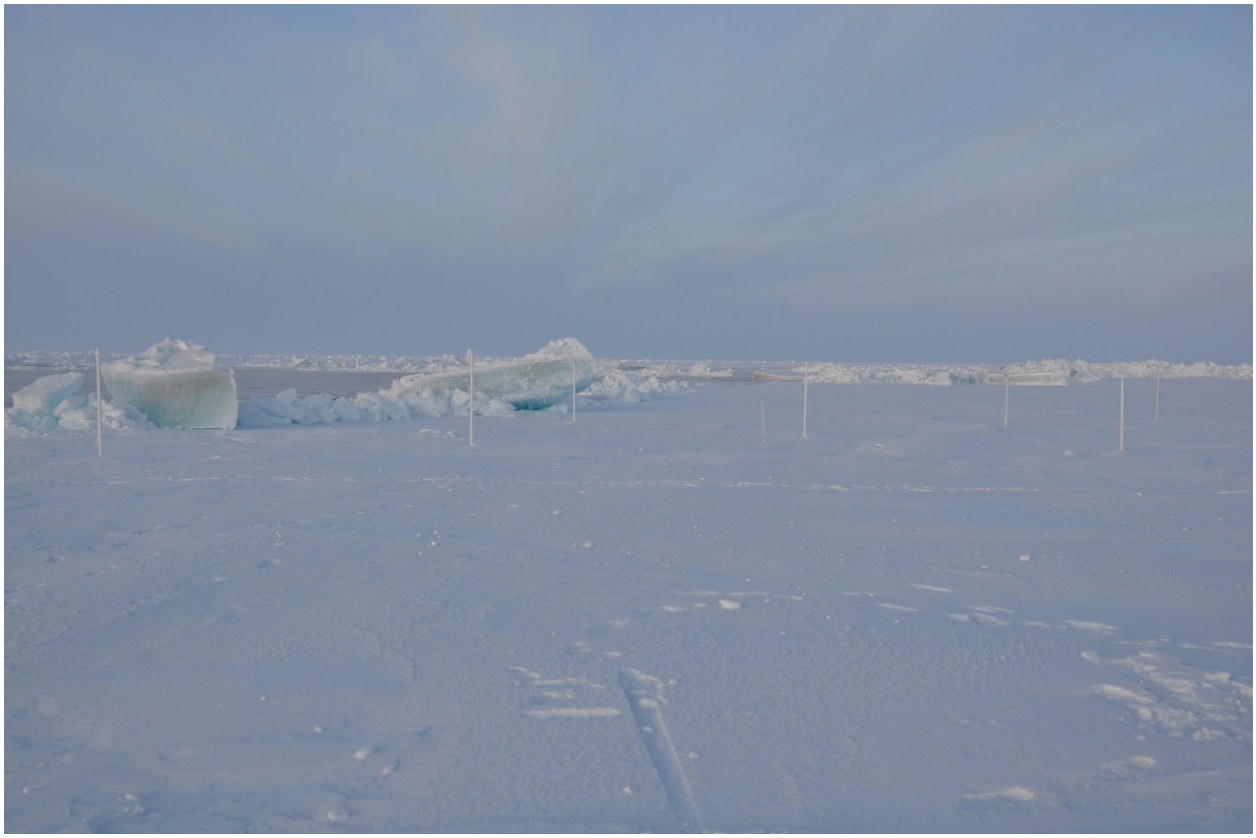

Fig. 4.7.4: *MET Stakes on March 17 after Rocket Trap Lead (left side of image) opened. Photo: David Clemens-Sewall.*

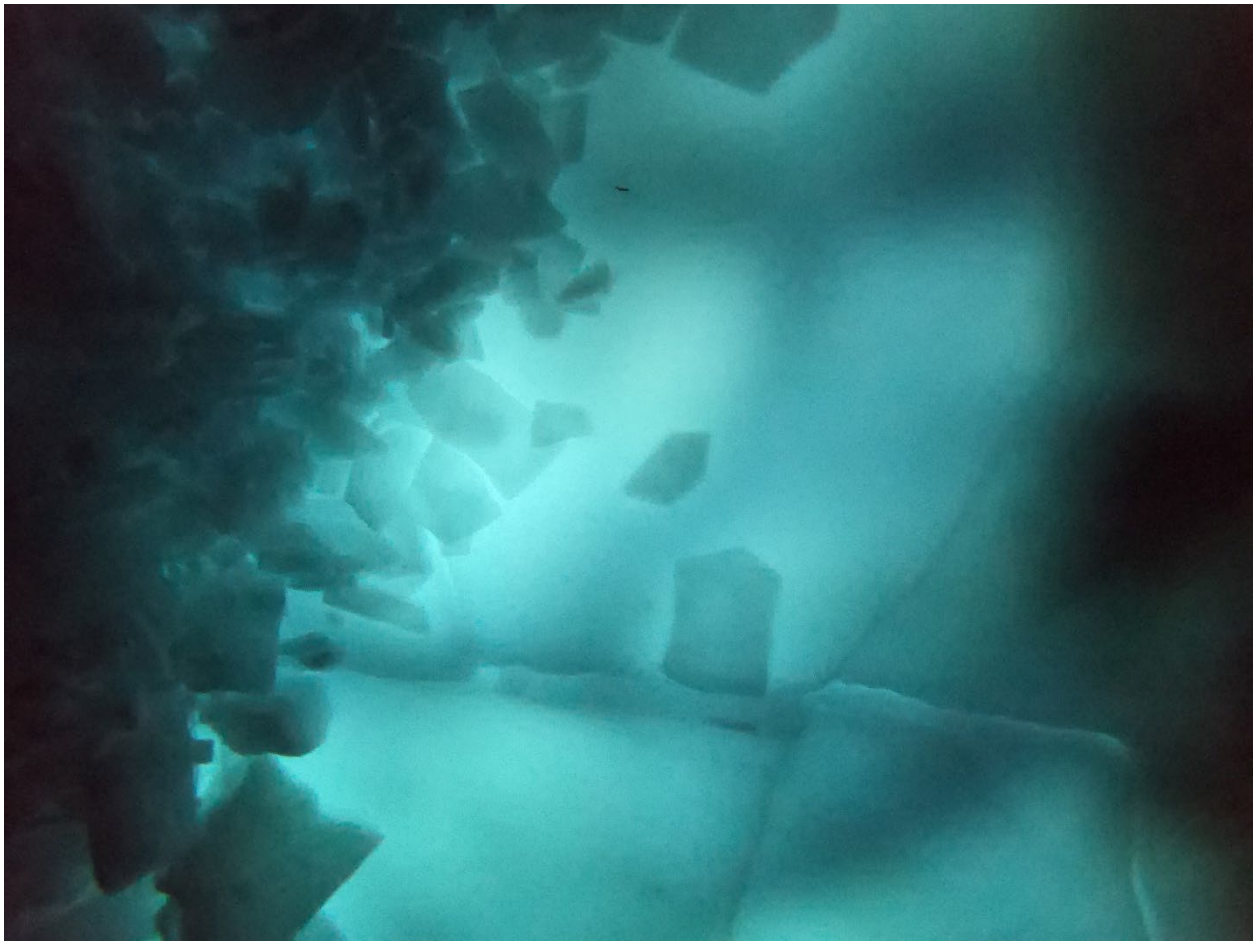

Fig. 4.7.5: *View of part of MET Stakes from underneath on April 14. An undamaged hotwire crossbar is visible at the top of the image. The rafting on the left side of the image pinned four out of the nine hotwires at the site. Photo: Eric Brossier.*

4.7.3.6 Ridge Ranch

Ridge Ranch was installed during leg 2, on level first year ice. The site is adjacent to Fort Ridge (the ridge observatory). In addition to the hotwire gauges, the Ridge Ranch plot has measuring tape on the underside of the stakes, which is readable by the ROV.

On March 18, the smaller secondary ridge on the Northern Transect side of Ft. Ridge broke apart and the subsequent dynamics would destroy Ft. Ridge and transport the Ridge Ranch outside of the ROV's range. The stakes were unaffected by the dynamics. But were now adjacent to a large, frequently active lead for the remainder of Leg 3. In April it was observed that some of the stakes closes to the lead were seeing either basal melt or reductions in their growth rates. Torsten Kanzow (cruise leader and Team Ocean), conducted fishing rod CTD's at the site but found only a stable mixed layer. Ridge Ranch is the only stakes site that was still fully operational on May 16 when Polarstern abandoned the Central Observatory.

4.7.2.7 Runaway Stakes

Runaway Stakes was installed during leg 2, on first year ice. The site is directly next to the Polarsten runway. It covers level first year ice, crosses a small ridge, and on one end borders a larger ridge. During Leg 2 the runway was expanded significantly which definitely influenced snow distribution and likely influenced the thermodynamics at this site.

Only four of the stakes here still had functioning hot wires at the beginning of Leg 3. Early in the morning of March 20 cracks fragmented Runaway Stakes. All fourteen stakes survived until May 11 but due to the challenges accessing the site and the impact of the runway we did not prioritize measuring this site. All fourteen stakes were drilled for thickness on May 11. The site was still present on May 16 and may be resumed with the addition of new hot wires.

4.7.2.8 MISS Stakes

MISS Stakes were installed on the ROV lead on April 24 on one month old ice. The site included three stakes (see Figure 4.7.6) on level lead ice. We measured this site four times between April 24 and May 12. The site was destroyed by the May 12-13 ice dynamics event and is no longer operational.

Fig. 4.7.6: *MISS Stakes on May 12. Photo taken from the ridge between the lead and the logistics area. The lead optics grid is visible as the flags in the distance. Photo: David Clemens-Sewall.*

4.7.2.9 STEAK Stakes

STEAK Stakes were installed in lead ice of three different ages on April 28 in the stern lead. The ice continued rafting shortly after installation and so most of the hot wires ceased to function. The ice was drilled for thickness afterwards. The site was destroyed in the May 12-13 dynamics event and is no longer operational.

4.7.2.8 Return of the Met Stakes

Return of the Met Stakes were installed on May the fourth to complement the SIMB at Met City. The site was destroyed in the May 12-13 dynamics event and is no longer operational.

4.7.2.4 Lead Coring for Snow Mass Budget

One aspect of snow mass balance, the snow that is blown into open water and incorporated into new lead ice became potentially important on Leg 3 due to the frequent presence of open water from dynamics events. This aspect of snow mass balance is not captured by traditional IMB methods or TLS mapping of snow redistribution (Section 4.3). To quantify the snow loss into leads we also collected 47 cores along transects of lead ice. Some of these we sectioned and others we melted whole for a total 101 salinity and d18O samples. The d18O will be analyzed to determine the mass of snow incorporated into the lead ice to complete the snow budget.

4.7.3. Preliminary (expected) results

On Leg 3 we observed a reduction in the sea ice growth rate across all ice types (Figure 4.7.7). By May 12, growth rates on First and Second Year Ice had fallen to zero within our measurement uncertainty. Snow accumulation was observed to be very patchy, most stakes received no new snow accumulation on most measurements on Leg 3 but occasionally a drift would include a stake in which case it received several centimeters or more.

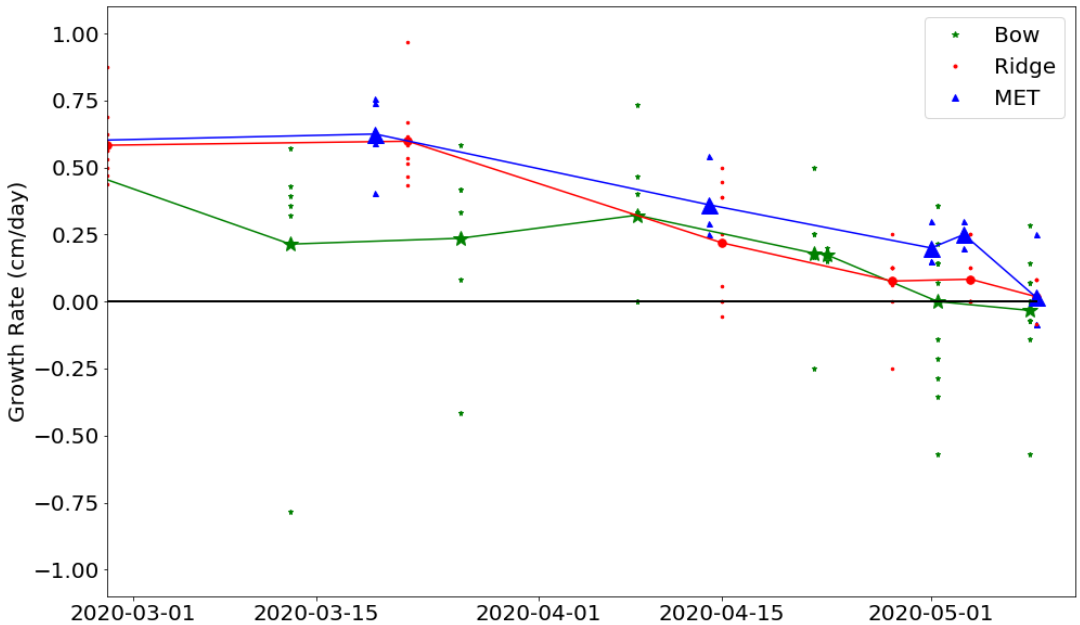

Fig. 4.7.7: *Ice growth rates at three of the stakes sites throughout Leg 3. The smaller symbols show the data for each stake. The larger symbols and lines show averages for all stakes at the indicated site. Note the decline in growth rates at all sites throughout the leg.*

4.7.4 Data management

All data are handled, documented, archived and published following the MOSAiC data policy (see APPENDIX). All device operations were logged in the AWI sensorweb portal and all sensor raw data files are stored in platform section of MCS.

4.8 Transect

Robert Ricker[1], Stefanie Arndt[1], Polona Itkin[2,3] (not on board), Stefan Hendricks[1] (not on board)

[1]DE.AWI
[2]NO.UiT
[3]US.CSU

4.8.1 Objectives

Total sea ice thickness and snow depth measurements on transects are the only direct spatially distributed snow and ice mass balance (IMB) measurements at MOSAiC Central Observatory. The transect of sea ice and snow depth measurements cover the spatial variability on a kilometer scale (CO scale).

Although a part of the full seasonal cycle observations, the transition to spring phase measurements collected during leg 3 of MOSAiC will help the specific process-related research topics such as:

- Sea ice and snow mass balance within the central observatory during spring
- accumulation of snow in the ridges and leads
- re-distribution of snow by drifting snow events - especially with combination with data collected by the TLS (see Section 4.3) and ALS (see Section 4.4)
- ice growth/heat fluxes under spatially patchy snow cover
- consolidation of the ridges

4.8.2 Work at sea

The work for the transect task was done on a regular weekly base, normally on Thursday afternoons. If weather conditions didn't allow, measurements have been postponed. All the instruments involved in transect are listed in Table 4.8.1. All transect surveys and corresponding device operation ID's are listed in Table 4.8.2.

Collocated observations of sea-ice thickness and snow depth on sea ice along transect lines that are representative for ice conditions in the CO. Measurements were done using a combination of a broadband electromagnetic induction sensors (Geophex GEM-2) and a MagnaProbe. The GEM-2 was towed in a pulk and measuring the total (ice + snow) thickness, while the MagnaProbe measures snow depth by means of a sliding disc on a rod that stays on the top snow surface along a rod that is pushed down to the snow/ice interface.

During leg 3, only GEM-2 and MagnaProbe measurements have been carried out on the transects. Remote Sensing transects have not been carried out.

The leg 3 ICE team continued the regular sampling at the transect lines established in the form of two main loops on different ice types. The loops were named for the original location in the CO.

1. Northern loop: located on thick and deformed remnant ice. This loop includes a 200-m-long snow structure transect.
2. Southern loop: located in an area of undeformed remnant ice, which however, was dominated by a large fraction of melted through and now refrozen melt ponds with thin ice (i.e. similar to first-year ice). This loop experienced significant deformation in the mid-November shear event.

The location of the two loops is illustrated in Figure 4.8.1.

Apart from the regular transect we also performed several other transects:

- Ridge Transects: Transects of snow depth and ice thickness were accomplished at Fort Ridge, Alli's Ridge, David's Ridge and Eco Ridge.
- Transect of Snow 1: This transect was carried out to monitor the development of the ice and snow cover in the Snow 1 snow pit sampling area.
- Transects at the RS site: This transect was carried out in order to characterize the snow and ice conditions at the remote sensing site in order to assist interpretation of the microwave signals.

Tab. 4.8.1: *Overview of sensors used on sea ice transect*

Sensor	Description	Device URN	Geophysical Parameter
GEM-2	Geophex GEM-2 Broadband Electromagnetic Induction Sensor	pack_ice:ice_ps:gem2-556	Total (sea ice + snow) thickness
MagnaProbe	GPS snow depth probe	pack_ice:ice_ps:magnaprobe-anja	Snow depth on sea ice

Tab. 4.8.2: *Overview of device operations of the mass balance work on the sea ice transects*

Transect Date	Ice+Snow Locations	GEM-2 ice thickness	Magna-Probe snow depth
05.03.20	Fort Ridge	PS122-3_30-54	PS122-3_30-85
	Northern Loop	PS122-3_30-72	PS122-3_30-88
	Southern Loop	PS122-3_30-71	PS122-3_30-89
	Calibration	PS122-3_30-74	
20.03.20	Northern Loop	PS122-3_32-94	PS122-3_32-95
26.03.20	Northern Loop	PS122-3_33-86	PS122-3_33-91
	Lead	PS122-3_33-87	PS122-3_33-92
	Calibration	PS122-3_33-88	
30.03.20	Southern Loop	PS122-3_34-14	PS122-3_34-15
03.04.20	Northern Loop	PS122-3_34-85	PS122-3_34-88
	RS Site	PS122-3_34-86	PS122-3_34-89
	Calibration	PS122-3_34-87	
06.04.20	Southern Loop	PS122-3_35-18	PS122-3_35-20
	Snow 1 Transect	PS122-3_35-19	PS122-3_35-21
10.04.20	Alli's Ridge	PS122-3_35-115	PS122-3_35-112

	David's Ridge	PS122-3_35-116	PS122-3_35-114
	Calibration	PS122-3_35-117	
16.04.20	Northern Loop	PS122-3_36-150	PS122-3_36-153
	David's Ridge	PS122-3_36-146	PS122-3_36-145
	Calibration	PS122-3_36-151	
24.04.20	Northern Loop	PS122-3_37-79	PS122-3_37-82
	David's Ridge	PS122-3_37-80	PS122-3_37-83
	Eco Ridge	PS122-3_37-81	PS122-3_37-84
	Calibration	PS122-3_37-78	
26.04.20	Southern Loop	PS122-3_37-135	PS122-3_37-134
30.04.20	Northern Loop	PS122-3_38-76	PS122-3_38-80
	David's Ridge	PS122-3_38-77	PS122-3_38-81
	RS Site	PS122-3_38-79	PS122-3_38-82
	Calibration	PS122-3_38-78	
07.05.20	Northern Loop	PS122-3_39-129	PS122-3_39-131
	Southern Loop	PS122-3_39-127	PS122-3_39-132
	David's Ridge	PS122-3_39-130	PS122-3_39-133
	Calibration	PS122-3_39-126	

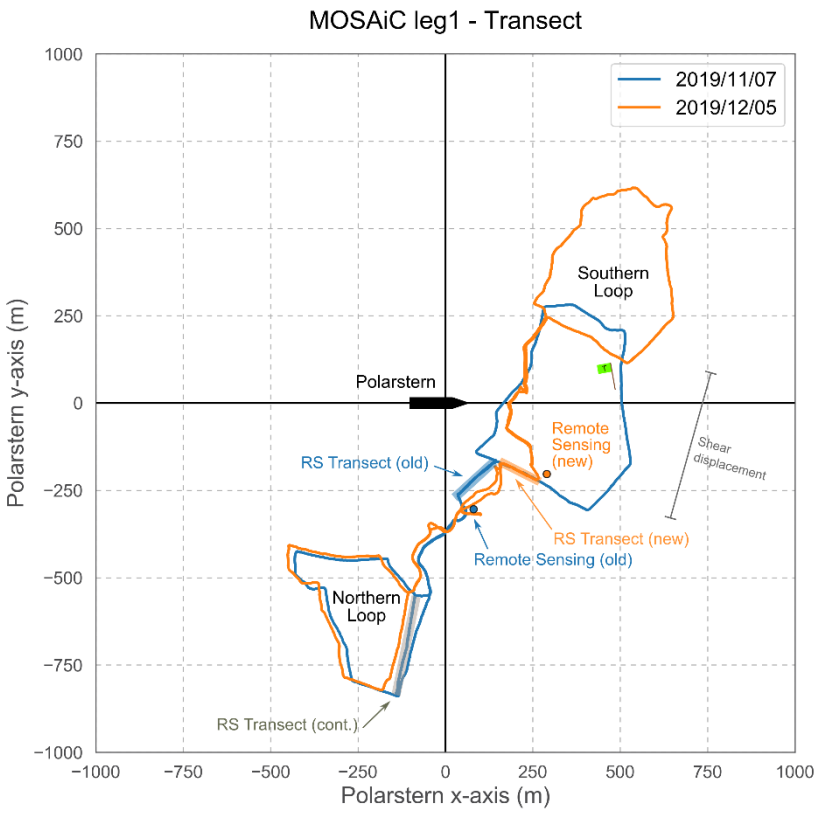

Fig. 4.8.1: *Location of the transect lines in the CO before (2019/11/07) and after (2019/12/05) the mid-November shear event. For leg 3 only the latter are relevant. The earlier tracks from leg 1 are left on the figure for comparison. Coordinate reference system is defined by Polarstern location and heading.*

4.8.3 Preliminary results

Quickview total (ice + snow) thickness from the GEM-2 results were produced after each transect activity for the purpose of quality control and initial evaluation of ice conditions. Exemplary quickview products at full sensor resolution are shown in Figure 4.8.2. It is shown that the Northern and Southern transect loops are quite different with regard to the ice thickness distribution. The Northern loop is characterized by thick and deformed 2nd year ice, while the Sothern loop also contains first-year ice and generally thinner ice.

Figure 4.8.3 shows boxplots of snow depth for the Northern and Southern transect loops from 23 October 2019 – 07 May 2020. In line with the total thickness measurements by the GEM-2, MagnaProbe measurements indicate that thicker snow layer can be found along the Northern transect loop.

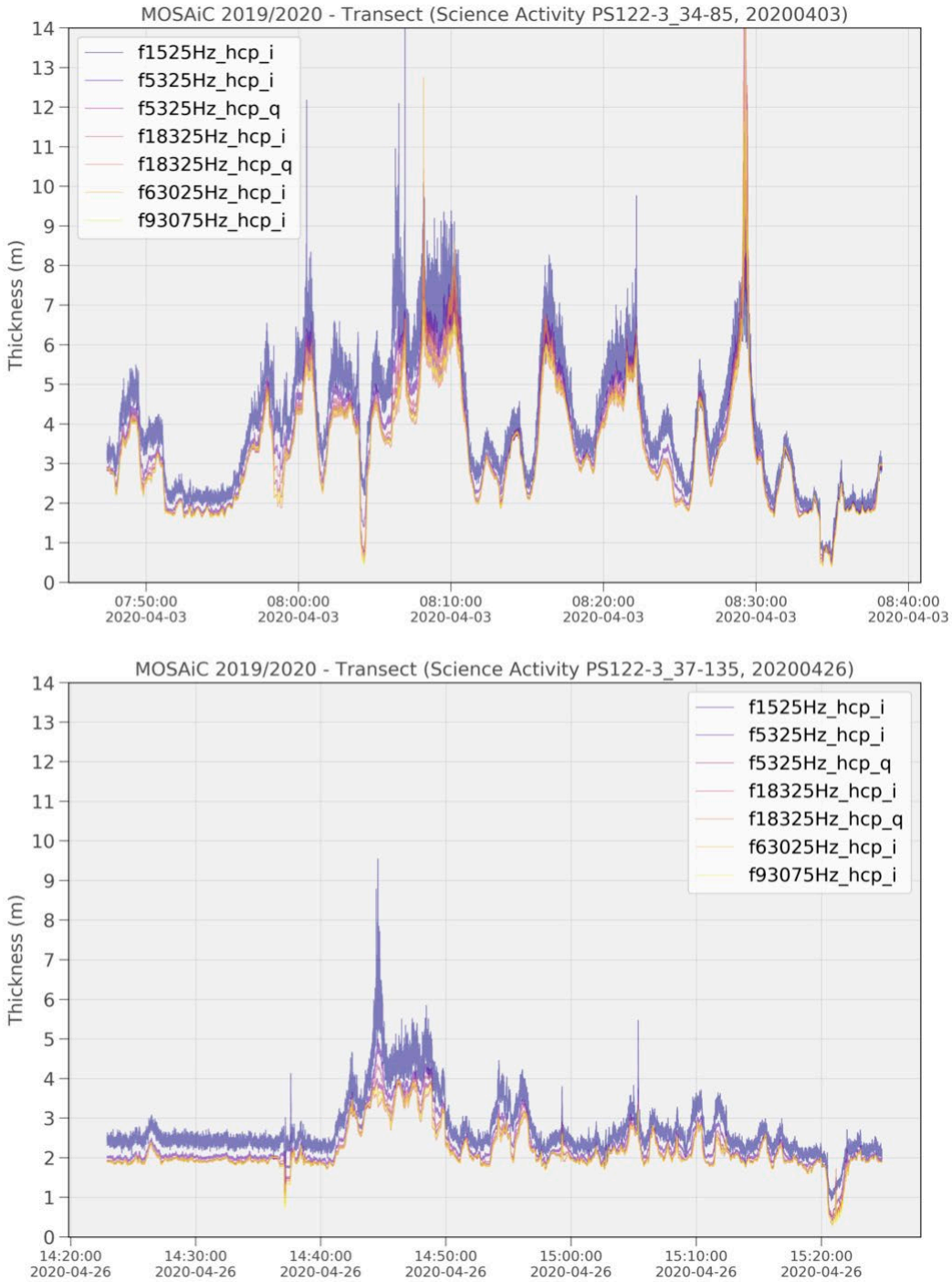

Fig. 4.8.2: *Quick looks of total sea ice thickness (snow+ice) from GEM-2. Upper panel shows sea ice thickness along the Northern transect from 3 April 2020. Bottom panel shows sea ice thickness along the Southern transect from 26 April 2020. The results are not corrected for different walking speeds or periods of the sensor without moving.*

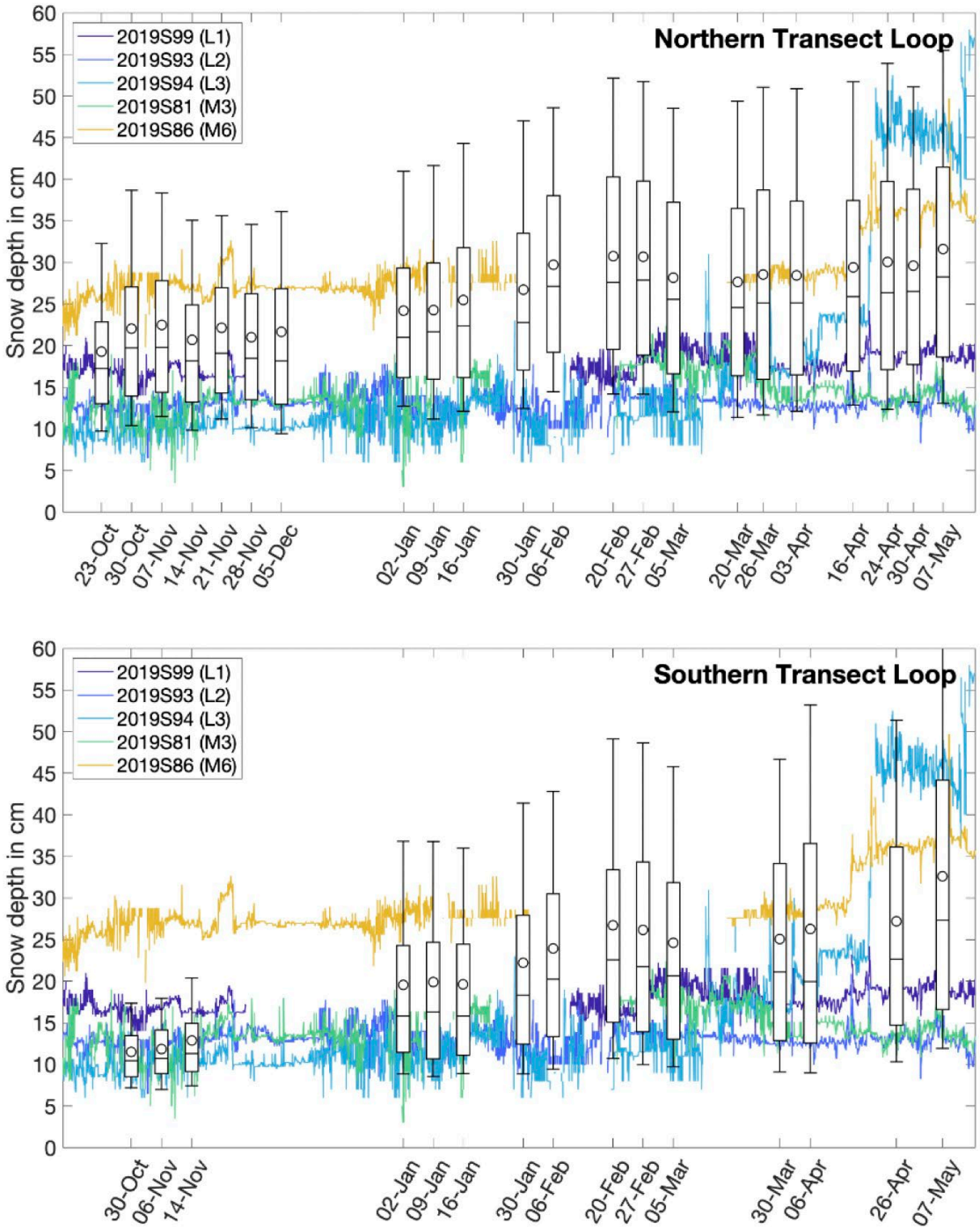

Fig. 4.8.3: *Box plots of Northern and Southern transect MagnaProbe measurements from 23 October 2019 – 07 May 2020. Solid colored lines in the background indicate snow depth derived from snow buoys at L- and M-Sites for comparison. Circles indicate mean values; horizontal line markers indicate median values.*

4.8.4 Data management

All data are handled, documented, archived and published following the MOSAiC data policy (see APPENDIX). All device operations were logged in the AWI sensorweb portal and all sensor raw data files are stored in platform section of MCS. Final geophysical parameters will be made available via the workspace section of MCS and archived in the PANGAEA data repository according the MOSAiC data policy.

4.9 Ice Dynamics

Jennifer Hutchings[6], Igor Sheikin[3], David Clemens-Sewall[2], Alexey Niubom[3], Polona Itkin[1] (not onboard), Ian Raphael[2] (not onboard), Egor Shimanchuk[3] (not onboard), Jari Haapala[4] (not onboard), Andrea Haase[5] (not onboard), Phil Hwang[7] (not onboard), Nikolay Kolabutin[3] (not onboard), Ruibo Lei[8] (not onboard), Mikko Lensu[4] (not onboard), Annu Oikkonen[4] (not onboard), Chris Polashenski[2] (not onboard), Victor Smirnov[3] (not onboard)

[1]US.UiT/CSU
[2]US.Dartmouth
[3]RU.AARI
[4]FI.FMI
[5]DE.HSVA
[6]US.Oregon SU
[7]US.UHud
[8]CH.PRIC

4.9.1 Objectives

An overall objective of ice dynamics research at MOSAiC is to deepen the understanding on how pack ice moves and deforms over a full annual cycle. In particular, we are examining spatial and temporal scales of motion and deformation and how those vary regionally and seasonally. We also aim to establish a relationship between deformation scales and physical characteristics of pack ice (in connection with data from IMB buoys, DTC, ice cores etc). The seismic stations obtain data on waves on ice and fracturing of the pack ice for a development of forecast methods for sea ice breaking.

4.9.2 Overview of measurement system

Ice dynamics research is based on the local measurements at the Central Observatory, ice drift observations from the Distributed Network and large scale satellite products. For a collection data on local scale, we established a MOSAiC Small scale Ice Dynamics Observing System (SIDOS) on the Central Observatory. The system includes following components :

- Laser strain observatory - LSO (DC)
- GNSS (Uhud) and DGPS stations (DC)
- Seismic stations (AARI)
- Stress gauges (DC, FMI)
- Stress panels (HSVA)
- Ice radar (FMI)

Leg 2 and Leg 1 installed seismic stations, stress gauges, panels and GNSS stations on the ice floe. The layout of instruments during much of Leg 3 is shown in figure 4.9.1. During leg 3 ice dynamics acted to reorganize the location of measurements relative to each other and the location of GNSS stations was changed as more stations were added. Compare to the similar map in Leg 2 cruise report to see evolution of the measurement locations.

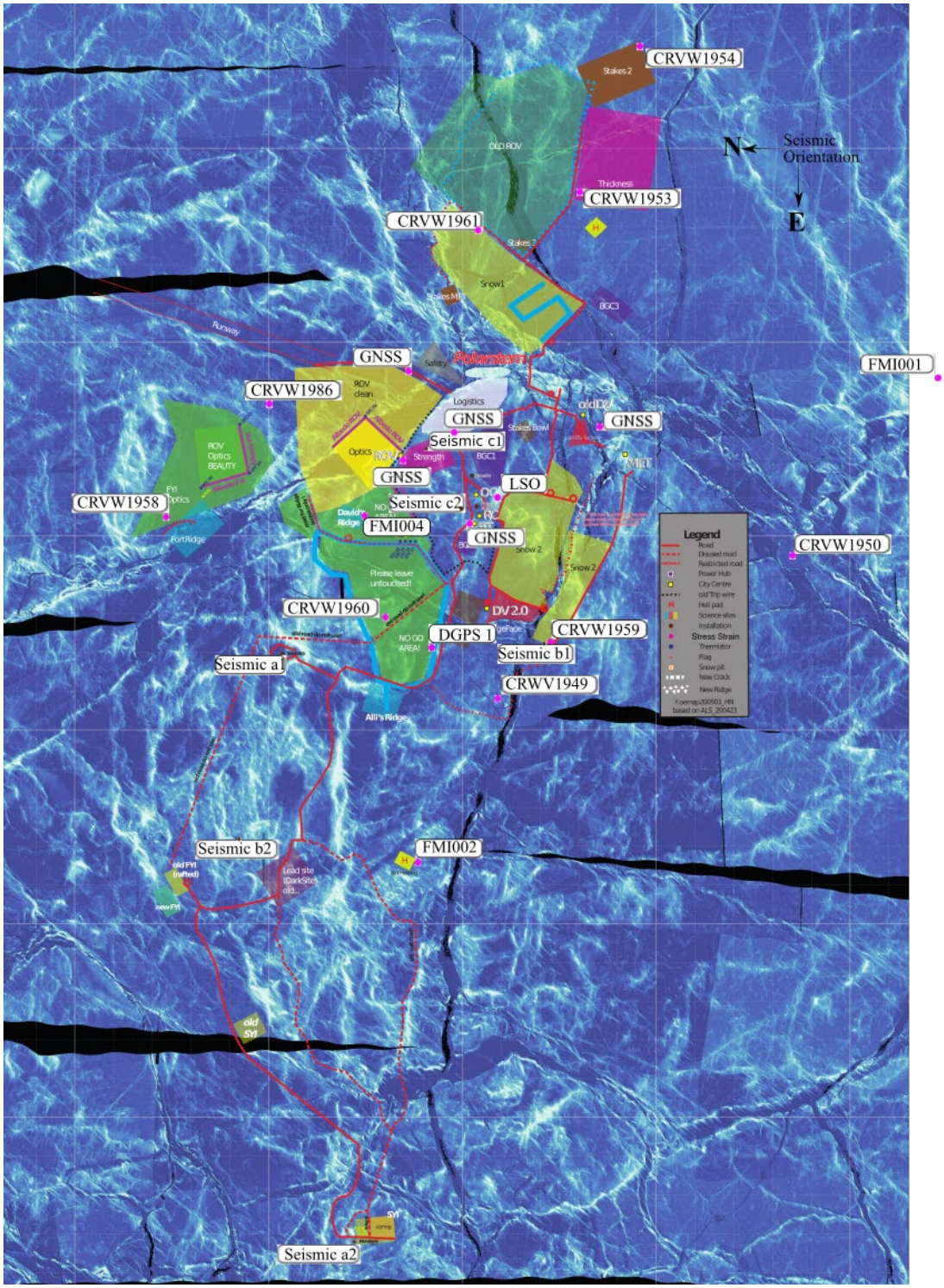

Fig. 4.9.1: *Schematic figure of the MOSAiC Small scale Ice Dynamics Observing System (SIDOS) during Leg 3 on May 4th. Stress sensors were in the same locations as leg 2, though ridging resulted in the loss of two sensors early in leg3 and redistribution of the relative locations. The location of the LSO theodolite is marked, however this was deployed at a later date. Two sites are marked for each seismic station: a1, b1 and c1 are the locations of alpha, beta and gamma stations at the start of leg 3, these were moved to sites a2, b2 and c2 in April.*

4.9.2 Work at sea

On leg 3 of MOSAiC we maintained the SIDOS (Figure 4.9.1) established during leg 2 and 1. In addition, we relocated one GNSS station, the seismic stations and deployed two extra GNSS stations. Most of the time allocated to the dynamics task was used for data download and service (battery exchange) in the existing network.

At the end of Leg 3 we deployed the Laser Strain Observatory (LSO) that was not working in temperatures below -17C. The seismic stations were recovered prior to leaving for resupply in Spitzbergen. A floe dynamics observatory, consisting of LSO, one DGPS and two GNSS buoys was left in the CO after departure on May 16th.

Laser Strain Observatory (LSO)

LSO provides high-precision plastic and elastic ice strain data. The observatory is composed of an array of retroreflectors (currently 17) fixed in the ice on metal posts, and an autonomous laser theodolite that tracks the displacement of the reflectors over time with mm-precision. This displacement measurement can be used to determine strain rate. The base station is accessible via the PackIce WLAN network through which data can be viewed in real-time from Polarstern.

The Leica TM50 base station was inoperable throughout most of Leg 3 due to low ambient temperatures. The LSO was deployed and running from May 5th. The central floe, defined by the area between active cracks that Ocean City was on, was substantially smaller than during leg 2, such that many of the reflectors placed during leg 2 were too mobile to be tracked by the theodolite tracking their motion.

Tab. 4.9.1: *Configurations of the LSO during Leg 3.*

May 5th	Running with 5 reflectors
May 6th	Running with 14 reflectors
May 7th	Outage when put on battery power. Put back on line power.
May 10th	Sporadic data outages while trouble shooting battery power issues.
May 11th	Running on battery power.
May 12-13	Extensive cracking and shrinking of the central floe. Many reflectors can no longer be tracked.
May 15th	Running with 17 reflectors on the now smaller central floe. Short outage due to a tilt overage error that required resiting all reflectors.
May 16th	Final data download and checks. Closed boxes and left the ice station hopefully to return on leg 4.

GNSS and DGPS stations

The GNSS and DGPS stations measure ice motion on high precision and high sampling rate (1 and 2 s) as well as a constant reference frame for floe-relative coordinate transformations. At the end of Leg 2 three GNSS stations were deployed in the CO: in the logistic area (S1), at the remote sensing hut (S2) and at the Balloon Town (S3).

We relocated S1 to ROV on March 13th. It failed to collect data as it had been shorted during a storm event.

A new station was deployed at Remote Sensing on March 12th (S6). This station was recovered on March 26th and redeployed near the former Met City DGPS site on March 31st.

A new station was deployed in the logistics area (S5) on March 12, ensuring three stations were collecting data on the same floe.

Since the Remote Sensing site experienced significant deformation, which was measured with S2 and S6, this area became difficult to access. We relocated S2 to the ROV hut on March 18th.

We encountered some problems using these stations. High winds caused the battery cables to rub against the battery boxes, fray and short the batteries. We were unable to download data in the field in the cold temperatures, even when running ethernet cables to nearby huts. S3 ethernet port had become damaged and S1 instrument was damaged by a short. We decided to do less frequent data downloads than battery changes and we brought the GNSS buoys (yellow pelican cases) onto the ship for data download. We also started a program of near time coincident battery changes so that we could maximize concurrent times between the 5 deployed instruments when data was collected.

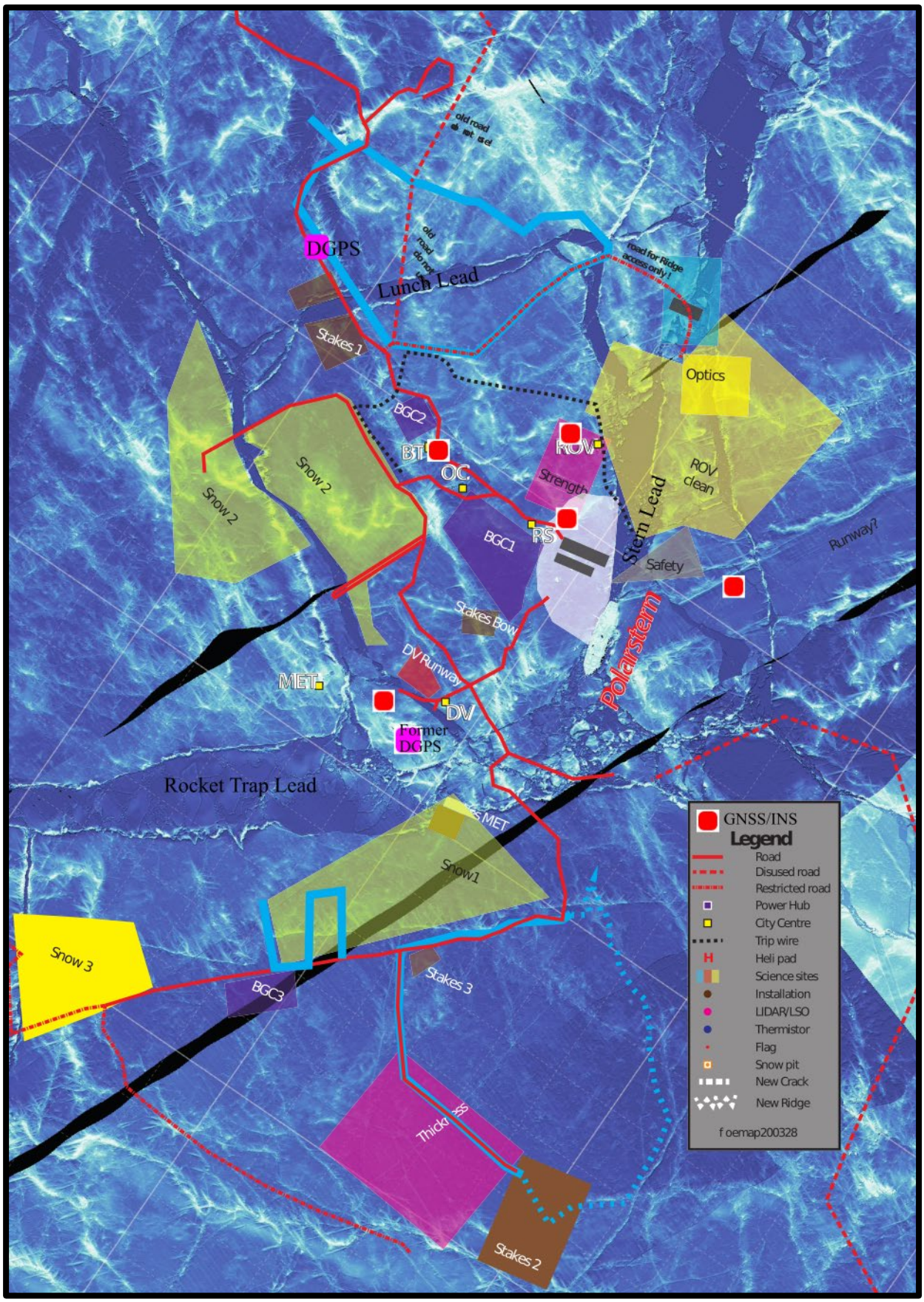

***Fig: 4.9.2**: Location of GNSS/INS stations and DGPS stations on March 28th. The locations moved with the ice, and some installations were deployed later. The DGPS near Met City had been removed.*

Two Trimble NetRS DGPS units were deployed by leg 2 within the CO (one at MET City and one at the Big Block on the Northern Transect). The station at the Northern transect requires regular battery exchange and data download, while the station at the MET city is connected to the line power and data can be accessed via PackIce WLAN network. For location overview see Figure 4.8.1 in the leg 2 cruise report. The DGPS at Met City was decommissioned on March 11, 2020 when power was pulled from the region due to mobile ice, and we could not re-establish battery power due to issues with the trimble power input port and a later shorting of the instrument.

At the end of leg 3 we brought the DGPS station from Big Block and redeployed in the CO close to Ocean City and next to the LSO theodolite. All GNSS stations were recovered, and on May 12th we redeployed two stations. S2 is deployed along the road between the ship and Balloon Town and is collocated with an LSO reflector. S5 was deployed at Balloon Town in exactly the same location S3 had occupied. We left the floe on May 16th with LSO and 17 reflectors, one DGPS and two GNSS buoys running.

Seismic stations

Each of the three seismic stations (Alfa, Beta, Gamma) includes seismometer CME 4311, tiltmeter ИН-Д3-360, autonomous recorder “Baykal-8” for logging signals, GPS-antenna, antenna for signal transmission to the base and battery for powering station. Measurements were recorder to the “Baykal-8” datalogger with 100 Hz frequency. Data of the seismic stations were also transmitted by the wireless connection to a laptop deployed onboard the *Polarstern for a* continuous visual monitoring of seismic observations.

The stations were deployed close to the logistic area during leg 1, and in leg 2 we distributed them over larger distances in the CO. Gamma remained close to the logistic area (close to the new ROV site and at the sampling site for mechanics experiments), Beta was deployed at the northern end of Snow2 sampling area and Alfa was deployed north of the Alli’s Ridge. All stations require regular battery service.

During leg 3 special places were prepared to reinstall these sensors for their work in the summer, because there is a risk of melt ponds affecting the winter installation sites. On April 24, the station close the ROV was reinstalled in the CO close the Ocean City. A site was chosen on a smooth two-year-old ridge of height less than 1 meter. A special post with reflective heat coating to depth 1,5 meters, with sensors installed on and all this is in a sunshield with a thermocouple. On April 26, the seismic station close Snow2 was reinstalled to a new place near the FYI coring site. On May 1, the seismic station “North” was reinstalled at the SYI coring site. May 12 was the end of the work of the station at SYI, and the instruments were recovered. May 15 was the end of data collection at the CO and FYI sites.

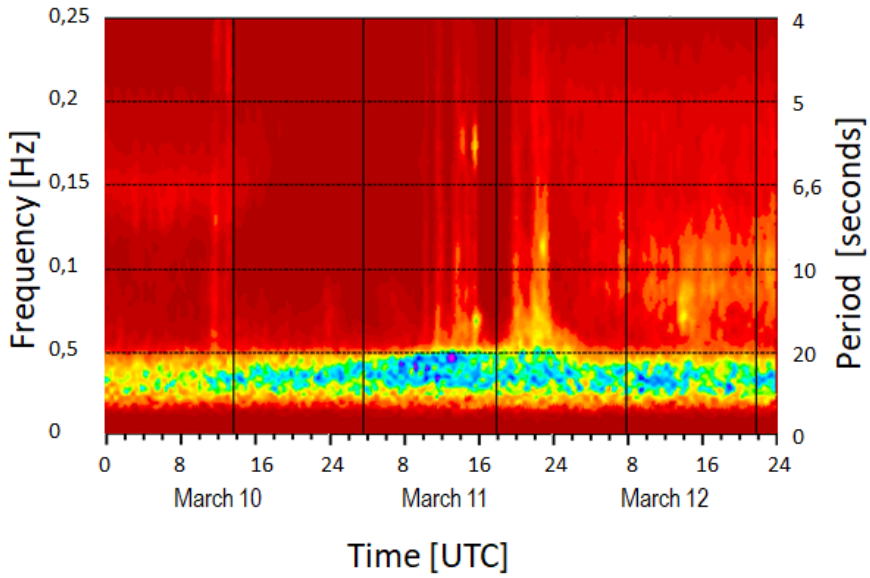

***Fig. 4.9.3**: Continuous Wavelet Time-Frequency Spectrum of ice fluctuations in vertical direction. seismic station «North», seismometer CME 4311. March 10-12 (2020)*

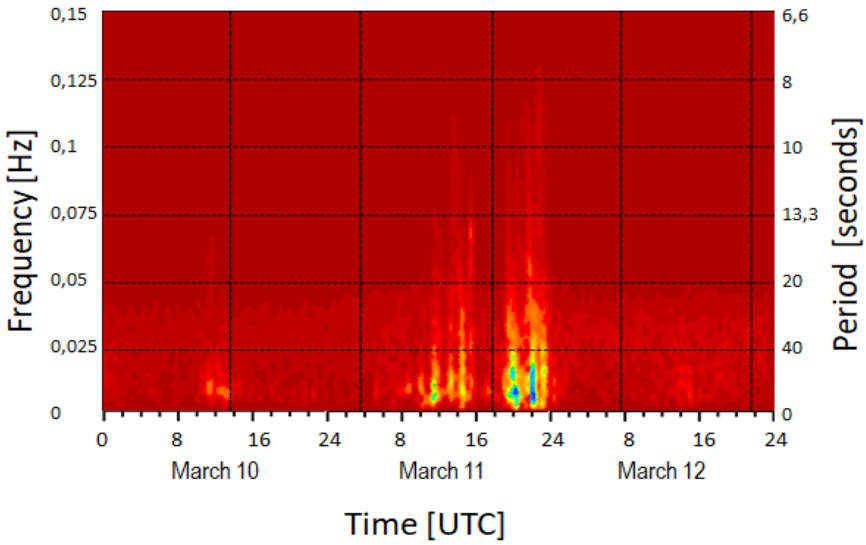

***Fig. 4.9.4**: Continuous Wavelet Time-Frequency Spectrum of ice fluctuations in horizontal (North) direction. seismic station «North», seismometer CME 4311. March 10-12 (2020)*

Delta also requires regular data download. Unfortunately, L1 was not revisited on Leg 3. There was a ridging event at L1 in early March that destroyed some buoys. The delta seismic station has not been located since this event.

Stress gauges

The sensors measure local horizontal ice stress by measuring the change in frequency of three internal, actively vibrating wires. Using a network of stress sensors, the DGPS/GNSS stations, and the LSO, we will approximate the stress field and responding strains within the local floe.

The sensors are installed primarily within and around the CO, though some were installed as far as 2.5km from Polarstern (for detailed locations see Figure 4.8.1 in the leg 2 cruise report).

Eight Dartmouth College/CRREL Geokon vibrating-wire stress gauges were installed during Leg 1. These sensors record stress every minute. In addition, five identical sensors from FMI were installed which record stress every 10 minutes. One DC/CRREL sensor was destroyed in mid-November, leaving twelve intact sensors All gauges from leg 1 were installed in the remnant/second-year ice.

During Leg 2, three more DC/CRREL sensors were deployed in the CO (one in the remnant ice of the N transect loop and two in the FYI of the ROV observatory) , making fifteen operational sensors at the end of Leg 2. They required infrequent battery exchange and data download, but otherwise operated unattended. All gauges were deployed on level pans of ice of diameter at least 100 m.

During Leg 3 we lost one FMI sensor (FMI003) to ridging in Rocket Trap lead on approximately March 17. By March 22, the first time we could reaccess the area, the datalogger had been crushed and submerged below the water. We managed to recover the sensor from the rubble but the datalogger and data was lost.

The DC/CRREL sensors transmit data to the ship via radio link every 12 hours although occasionally the radio links would not communicate for a number of days before resuming. At the end of leg 3, 5 DC/CRREL sensors were definitely still working. Two more (1950 and 1954) stopped communicating on May 14 when the ship relocated further from them and are presumed to still have been operating. One sensor, 1949, continued transmitting until May 15, after the May 12-13 deformation event, but given it's proximity to a ridge was likely destroyed shortly thereafter. Sensor 1959 was destroyed in the May 12-13 deformation event. Sensor 1987 was destroyed by Rocket Trap lead on March 15. The five definitely working DC/CRREL stress sensors transmitted their last data of leg 3 early in the morning of May 17, as Polarstern abandoned the Mosaic Floe.

Stress panels

Stress panels deployed in the logistic area during leg 1 and the stress and temperature sensors deployed in the ship hull in void 92 were all operating unattended during leg 3. The ship experienced large movements during to ridging onto the ship at various times from March 11th onwards, and did not consistently hold station for the rest of the leg. During this period in March the location of the panels relative to the ship moved repeatedly sternward and bow-ward and there was some rotation of the panels relative to the ship.

There is a gap in data between March 24th and April 11th when power was cut to installations on the ice, and the panels were removed on March 29th because we thought the ship would move to a new anchor point. We reinstalled the panels between April 8th and 11th in the same location as previously however in front of the chainsaw hole the panels were taken out of and only 20m from the ship hull. The trench holding the panels was flooded on the 11th at 14:45Z, and topped up with sea watch on April 13th. A crack extending past the panels late on April 28th. The logger box and panels were recovered after this.

***Fig. 4.9.5**: Shown on right is recovery of panels on March 29th. The crack the formed during hand over between leg 2 and 3 runs beside the middle panel. [left] Panel location on March 20 is between the red flags. The panels had be installed perpendicular to void 92, and did not move from this location until March 11th. There was subsequent motion of the ship relative to the floe from March 11th onwards. On March 15th the ship moved about 5m forward relative to the stress panels, moving the panels to be in line with the gangway onto the ice. On March 20th the ship moved backwards, and new position of the panels is shown in the photograph on March 20.*

***Tab. 4.9.2**: Movements of panels relative to ship*

March 11	crack runs through the ship and opens to lead
March 15	the lead to the stern rafted and ridged. Ship broke anchor lines and moved forward relative to the ice. Panels became aligned with the gangway from the ship to the ice. After the movement the ice relaxed and opened between the ship and ice disconnecting panels from ship. This opening subsequently froze over.
March 18	opening between ship and logistics area.
March 19	this opening is closed.
March 20	broke anchor lines. Ship moved back relative to the ice. Power outage starts.
March 23	ship moved forward 80m.
March 24	opening between ship and ice of about 5m. ship rotated about 7 degrees.
April 19	ship jolted and leaned to port. Ridging to stern pushed the ship towards the pressure panels.
April 24	opening between the ship and panels.
Aptil 27	ship moved backward such that panels became aligned with the bow.
April 28	jogging 90 degrees past the panels. If this opened and ridged it could destroy the panels so we recovered them.

Data was downloaded from void 92 on May 4th. Inspection of Leg 1 data back on land identified that some of the strain gauges in the void were not recording. On May 18th the system was rebooted and appears to be functioning as normal again.

Ice radar

In order to obtain data of local ice dynamics in high temporal and spatial scale, we used a system which digitizes the raw analogical ship radar data in a manner that echoes from the sea ice features, which normally are considered as a noise in marine applications, are digitized in high resolution. The radar signal digitizing unit, developed by the Imagesoft ltd., was connected to the antenna of the WAMOS radar. The set-up of the system is similar than used for the N-ICE2015 campaign (Oikkonen et al, 2017).

During the MOSAiC, processed images of every radar loop have been stored. Interval of those images is about 2 seconds. Digitizing area covers 20 x 20 kilometers area with 8.3 meters horizontal resolution. Continuous recordings begin on 25th October 2019. On leg 3 we continued with the collection and processing of the data.

Leg 3 was exceptionally dynamics, and notes were maintained of all the deformation events observable in the RADAR. These notes are summarized in the preliminary results section 4.9.3.

There were two glitches in data collection, which have not resulted in loss of data. On May 4th at 1am UTC the RADAR Server clock moved forward one hour to British Summer Time. This was not corrected on the ship, and the apparent one hour gap in data is not a real gap. On April 23 the NAS storage for the RADAR became filled. Unfortunately Leg 1 data was deleted from the NAS to make space for more data storage. This data was checked to be on the MCS and backed up on shore. A second NAS server (nas2) was installed on May 8th. There is now sufficient storage for the remainder of MOSAiC.

Sea ice strength/mechanics measurements

Aim of the ice strength measurements is to determine local strength of different ice types and their seasonal variations. Measurements of vertical and horizontal ice strength were carried out according to a methodology developed in Ice Physics Laboratory of the AARI (patent №2348018) and described in “Methodic manual for studying physical-mechanical characteristics of ice formations as initial data for calculation of ice loading on shores, bottom and sea constructions” (SPb, AARI, 2011, p. 179).

For these measurements, a 50 meters x 50 meters area named ‘seismics’ was reserved. The site contains level second-year ice and it is located just next to the ROV site, next to the seismic station at the logistic area. Local ice strength measurements were conducted with an automatic hydro complex “ЛГК 131-01” borehole probe-indenter “ЛГЦ095.055.0050.002”.

Local ice strength measurements

Measurements are carried out in the following way. First, the location of measurements was cleaned from snow, snow and ice surface temperatures were measured. Then at this point a hole with diameter 250 mm is drilled through vertically the ice. After that the hole is cleaned from brash ice and a probe-indenter deployed on a tripod over the hole. After testing of the system, the probe-indenter was oriented to the selected direction and lowered down into hole on 30 cm depth and first measurement was made. The following measurements were made every 30 cm (30,60,90,120,150,180 cm)

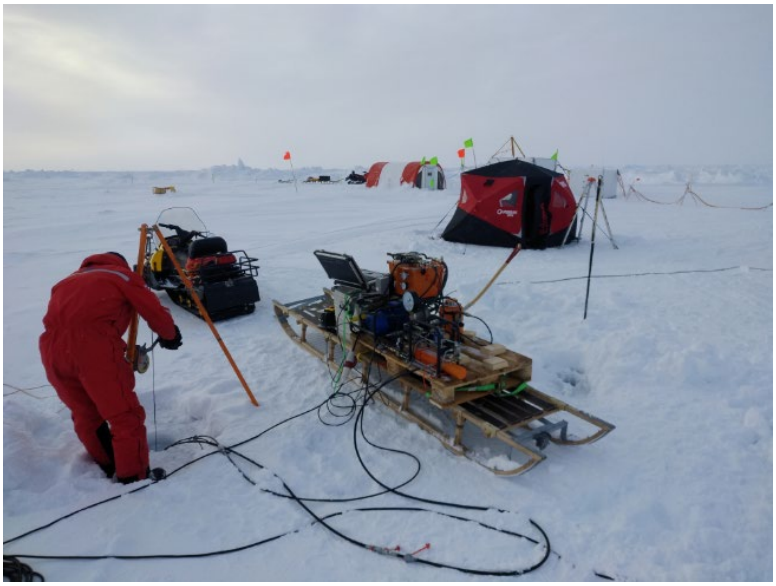

***Fig. 4.9.6**: Immersion of the probe indenter into the ice well to determine local ice strength using an automatic hydro complex "ЛГК 131-01".*

Measured strengths are given in Tables 4.9.3. to 4.9.5

***Tab. 4.9.3**: Results of the ice strength measurements from AARI borehole jack 25.03.2020*

Point	H_{snow} (cm)	H_{ice} (cm)	H_{raft} (cm)	LocStr30 (MPa)	LocStr60 (MPa)	LocStr90 (MPa)	LocStr120 (MPa)	LocStr150 (MPa)
t1	8	175	168	35,7	45,0	45,0	45,3	
t2	8	175	168	37,6	38,2	33,2	31,5	4,9
t3	8	175	168	46,1	45,1	44,3	43,5	
t4	8	175	168	41,0	38,3	36,2	29,3	4,6

***Tab. 4.9.4:** Results of the ice strength measurements from AARI borehole jack 11.04.2020*

Point	H_{snow} (cm)	H_{ice} (cm)	H_{raft} (cm)	LocStr30 (MPa)	LocStr60 (MPa)	LocStr90 (MPa)	LocStr120 (MPa)	LocStr150 (MPa)
t1	22	152	143	41,4	34,9	39,5	28,6	7,9
t2	23	150	143	41,5	33,2	30,3	28,0	
t3	23	151	143	38,4	32,3	34,6	26,2	
t4	24	150	143	41,6	38,1	34,1	25,4	

Tab. 4.9.5: *Results of the ice strength measurements from AARI borehole jack 08.05.2020*

Point	H_{snow} (cm)	H_{ice} (cm)	H_{raft} (cm)	LocStr30 (MPa)	LocStr60 (MPa)	LocStr90 (MPa)	LocStr120 (MPa)	LocStr150 (MPa)	LocStr180 (MPa)
t1	16	200	187	29,8	29,7	30,2	29,0	24,7	21,9
t2	15	199	187	30,3	33,2	26,6	31,3	29,5	19,8
t3	15	199	188	34,7	29,3	29,7	29,9	22,7	5,6
t4	15	200	188	33,8	32,1	26,5	28,8	24,8	3,4

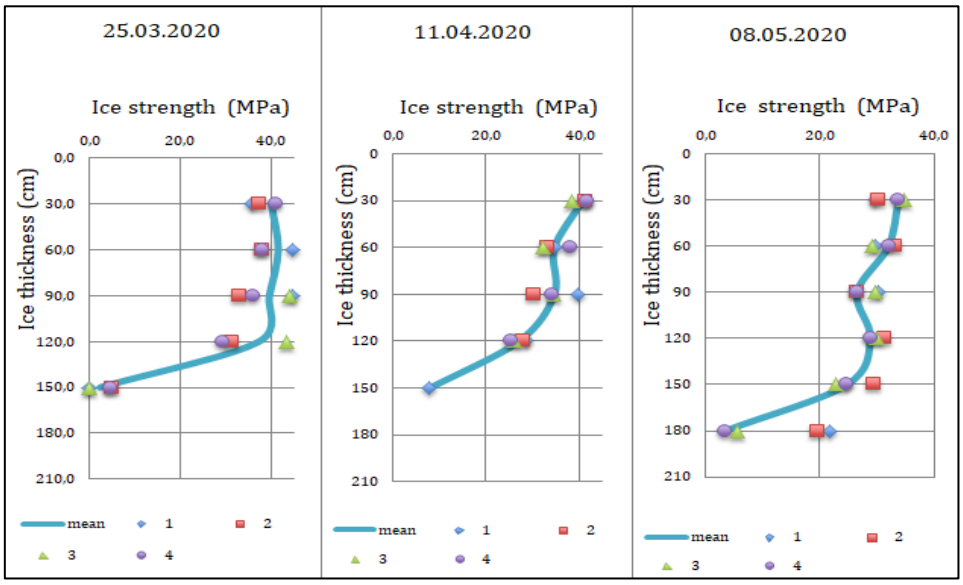

Fig 4.9.7*: Results of the ice strength measurements from AARI borehole jack.*

<u>Uniaxial compressive strength measurements.</u>

Vertical and horizontal ice samples were tested.

The ice cores for vertical ice strength measurements were taken with a “Kovacs” 14 cm ice corer. For the horizontal strength measurements, a selection of large ice samples along the entire thickness of ice with width 45 cm we taken. These samples were also retrieved using a “Kovacs” 14 cm ice corer and winch fixed on tripod.

The number of measurements taken during Leg 3: 160

Vertical ice strength measurements were conducted on: March 10, April 15, April 19, May 2 (2020)

Horizontal strength measurements: March 23, April 15, May 2 (2020)
On April 19, vertical samples of young ice were tested. In other cases, measurements were conducted as per the usual standard procedure.

Fig. 4.9.8*: Selection of large ice sample thickness 190 cm and width size 45 cm. Right – block ice raised by the winch fixed on tripod.*

Fig. 4.9.9: *Preparation of horizontal ice samples*

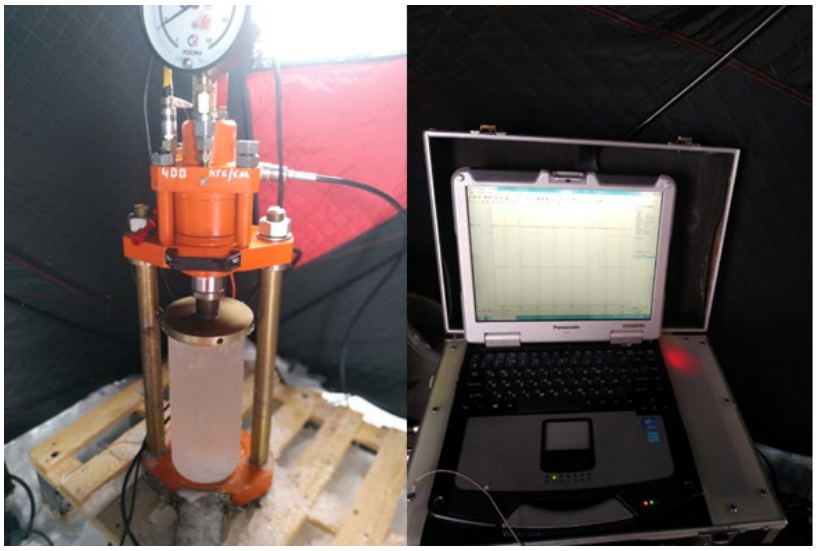

Fig. 4.9.10*: Uniaxial compressive strength measurements ice of horizontal direction.*

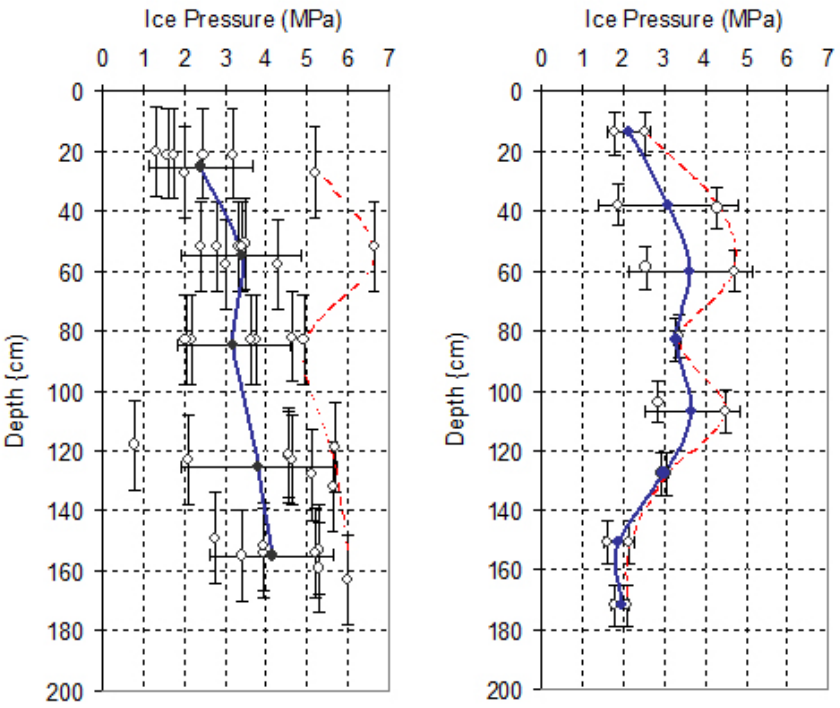

***Fig. 4.9.11**: Uniaxial compressive strength measurements, left plot: in vertical direction, right plot: horizontal direction May 2 (2020).*

Additional ice cores were taken for temperature, salinity, density and texture analysis.

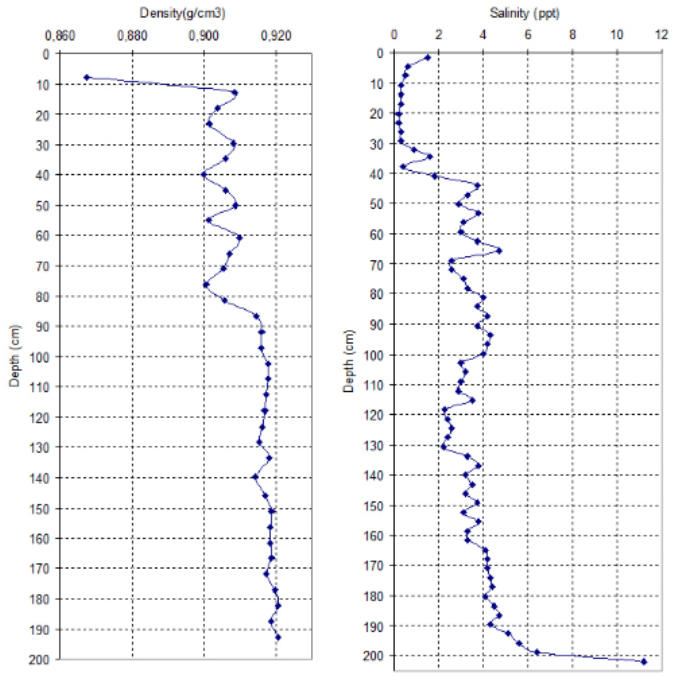

***Fig. 4.9.12**: density and salinity of ice cores May 5 (2020)*

4.9.3 Preliminary results

Leg3 was characterized by unstable ice conditions in the CO. The ship was located in a shear zone after March 11, and the action of the shear zone oscillated across two different direction. The ship and Met City were located in a junction between lead systems and eventually this because a normal shear zone between two working leads. At which point the CO disintegrated into smaller floes (May 13) and it was decided to recover on ice installations before leaving the CO for resupply on May 16.

David Clemens-Sewall and Jenny Hutchings compiled the following list of cracking events in the CO and vicinity. Cracks, Leads and Ridges are referred to by names given below. A cartoon showing the approximate location of all these features relative to the ice station layout at the end of leg 2 is shown in Figure 4.9.13. By the end of leg 3 the icescape had completely changed through the working of these features (Figure 4.9.14).

Names of Leads/Ridges

- Rocket Trap Lead: Named after the rocket traps the lead consumed. This is the lead the formed to the bow of the ship and extended through the ship to the Stern Lead.
- Stern Lead (or ship lead): The crack the formed through the ship on March 11th. One side of this to the stern of the ship became referred to as Stern Lead.
- The Rocket Trap and Stern leads were collectively called Ship Lead when they first formed.
- Met City Lead: Crack that opened on March 11th and worked since then cutting of access and power lines to Met City at many times.
- Drone Ville crack: A crack that opened between Rocket Trap lead and Met City Lead, causing the DGPS/LSO site to become an island.
- Lunch Lead (which David and I called Igor's lead for a while due to his frequent crossing of this lead to get to his seismic station): Named by logistics team after their lunch spot one nice day. Opened on March 13th.
- Extension to Lunch Lead: Formed after lunch lead, running on the other side of Met City lead parallel to lunch lead and Rocket Trap lead. There is a kink between lunch lead and the extension, and they formed at different times.
- David's Ridge*: A small ridge that formed across the northern transect on route to Fort Ridge.
- New Fort Ridge ridge*: A large ridge that formed through the Fort Ridge area. The old ridge being studied at fort ridge was consumed by ridging events that created the new fort ridge.
- Paul's Crack: Named after Paul's foot that found the crack. Parallel to Met City lead between the ship and Droneville.
- Snow1/Met City Lead: The Met City lead at one point joined with Rocket Trap lead, and then later in April joined with the lead that extended through Snow 1. These are not distinct leads, and the intersections between the original leads were expressed as kinks in the new leads. For example, the Snow1/Met City lead junction was an area of normal faulting around Met City, and was the event that cause the Met City thick second year ice floe to split in half.
- Stakes 3 crack: Formed in snow 1 on April 4th.

* The timing of cracking events leading to the formation of ridges in the Fort Ridge area can not be estimated from RADAR or panomax.

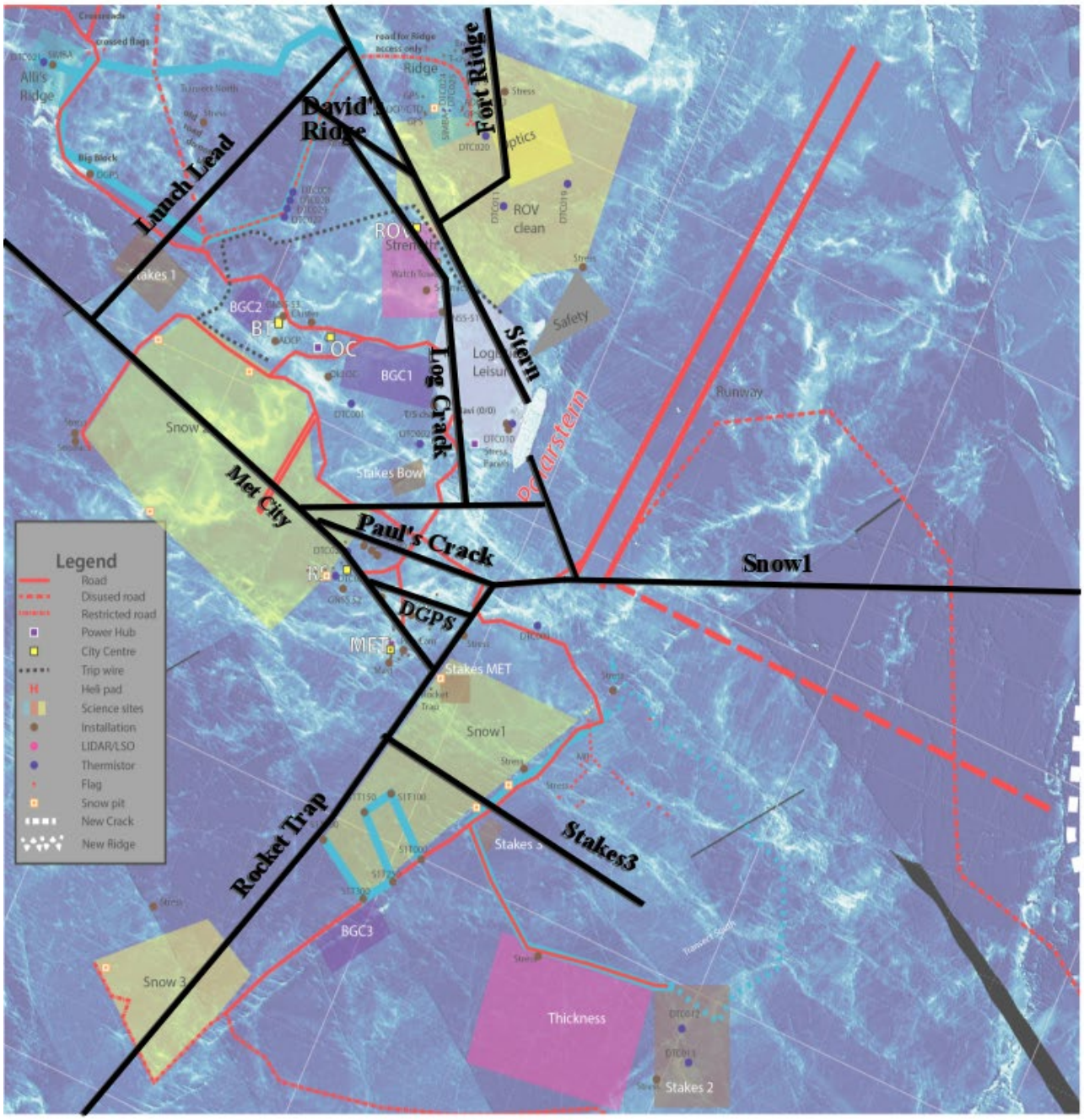

***Fig 4.9.13**: Cartoon of approximate location of cracks, leads and new ridges that formed during Leg3 up until May 11th, relative to the layout of the central observatory at the start of leg 3.*

This is a list of when cracks and ridges formed. We note the time when a crack first formed based on visualizations provided by the panomax 360degree camera and the FMI ice radar. The aim of this narrative is to provide context for strain measurements that show deformation over larger spatial scales. We wish to track where the cracks are that accumulate this deformation and identify their location relative to stress sensors and seismic stations.

All times are UTC. We note the time of when a crack was first observed, or for event recorded for specific features when they began to open or ridge. We have not noted all the incidents of lead opening or ridging, just highlighting some events. We do, however, try to note all the crack formations in the CO. These are dynamic cracks that we can track with RADAR or panomax.

Event 0 (at a distance from the ship, not directly affecting the CO)

March 4
0800 Lead opened approximately 1.5km from ship to bow of ship.

March 6
shearing along line between the closing lead and ship, at about 30 degrees clockwise to the lead.

Event 1 (it all started with a crack running through the ship that opened to a lead)

March 11
0700-0720 Rocket Trap crack opens (Panomax)
0840-0850 Rocket Trap crack rotation in RADAR
0850-0900 Goes back
Extends through RADAR image.

Panomax: 1040 ship crack opens
Radar: 1040
Ship crack opened
Radar shows rotation at this time.

Both cracks open over the next hour (panomax)
Very open at 14:20

David thinks a crack forms across ROV area (making Fort Ridge an island). Not sure when, cant find in panomax or radar

1440 (panomax)
Met City crack opens

Echelon cracks at junction (panomax)

Met City sheared to starboard
1940-2000

Over next hours shears, with Met City moving to starboard
2300 shearing ends

March 12
Cracks and leads making small movements throughout the day. Not noteworthy, working but small movement.

March 13
0520 - crack opened between Met City lead and Ship Crack (splitting stakes1 in half)
Classic zigzag crack pattern (weakness not parallel to direction of crack). This is Lunch Lead.
0600 - Extension to stakes1/Igor's crack that is observed in Manuel's drone flights on the 17th. This is an extension of the Lunch Lead (aka Igor's lead) that parallels Rocket Trap lead.

March 14
Leads working throughout
0200 Met City sheared away
0220-0240 New crack through ROV area. Now a ridge in front of optics area.
0300 Rocket Trap lead opened up
0300 Opening of ship/ROV leads and Met City lead
2100 Opening Rocket trap lead

March 15
Ship lead opens and closes, shearing. Relative motion is the ice on the side away from the ship is moving away from the bow.
1400-1520 Ship moved relative to the ice. Ice in logistics area moving towards ship lead.
1800 Crack across the runway
/Users/jenny/LEG3/CO_Cracks/RADAR_Panomax_Log_11-26March.txt

March 19
DroneVille crack opens
There is another crack by the 26th much earlier (must be the same system)

March 20-21
Stern lead opens and moves back and forth a bit.

March 23
Crack through Snow 1
By the 27th crack formed along far edge of snow 1
Also, on March 23rd between 0400 and 0420 crack opened between Met City and former (then current) Remote Sensing.

March 24
Met city/RS lead opened a bit more.

At some time between the 11th and 23rd there were more ridges formed through ROV. WE can not identify time from RADAR because the region is in the RADAR shadow. It is also too far away to identify in the panomax.

March 25
14:00 Stern (ship) lead opened

March 27
17:20 Rocket Trap lead opens

March 29-31
Rocket trap lead ridging.
Stern lead opening and moving March 29 and 30.

April 1
Cracks opened between Ship and Met City.

April 2
Rocket Trap lead opened from ship in direction bow pointing. Diverted

April 3
Rocket Trap lead opening more, and extends into horizon

April 4
Stakes 3 crack opens through Snow 1 at 0200
Freezes up, then opens a bit more from 1400-2300ish

April 5
Rocket Trap lead (that ship is in) ridges onto ship at about 6:30am UTC.
Stakes 3 crack direction of motion changes at 0200 such that ridging occurs in Snow 1 and shear inside the S. Transect. Around 1700 direction of motion changes again such that now Stakes 3 piece moving away from Snow 1 and other half of S. Transect piece.

April 6
Paul's crack opened between ship and Drone Ville.
Continuation of movements in Stakes 3 lead from April 5.

April 7
New cracks between Paul's crack and Drone Ville/ Met City. < 30cm wide.

April 8-15

Small movements in Stakes 3 lead but no new cracks/ridges

Event 2 (or continuation of event 1 after lull in dynamics? The same leads are working)

April 15

Preexisting cracks opened very slightly (order centimeters). Some of the cracks had beautiful echelon shear crack patterns in the nilas forming on them. The ice pack around the ship was shearing very slightly and closing in the stern-bow direction.

April 17

05:20 Rocket Trap lead opened again, but did not extend all the way to the ship. It followed a jog up a preexisting lead running beside Stakes 3. This preexisting lead was following a crack already in place (Paul's crack which extends past Stakes 3 and is the crack David put his foot in when coring on April 15th).

13:40 Paul's crack opened between ship and Drone Ville. More cracks opened between ship and Met City. DroneVille is now an island together with Met City.

Shears and opens slightly until

22:00 opening to form island at around Met City and new cracks extending on other side of Rocket Trap Lead.

April 18

11:20 Paul's Crack and crack through stakes 3 became a lead.

April 19

08:40 New crack to port of ship between runway and stakes 3.

14:40 Cracks (incl. Paul's crack) open into leads between ship and Met City. New crack that formed at 08:40 opens into a lead.

Met City Power disconnected at this time.

April 20 (storm)

Shearing 2km from Portside of the ship visible in ice radar.

20:20 Met City Cracks opening

April 21

leads closing, Met City lead opening. The whole area ahead of the ship is working since the 18th.

April 22

06:00 Crack on port side of ship running bow to stern opens

11:20 Opens again

April 23

Found crack across road just before 2nd year ice. Not sure when this opened, it was less than a meter wide the morning of the 23rd. Probably associated with openings on the 22nd.

The leads that formed on the 19th continue to work in the following days, forming a shear zone between the ship and Met City.

April 26

13:20 Crack across stern lead opens.

April 27

4-5am ridging heard at ship, Met City Ridge shearing 05:00. During the day we saw opening running 9-11 o'clock relative to the ship and shearing along 1'oclock.

22:20 Crack across logistics area. This crack runs past ROV (splitting ROV and mechanics site), and runs all the way through David's Ridge.

The Met City shear zone continues to work. Log area crack stabilizes.

April 29

06:40 opening of the leads between ship and met city.

These continue to work, on may 1st met city leads had closed. Opening and ridging of cracks in snow 1 throughout the next few days.

The leads and cracks in the shear zone continue to work. May 2nd 0100 opening in snow 1 lead.

May 3

0300 Snow1/Met City lead opening

Shear zone continues to work. Shearing along Snow1/Met City lead. On May 6th a morning Met City scouting party witnessed the shearing.

May 6

06:40 Crack behind Met City, making Met City an island in the shear zone. The shear zone is growing in width, cracking ice next to it.

May 7

14:20 Snow 1/Rocket Trap lead opened

Rocket Trap / Snow 1 / Met City / south extension to Lunch leads continue to work, and there is shearing in wider area of radar scene, over the following days. A little quieter on the 10th and 11th.

May 12

09:50 Leads opening along starboard of ship in RADAR, about 2km from ship.

14:40 Logistics Area crack opens, and becomes extension of Rocket Trap Lead.

15:40 Cracks formed in CO (on bridge watch, watched the one split remote sensing from main floe in less than 5 minutes).

19:20 Rocket Trap lead is moving.

Continuing through the May 13th Storm we see these leads working, the Snow1/Met City shear zone works. The whole region around us is broken up into smaller floes. Not recording all these actions. In the Panomax you can see cracking and smaller floes forming. This may be related to the action in the shear zone, however it is not clear if there was also not some swell involvement or differential wind forcing across floes.

May 13

08:20 Stern Lead opens

May 14

ship repositions to recover installations from the now rather small CO central floe.

May 15

evening/night Met City ridged to oblivion.

May 16

we left the floe for our journey to Spitzbergen.

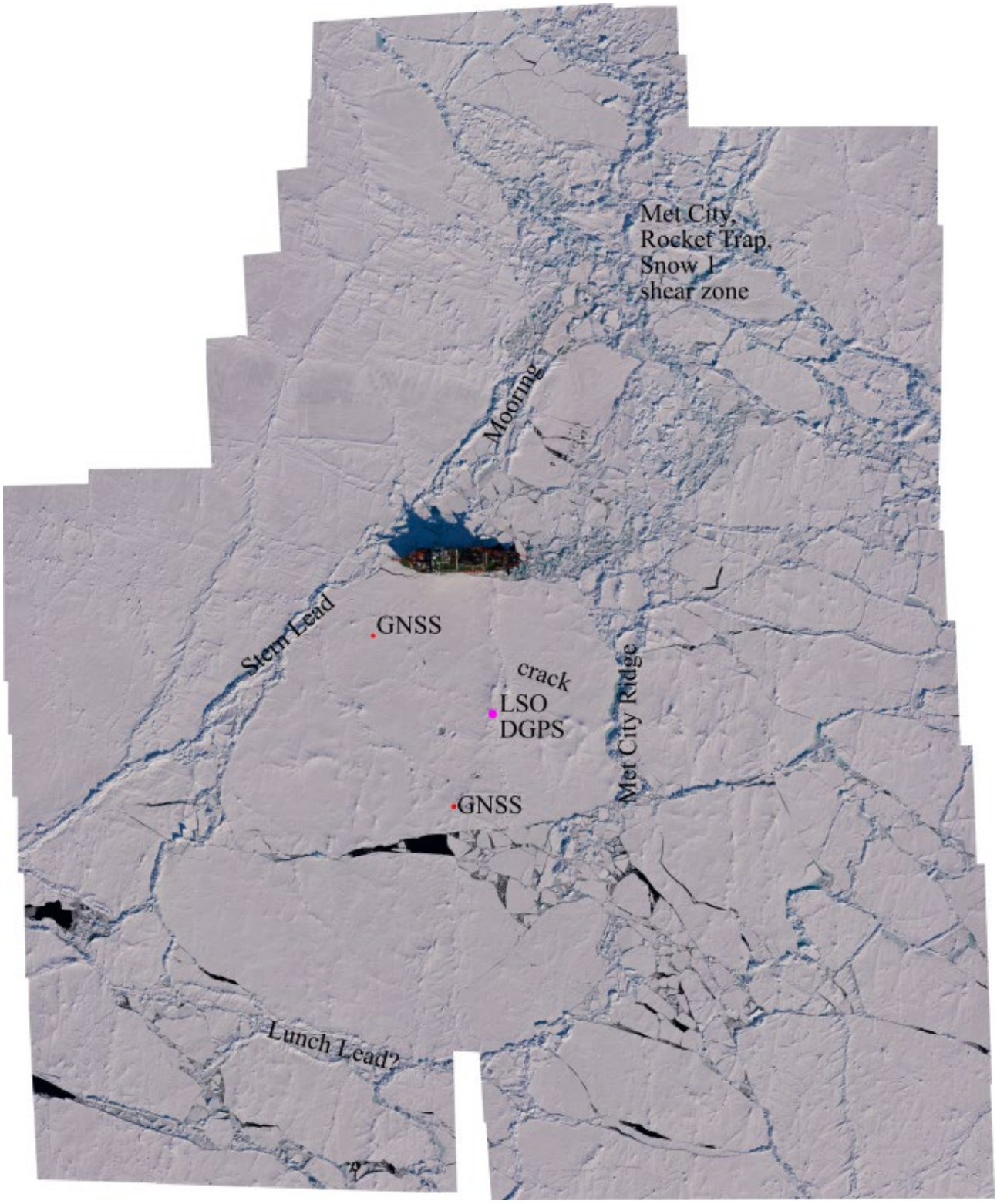

Fig. 4.9.14*: May 16th, the main floe of the central observatory has cracked into several pieces in response to the shear zone on the right of this image. Dynamics installations left on the central floe are marked. There was shear and ridging of the dynamic features we had tracked in the central observatory since March 11th, and the ridges and shear zones associated with these are marked. Mosaic of drone images provided by Manuel Ernst.*

4.9.4 Data management

All data are handled, documented, archived and published following the MOSAiC data policy (see APPENDIX). All device operations were logged in the AWI sensorweb portal and all sensor raw data files are stored in platform section of MCS.

4.8.5 References

Oikkonen A, Haapala J, Lensu M, Karvonen J, Itkin P (2017), Small-scale sea ice deformation during N-ICE2015: From compact pack ice to marginal ice zone, J. Geophys. Res. Oceans, 122, 5105–5120, doi:10.1002/2016JC012387.

4.10 Ridge Studies

Stefanie Arndt[1], David Clemens-Sewall[2], Robert Ricker[1], Amy Macfarlane[3], Philipp Anhaus[1], Steven Fons[4], Polona Itkin[5] (not on board), Mats Granskog[6] (not on board), Knut Vilhelm Høyland[7] (not on board), Glen Liston[8] (not on board), Don Perovich[5] (not on board), Mario Hoppmann[1] (not on board), Yusuke Kawaguchi[9] (not on board)

[1]DE.AWI
[2]US.Dartmouth
[3]DE.WSL/SLF
[4]US.NASA
[5]US.UiT/CSU
[6]NO.NPI
[7]NO.NTNU
[8]US.CSU
[9]JP.UTokyo

4.10.1 Objectives

Pressure ridges are formed by pilling up of crushed ice blocks during sea ice convergence. Often the features also shear. While the ridge sail is the obvious surface part of the ridge, the submerged part – ridge keel, is typically much larger and voluminous, taking up to 90% of the ridge volume. Both sails and keels are important surface roughness features that cause turbulence in atmosphere and ocean. During Leg 3 new ridge site in addition to the ones chosen on Leg 2 have been investigated in order to answer the following research questions:

- The ridge consolidation: The body a new pressure ridges is composed of ice blocks and air and water pockets between them – voids. The water-filled voids? will gradually freeze during cold season and the ridge will eventually consolidate. Since the winter observations of the ridges are rare, MOSAiC offers a unique opportunity to observe the ridge consolidation with direct observations (drilling and coring) and remotely (electro-magnetic induction)
- Redistribution of snow in the deformed ice: Ridges are traps for snow and MOSAiC gives an opportunity to observe seasonal development of snow thickness and stratigraphy in the ridge and its surroundings.
- Ridge-associated ecosystems: Pressure ridges remain the least studied Arctic ice-associated ecosystem, with a basic lack of data for the winter season and limited studies from other seasons. Neither are ridges represented in ecosystem models, they neglect the complex structure of ridge habitats, which is quite different from the level ice described in models. It is expected that pressure ridges will become an increasingly important component of the new Arctic sea ice regime dominated by FYI where the largest portion of the level ice melts completely in summer.

4.10.2 Work at sea

In the beginning of Leg 3, we continued the work in the established Sea Ice Ridge Observatory of ‘Fort Ridge’ on the Eastern flank of the main floe of the CO. However, during the break-up event on March 18, the ridge started to disintegrate and flatten, and therefore lost its ‘ridge status’.

We therefore scouted for new ridge sites in order to continue sampling also from elevated ice surfaces. As the numerous requests from team ICE and ECO could not be covered within one ridge site, two ridge sites have been identified for the ridge studies focusing on different aspects, as outlined below.

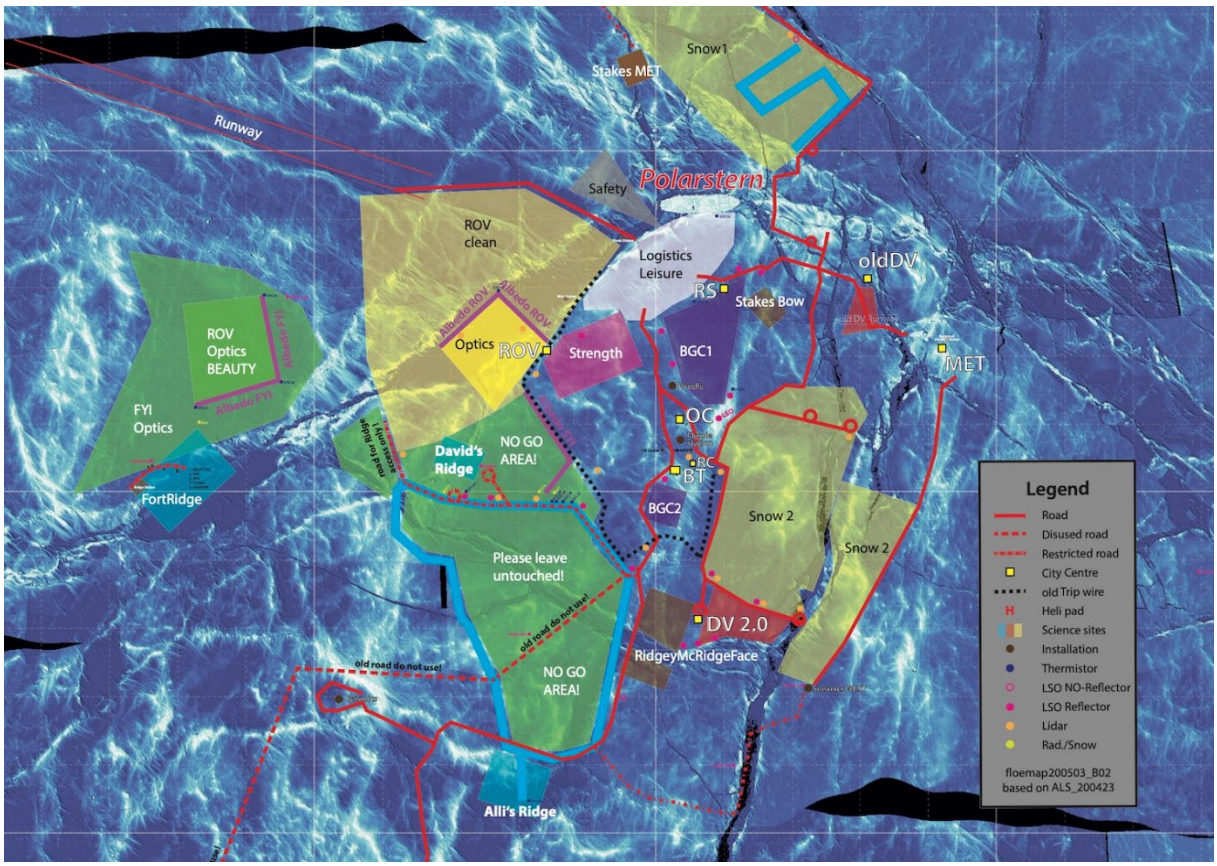

Fig. 4.10.1: *During Leg 3, on-site work was conducted on four ridge observatories: Fort Ridge, Alli’s Ridge, David’s Ridge and RidgeyMcRidgeFace.*

4.10.2.1 David’s Ridge

David’s Ridge starts near the former ROV tent and cuts through the near part of the Northern Transect. The ridge was formed in two stages. On March 11 between 10:20 and 10:30 UTC a crack opened up that would become David’s ridge, the ROV lead, and cut through the logistics area to the ship. By March 14, this crack was around 50 m wide near the Northern Transect (see lidar scan on March 14 for exact geometry) although it had experienced shear motion such that portions of the crack were closer together. The distance between two lidar reflectors on either side of the crack grew by 19 m. Nearer to the ROV tent shear motion had already started to build that section of David’s Ridge. Between March 15 and March 18 (most likely on March 15) the crack underwent further shear motion with the Ft. Ridge side moving towards map North and built an approximately 1 m high ridge (see lidar scan from March 18 for exact

geometry). Anecdotally this original version of David's ridge seemed to be mostly composed of ice that had formed in the March 11 crack.

Between March 18 and April 4, shear motion continued and increased the height of David's Ridge to approximately 2 m. This episode of growth may have deformed some of the Second Year Ice as well. The sense of motion was the same as before, the Ft. Ridge side moved towards map North. On April 6, a crack formed cutting through the ROV lead, the portion of David's ridge closest to the ROV site (that had already started ridging on March 14), and across the N Transect to the Stakes 1 lead following the edge of a small, old ridge. This crack was 3 m wide in places. Considerable snow drifts accumulated around David's Ridge but no major dynamics happened until April 27, 2200 UTC. On April 27 between 2200 and 2220 the "Logistics Crack" formed through the logistics area, separating the ROV hut from the Mechanics site, and along the spine of David's Ridge. The sense of motion was the piece of ice with Balloon Town and the 4 DTC's moving towards map North. Along David's Ridge this created an opening of about 2 m. Some additional movement happened in the N Transect portion of the April 6 crack as well. No additional movement happened until May 12. On May 12-13 the large dynamics event which caused the floe to break apart generated convergence at David's Ridge and raised the ridge to be approximately 2.5 – 3 m tall.

One big advantage was that the ridge is located within the operation range of the ROV site. The ridge is approximately 180 m long (measured from where it intersected other ridges on May 9) with 1.5 to 2 meters sail elevation over the level ice surface. The keel depth goes down to a maximum of 8 to 9 meters according to ROV multibeam surveys (Figure 4.10.2).

While on the one site of the ridge, the marked transects are ends on the turning circle close to the Northern Transect path, the other site indicates a "secondary" ridge (Figure 4.10.3).

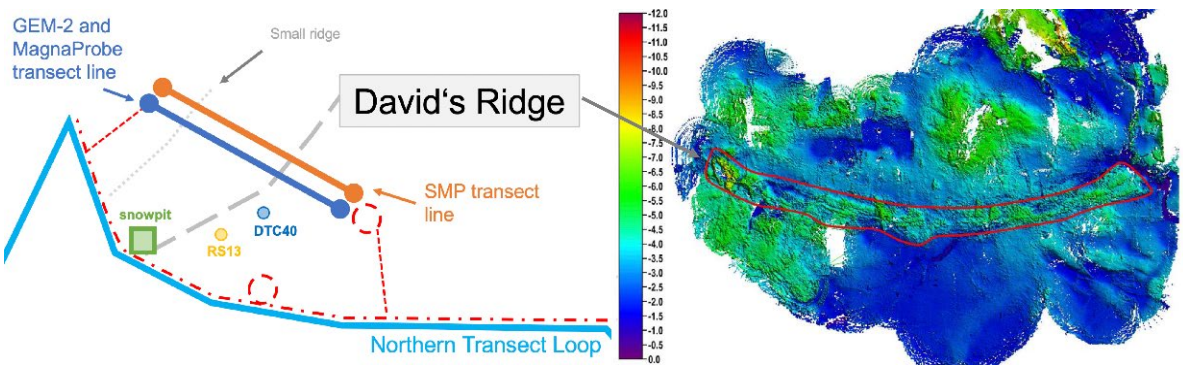

Fig. 4.10.2: *(left) Schematic of David's Ridge indicating all transect lines and installations. (right) High-resolution multibeam survey of David's Ridge (red area) and its surrounding showing the revealed ice draft of the area.*

Since the set-up of the observatory, the following on-site measurements have been performed during Leg 3:

- weekly sea-ice thickness and snow depth transects with GEM-2 and MagnaProbe
- weekly SMP transect
- one snow pit
- weekly ROV multibeam surveys at 20 m depth and high resolution along and across ridge transects at 10 m depth performed once one week prior to the latest major ice dynamic and destruction event?
- Optic transects as close as possible to the ice-ocean interface
- Terrestrial Laser Scans March 11, 14, 18; April 4, 11, 17, 22, 29, May 9. These scans were timed to bracket major dynamics events and blowing snow events.

In addition, the following sensors have been deployed on the ridge on May 06:

- Radiation station R13
- DTC40

Stress sensor FMI004 (which was deployed on leg 1) was at the end of the transect closest to Balloon Town. On May 4, a couple of Laser Strain Observing System reflectors were deployed near David's Ridge and record relative motion up to the May 12-13 storm. See the Dynamics section for more details on the dynamics instrumentation and measurements.

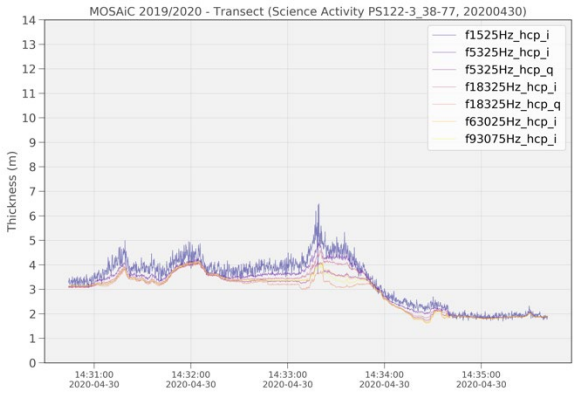

Fig. 4.10.3: *GEM-2 transect crossing David's Ridge on April 30. Transect starts left at small road, goes over a small ridge structure, David's Ridge, and ends finally at the turn circle close to the Northern Transect again (see Figure 4.10.2).*

4.10.2.2 Ridgey McRidgeFace Ridge aka ECO Ridge

Ridgey McRidgeFace ("RMRF") is located at the former Stakes 1 site. It was formed in the November 2019 deformation event between FYI and SYI floes, providing a diverse location for ice and water sampling by team ECO. The aim of using RMRF was to locate water-filled gap layers within the ridge and sample the water and surrounding ice for ecological parameters. Team ICE accompanied the sampling to drill ice cores for physical parameters (temperature, salinity, density) that would supplement the ecological data.

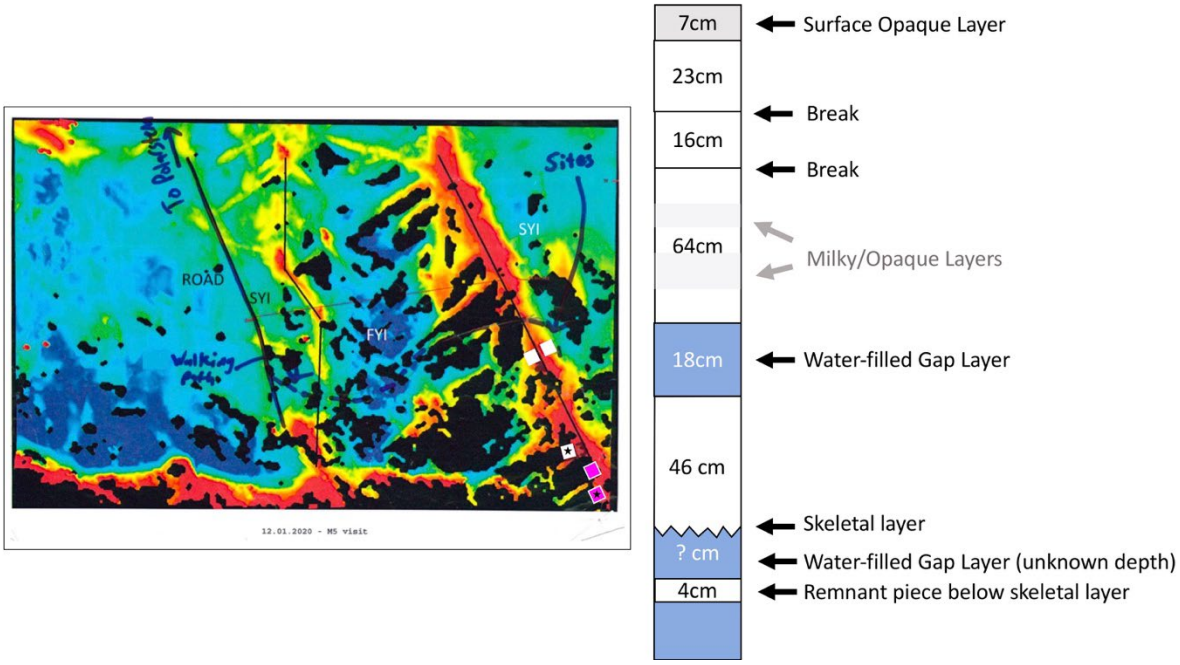

Fig. 4.10.4: *(Left) A TLS scan of "Ridgey McRidgeFace" (courtesy of D. Clemens-Sewall) with the ridge coring locations. White squares are locations from the first coring session (April 22), while pink squares are from the second ridge coring session (May 5). Stars indicate the plots where cores were taken. (Right) Profile of the SALO18 sea ice core drilled at RMRF on May 5. Water was pumped from the first gap layer.*

RMRF was visited twice during leg 3, on activity weeks 37 and 39. Each time, multiple locations were drilled with a thickness auger to search for the water-filled gaps. When one was found, 40L of water was pumped out by team ECO. Then, three ice cores were drilled: one for temperature, salinity and oxygen isotope analysis, one for team ECO who kept 10cm above the water-filled gap and 10cm below the gap for ecological processing, and one to measure sea ice density.

4.10.2.3 Alli's Ridge

During Leg 3, we walked once all three transects across Alli's Ridge (April 10) and read out the DTC data at the end of the leg (May 15).

4.10.2.4 Fort Ridge

As mentioned above, the Fort Ridge Observatory could not be used as a proper ridge observatory during Leg 3 due the disintegration of the ridge. However, several tasks have been performed before the break up, as outlined below. Also, all deployed installations during Leg 2 from team ICE are still in place. Therefore, the site had been visited several times for stakes reading and data downloads of the remaining DTCs on the ROV FYI optics grid nearby.

- The transect lines across Fort Ridge were sampled once during Leg 3 (March 05) before the ridge disintegrated.
- On March 08, the Ice-Mass-Balance Buoy R10 was deployed between the ROV FYI optics grid and Fort Ridge.

- Due to the upbreaking observatory and the respective ridging and lead opening, we rescued on March 23 DTC24 and DTC25.
- On May 10, a broken temperature sensor chain on buoy 2020T60 was replaced, and the buoy was left in its place on Fort Ridge.

4.10.3 Preliminary (expected) results

The different ridge observatories focusing on ridges of different ages, give the possibility to study age-related ridge processes and properties from both the sea-ice physics and interdisciplinary perspective.
These analyses will be mainly based on the autonomous systems deployed in the ridge observatories as well as the lab analysis of the ice core, after the termination of MOSAiC.

Ridges have a considerable impact on snow redistribution. The combined TLS and snow property datasets collected from David's Ridge will facilitate process-based studies of the impact of old and new ridges on snow processes.

Both AFZP-POPE buoys continue to operate as they did on leg 2. The dish plate antenna for communication on A-Deck of *Polarstern* had to be adjusted (but not moved) to account for a change in the ship's heading. AZFP-1 continues to log and store data on the internal memory of the buoy, while AZFP-2 sent data successfully during two data communication sessions on leg 3:

08.04.2020 Data recovery for the period 15.02.2020-19.03.2020
08.05.2020 Data recovery for the period 19.03.2020-08.05.2020

4.10.4 Data management

All data are handled, documented, archived and published following the MOSAiC data policy (see APPENDIX). All the instruments have been added into the system of SENSOR.awi.de and all the data has been or will be added to the MCS. The data will be submitted according the data policy of MOSAiC.

4.11 Remote Sensing Measurements

Lars Kaleschke[1], Reza Naderpour[2], Robert Ricker[1]

[1]DE.AWI
[2]DE.WSL/SLF

4.11.1 Objectives

The general objectives have been described in the MOSAiC science plan and in previous cruise reports. Here we only report about changes and the particular experiments conducted for leg 3 and otherwise refer to the aforementioned documents.

Leg 3 covers a period of strong change in environmental forcing conditions. The change of surface air temperature from below -40°C to above melting point and its associated change of the sea ice and snow surface properties has been observed with various active and passive instruments. These stationary measurements form the basis for a later analysis of the temporal variability. A relocation experiment towards the end of the time series enables to assess the spatial variability within the area of the remote sensing site which was governed by large artificial snow dunes in the lee of the instruments. Finally, we investigated the influence of the snow cover on the microwave brightness temperature by a dedicated snow removal experiment. The remote sensing measurements were accompanied by measurements of the

dielectric permittivity, ice cores, snow pits, aerial and terrestrial laser surface elevation and underwater draft ROV surveys, GEM sea ice thickness and magnaprobe snow depth tracks, and thermistor string installations.

The extensive data set collected will be useful for the verification of sea ice microwave radiative transfer models and various sea ice and snow physics parameterizations that are required to improve satellite retrieval algorithms for key sea ice and snow parameters.

4.11.2 Work at Sea

MOSAiC Central Observatory

Several remote sensing (RS) instruments were deployed and operated on the ice inside the Central Observatory (CO), in addition to those deployed on the ship itself. A unique advantage of the instruments deployed is that it provided for the first time a complete set of passive and active microwave observations collected over similar snow and ice types spanning frequencies from 1.4 to 89 GHz. Table 4.11.1 gives an overview on all instruments operating during Leg 3, the responsible person maintaining the instruments during Leg 3, and the responsible PI on land.

When Leg 3 arrived to the CO, the Remote Sensing Site 3 (RS3) was functional and measurements were ongoing with the following instruments: SSMI, GNSS-R, UWBRAD, L-Scat, C-Scat, Infrared and Visual Camera. ELBARA was not functioning because of its broken instrument computer. We managed to fix ELBARA and redeploy it at RS3 during the Leg2/3 handover and with the help from Leg 2 personnel. Furthermore, HUTRAD was deployed at RS3 which resulted in a total number of 9 functional instruments.

Tab. 4.11.1: *List of remote sensing instruments deployed/redeployed Leg 3*

Instrument	Details	PI	Institution	Leg 3 responsable
On the ice				
L-band Scatterometer	1.26 GHz scanning radar	R. Scharien	U. Victoria	R. Ricker
C-band Scatterometer	C-band (~5 GHz) scanning radar	J. Yackel	U Calgary	R. Ricker
MW Radiometer UWBRAD	Ultra-wideband 0.5 – 2 GHz radiometer (P to L-band)	J. Johnson	Ohio State University	L. Kaleschke
MW Radiometer ELBARA	1.4 GHz (L-band)	M. Schwank/ T. Casal	WSL/ESA	R. Naderpour
SSMI Radiometer	19, 37, 89 GHz (K, Ka, W-band)	J. Stroeve	U Manitoba	L. Kaleschke
GNSS-R	reflected GNSS signals from snow/ice	E. Cardellach/ T. Casal	ICE-CSIC/ESA	L. Kaleschke
Infrared Camera	Surface temperature	G. Spreen	U Bremen	R. Naderpour
Video Camera	Visual overview of RS site	G. Spreen	U Bremen	R. Naderpour

HUTRAD	6.85, 10.65, 18.70 GHz	J. Lemmetyinen/T. Casal	FMI/ESA	R. Naderpour/L. Kaleschke
HyperSpectral Camera	Specism IQ	G. Spreen	U. Bremen	R. Naderpour
On Polarstern				
GNSS-R & atmosphere	reflected GNSS signals from snow/ice and GNSS for atmospheric water vapor	M. Semmling	GFZ	L. Kaleschke
GNSS Ionosphere	Ionospheric scintillations for GNSS measurements	F. Fohlmeister	DLR	L. Kaleschke
MW Radiometer EMIRAD2	1.4 GHz (L-band)	S.Savstrup Kristensen/ T. Casal	DTU/ESA	L. Kaleschke

Refer to Leg 1 and Leg 2 Cruise Reports for detailed descriptions on location, instrument setup and activities of Remote Sensing Sites 1—3.

Remote Sensing Site 3 (start: 24.02.20202, end: 2020.03.11)

The RS3 was established and brought to operational status during Leg 2. Figure 4.11.1 shows a view of the RS3 in the beginning of Leg 3. The measurements were ongoing at this site until 11 March 2020 when a crack opened up at the site cutting the site away from the main floe. This crack passed by close vicinity of the RS hut as well as ELBARA, HUTRAD, and UWBRAD within a few meters. On the evening of 11 March, a team of four personnel from the ICE team and the logistics were dropped on site by helicopter to move the instruments away from the lead to save them from possibly drowning and/or being crushed by the anticipated ridge formation. Figure 4.11.2(a,b) show a picture of RS3 after the crack in the ice and the RS hut conditions after ridge formation at RS3, respectively.

Fig. 4.11.1: *Overview of RS3 site as of 19 Feb 2020. (Photo: Screenshot from the University of Bremen's visual camera, installed on top of the RS hut).*

Therefore, on 11 March 2020, all measurements on RS3 had be stopped. After the ridge formation and increased danger of serious damage to the RS hut and instruments, the decision to was made relocate the site. Therefore, given the highly dynamic ice conditions on the floe

hosting RS3 and the Met City, the instruments were brought to the logistic area to be redeployed at RS4.

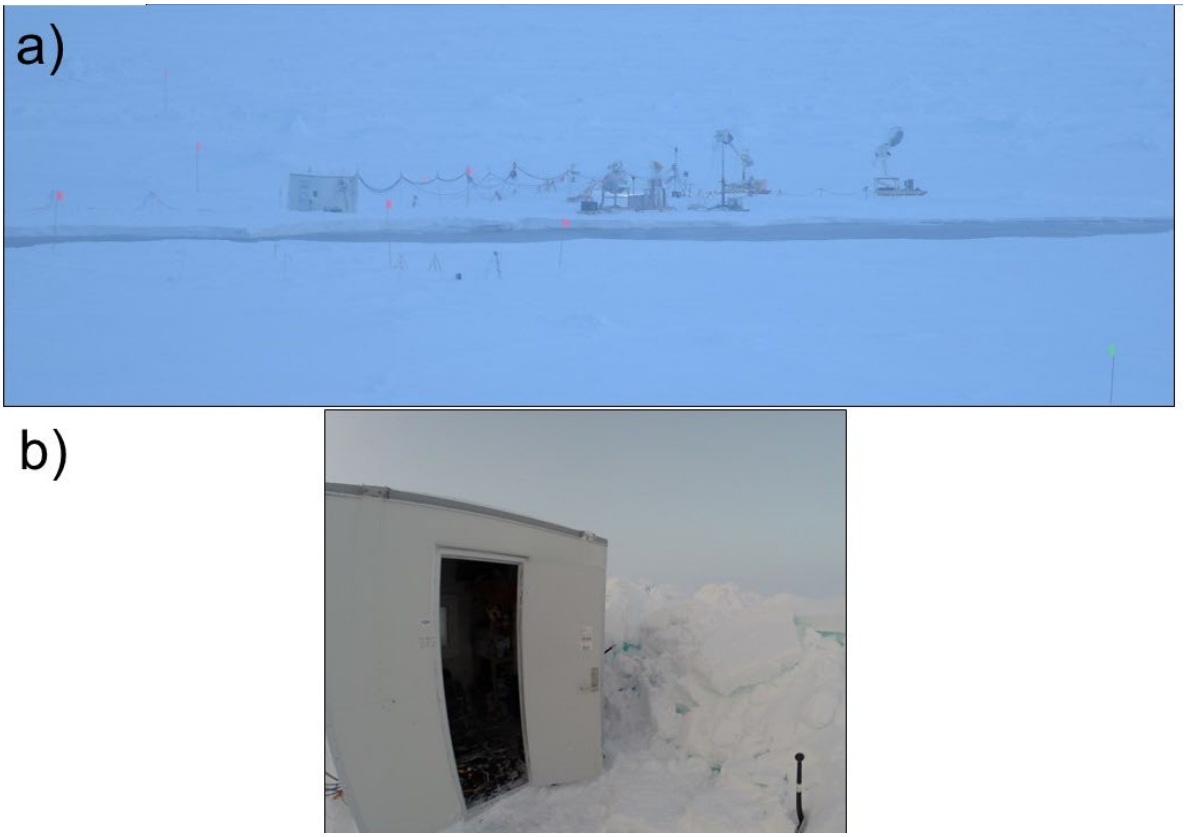

Fig. 4.11.2: *(a) Overview of RS3 site on 11 March 2020; (b) RS hut on 17 March 2020 endangered by the forming ice ridge. (photos: panel (a) by Reza Naderpour, panel (b) by Lars Kaleschke)*

Remote Sensing Site 4 (start: 2020.03.25, end: 2020.05.05)

We decided to situate the new remote sensing site (RS4) at the southern edge of the BGC1. Given the strong ice dynamics and the shrinking size of the stable parts of the floe, this decision made sense because a) it was situated on a fairly stable part of the floe, b) it would provide easy access to the site without necessary bear guarding and even in sub-optimal weather conditions, and c) it would make it exponentially easier to save the instruments given the short distance to the logistic area and reach of the ship's cranes. Figure 4.3.5 shows the location of instruments on a TLS snow map.

The following instruments, also listed in Table 4.11.1, were redeployed at RS4: ELBARA, HUTRAD, SSMI, GNSS-R, Infrared and Visual Camera, HyperSpectral Camera, and C-Scat. RS4's operation continued until the planned end date of scientific measurements on Leg 3 on the ice after which the instruments were packed and brought onboard Polarstern.

Onboard Polarstern

Ionospheric scintillation GNSS

A short term data collection problem of the ionospheric GNSS around 11 March was solved by removing snow from the antenna and a reboot of the receiver.

EMIRAD-2 L-band radiometer

A three-week EMIRAD-2 data gap from 25 March to 13 April was triggered by a power outage and subsequent instrument failures. A short-circuit of a thermostat in the EMIRAD-2 enclosure reestablished the power to the instrument. Further troubleshooting over the next three weeks identified a problem with the system clock of the internal computer which prevented the collection of new data. Data reports have been produced using a binary (Unpack.exe) and results were interpreted on land by DTU contact persons. A 24-hour sky calibration was performed on 23 April which subsequently revealed a potential degradation of the radiometer. DTU suggested more frequent (daily) sky calibrations which have been regularly performed since then. On 17 May EMIRAD-2 stopped producing data, a power-cycle helped to start the production of data again on 19 May.

Brief Description of the RS instruments used in Leg 3

In total 14 different instruments were operated as part of the Remote Sensing task during Leg 3, 10 on the ice and 4 onboard. All of the instruments listed in Table 4.11.1 worked at some point during Leg 3; however, some stopped measurements at a time. More specifically, L-Scat and UWBRAD were operational on RS3. However, L-Scat was damaged by falling on the ice during a strong storm and could not be repaired and redeployed at RS4. UWBRAD's operational status was unstable and irregularly faulty. Given its design and implementation (high center of gravity, no sled, and difficult to dismount) and with consideration of possible need of emergency rescue, UWBRAD was not redeployed at RS4.

A detailed description of the remote sensing instruments can be found in Leg 2 cruise report. Here we give a brief overview of the two new instruments, HUTRAD and the HyperSpectral Camera which were deployed during Leg 3.

HUTRAD

Helsinki University of Technology RADiometer (HUTRAD) is composed of three radiometer units measuring at 6.85 GHz, 10.65 GHz, and 18.70 GHz. The refurbishment of this instrument was finished in January 2020 and it was sent to MOSAiC for measurements of sea ice.

HUTRAD was assembled and put in operation at RS3 from 8—12 March, 2020. After relocation, HUTRAD measurements started again on April 3 and continued until the end of RS4 on 5 May 2020. Figure 4.11.3 shows HUTRAD operated at RS4 during Leg 3. Regular sky measurements at multiple elevation angles were performed for later calibration of HUTRAD data and computation of brightness temperatures.

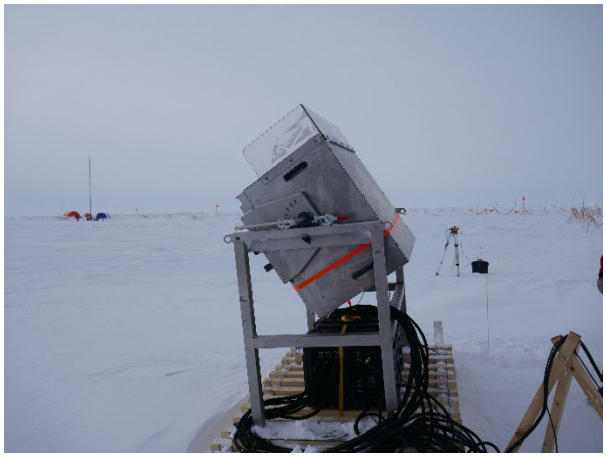

Fig. 4.11.3: *HUTRAD radiometer at RS4 performing sky measurement on 14 April 2020. (photo: Lars Kaleschke)*

HyperSpectral Camera

The HyperSpectral Camera (HS Cam) operates at a wavelength range of 400—1000 nm with a spectral resolution of 7 nm and 204 spectral bands. This camera was first tested on the ship and later installed at RS4 on 15 April 2020 as part of the optical remote sensing program of MOSAiC. HS camera was operated using time laps mode until 5 May 2020. However, its operation was sometimes stopped due to problems with power and battery charger for this setup and the thermal camera. The data from HS cam was uploaded to the MCS; however, the connection between the camera and its control toughpad could no longer be established. The technical problem is not yet identified. Figure 4.11.4 shows the HyperSpectral Camera (right) and Thermal/Visual Camera setup at RS 4.

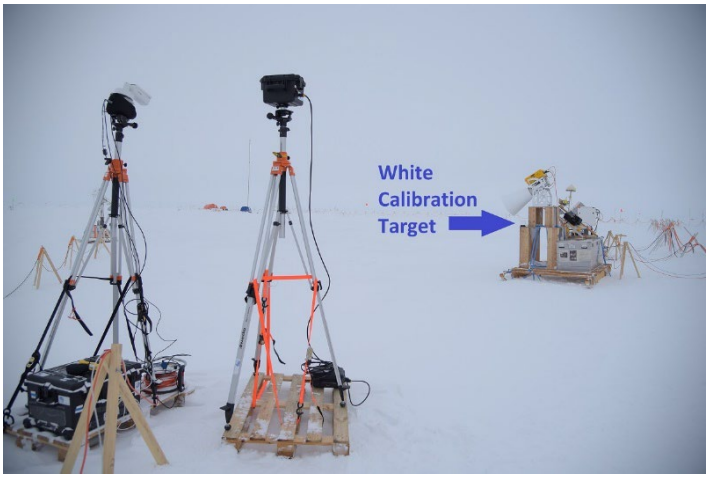

Fig. 4.11.4: *HyperSpectral Camera (right tripod) and Thermal+Visual Camera (left tripod) setups at RS 4 on 15 April 2020. The white calibration target for the HS cam was placed on the corner of ELBARA scaffold.(photo: Reza Naderpour)*

4.11.3 Preliminary (expected) results

All RS instruments (Table 4.11.1) will provide a time series of the seasonal development of their measured parameters, i.e., microwave brightness temperature and backscatter at different frequencies, reflected GNSS signals, infrared temperatures and visual images. Their variability and changes will depend on the atmospheric conditions, e.g., temperature and snow accumulation. The combination of on-ice remote sensing measurements together with the comprehensive snow and ice measurements will allow to improve microwave emission and scattering models of snow and ice, which in turn will lead to improved satellite remote sensing datasets.

Data recorded and stored in the MCS during legs 1—3 are primarily raw, uncalibrated measurements like backscatter power from the radars and voltages from the radiometers. We here show a few exemplary early results.

SSMI and HUTRAD brightness temperature time series

A main aim of the MOSAiC remote sensing program is to better understand the measured brightness temperatures as a function of sea-ice and snow in-situ parameters. We experienced a wide range of surface temperatures during leg 3. We here show that warming events and associated changes of the snow surface can lead to an underestimation of the ice concentration. The temperatures on 16 April and 19 April close to the melting point changed the snow surface characteristics and reduced the surface roughness. This was visible by strong specular surface reflection ("glaze effect") in the direction of the sun. The effect of a specular reflecting surface comes along with an increased polarization of the reflected electromagnetic waves.

The SSMI-radiometer is a passive microwave sensor that measures at frequencies of 19 GHz to 89 GHz, the same frequencies of the SSMI satellite series. The HUTRAD radiometers operate at three frequencies 6.9, 10.7, and 19 GHz that will be included for the Copernicus Radiometer (CIMR) mission. Unfortunately, the 37 GHz channel of the SSMI radiometer was malfunctioning, generating only random signals, and repairs were not successful. The thermal control and reference temperatures for the HUTRAD 10.7 GHz channel failed after 11 March resulting in fluctuations of the system temperature between -10°C to 10°C. Nevertheless, the 6.9 GHz and 19 GHz channel operated at a stable internal temperature of 10°C ± 0.02°C.

The following results are only preliminary by assuming a time constant linear relation of radiometer signals and brightness temperatures. Linear calibration coefficients were derived as a result of a linear regression using several (>10) measurements with cold (sky) and hot (ambient temperature) targets.

The SSMI system stores quick-look values which are useful to verify that the radiometer is producing reasonable data. The absolute values and scale of these quick-look values are not accurate. The HUTRAD system stores signal counts and the reference temperatures. We used microwave absorbers at different ambient temperatures as a hot load and the sky background at different elevation angles as cold load. These two methods allow to derive regression coefficients to calculate preliminary calibrated brightness temperatures from the SSMI quick-look values or HUTRAD signal counts, respectively. We used two different 24” x 24” x 0.5” microwave absorber plates named “PPG CUMMING MICROWAVE” C-RAM MMW2 and MT24 with the first one applicable for higher frequencies and the latter one for the lower frequency channel. In addition, we had absorber drums that came with the HUTRAD system. The latter ones were more difficult to handle and gave no stable calibration signal as tested on April 11. We henceforth used only the absorber plates MT24 and MMW2 hold together with the MT24 side towards the antenna for the lower frequencies and MMW2 for 89 GHz, respectively. The temperature was measured in between both plates using a HH376 RTD thermometer. For the clear sky calibration, we calculated the expected brightness temperatures using the atmospheric absorption coefficients of the Rosenkranz (1998/1999) model with temperature and humidity profiles from the near coincident 6-hourly radiosondes.

A manual change of the elevation angle is necessary for the HUTRAD instrument. The timings for elevation changes and calibrations were recorded in a field book, a transcript is stored on MCS in the HUTRAD folder. The SSMI instrument can scan at different elevation angles, however the elevation angle of the positioner is not correctly aligned to the measured radiation in the data set, it has a time delay which is not always constant. The time taken from a GPS sensor is recorded with gaps by the SSMI data logger.

The preliminary brightness temperature time series from HUTRAD (Figure 4.11.5) and SSMI (Figure 4.11.6) show some interesting variability associated with the warming events. Spurious jumps in the SSMI data are also the result of problems with the alignment with the incidence angle. To resolve these issues requires a more careful investigation and advanced post-processing.

We calculated the ice concentration from the 89 GHz channels using the ASI algorithm (Kaleschke et al.,2001). Because we know that the radiometer field of view was actually 100% covered with ice we can interpret deviations from this value as errors. It is evident that the

warming event had a substantial impact on the polarization and the derived ice concentration (Figure 4.11.7). The resulting underestimation of the ice concentration amounts up to 20%.

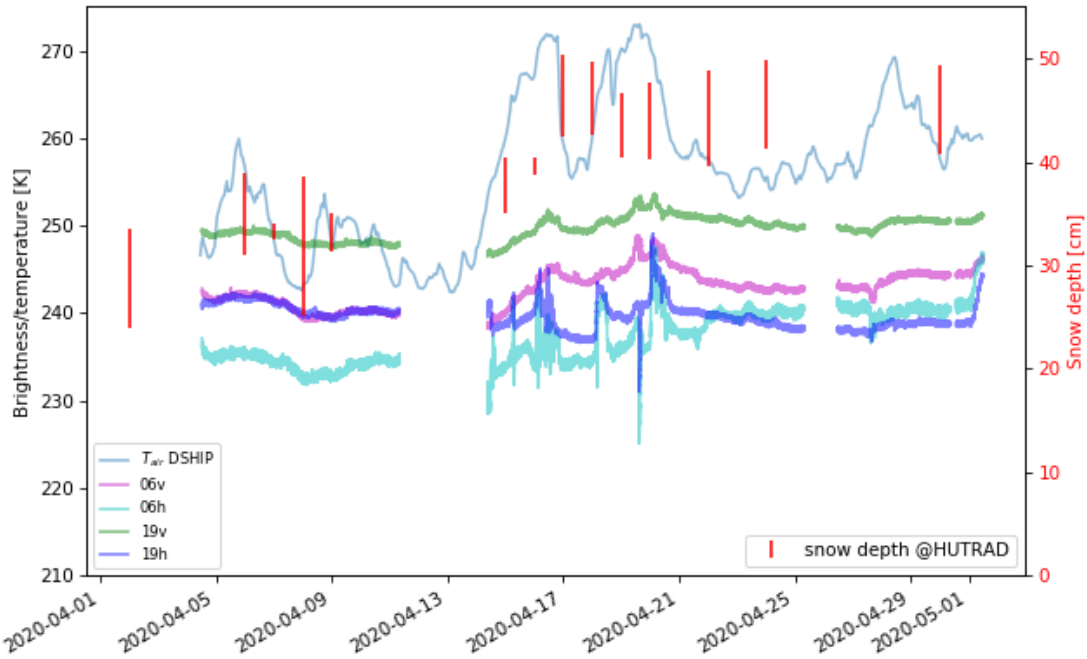

Fig 4.11.5: *Preliminary brightness temperature time series from HUTRAD at 45° elevation angle together with 29-m air temperature (DSHIP) and readings from a snow ruler. The red bars represent mean and standard deviation of snow depth in front of HUTRAD. Data for deviating elevation angles are not shown.*

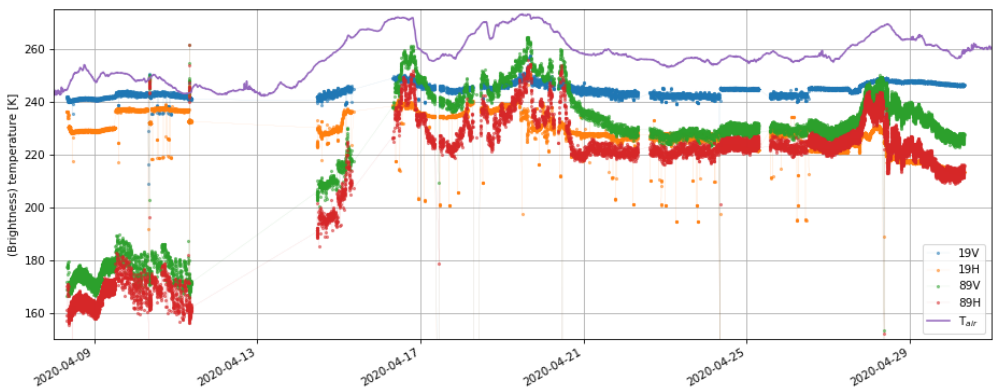

Fig 4.11.6: *Preliminary time series of vertically and horizontally polarized microwave brightness temperatures at 19 GHz and 89 GHz recorded with the SSMI radiometer during Leg 3. The selected incidence angle is 45° (not always true, see text). Data gaps are caused by different scanning modes and data recording problems of the system.*

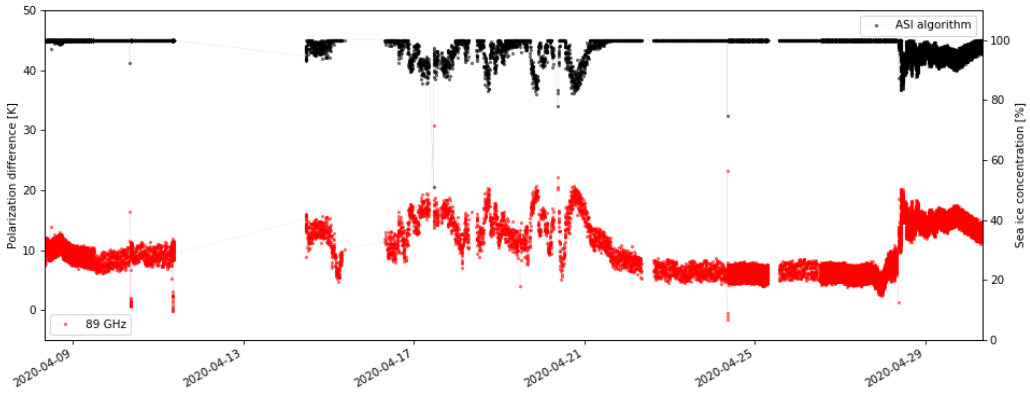

***Fig 4.11.7**: Ice concentration derived from the 89 GHz polarized brightness temperature difference (vertical minus horizontal polarization) according to the ASI algorithm (Kaleschke et al, 2001).*

4.11.4 Leg 3 Experimental Measurements

Spatial variability / displacement experiment

This experiment was designed and performed to investigate the heterogeneities of sea ice and snow cover properties and their effects on the radiometric signatures between 1.4 GHz and 18 GHz. The instrument displacement path was along two lines at two sides of the RS site. The radiometer measurements were performed at 14 flagged locations each one four meters away from the neighboring locations.

On April 30 snow depth was measured with a magnaprobe and sea ice thickness was measured with GEM along the marked locations while keeping some distance to avoid interference with metal objects and poles close to the site. Terrestrial Laser Scanning (TLS) was performed to acquire high resolution surface roughness and topography information. For each of the 14 flagged locations, three Snow Micro Pen (SMP) measurements were conducted to gain information on snow density profile and specific surface area and their local heterogeneities relevant to radiometers' footprint area(s). The "surface" open-end resonator sensor together with the FieldFox VNA was used to measure the complex permittivity of the snow surface. Accordingly, three measurements were conducted at each of the 14 flagged locations. These measurements were conducted in the frequency of 300 kHz to 5 GHz.

At each of the locations a multi angle measurement round was conducted with ELBARA within the angular range of 40° to 80° (nadir angle). Each measurement included three cycles of horizontal and vertical polarization loads. We skipped the HL, CL, and AL measurements to save time but sky measurements were performed at the beginning and end of the transect. The instrument is highly stable once it has reached its target physical temperature of 15°C. Unfortunately, the receiver pin for the horizontal polarization was broken; therefore, the measurements are limited to V pol.

After completing the displacement experiment path with ELBARA from flag 1 to 14, HUTRAD was placed to observe the undisturbed areas from flag 14 to 1. Measurements at two nominal angles of 45° and 60° were conducted at each flag. However, due to shortage of time, only flags 14 to 10 could be covered on May 1st. On May 2nd, measurements with HUTRAD at flagged location 1 to 14 were performed, this time with support of a Skidoo for pulling the instrument. Preceding sky measurements at 120° were conducted in addition to the measurements at 45° and 60° to better mark the change of positions. The different stations

are now obvious as a clear signal in the radiometer data and can be used to extract the multi-angle observations for the respective stations as presented in Figure 4.11.8.

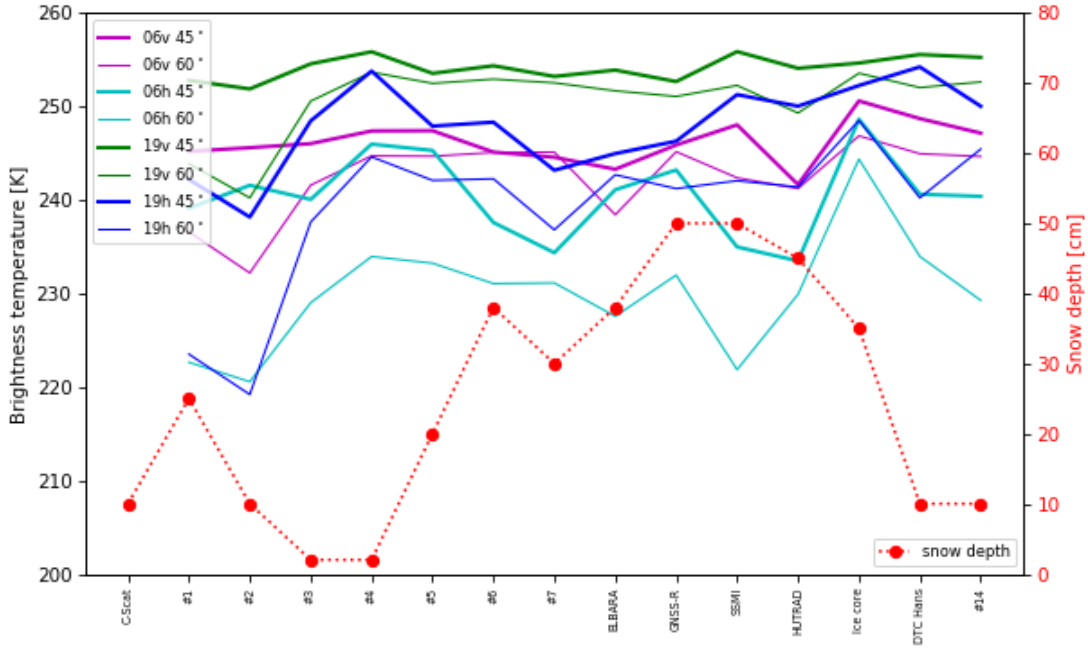

***Fig 4.11.8**.: Brightness temperatures measured with HUTRAD at 14 locations at the RS site on 2 May 2020. The graph shows brightness temperatures at two polarizations with two different elevation angles, respectively. In addition, the snow depth as measured with a ruler stick is indicated in red.*

Further to the radiometers, we also carried out a displacement experiment with C-Scat along a transect at the Remote Sensing site on 4 May 2020. Therefore, we have moved C-Scat along a 16 m transect with scanning positions every 4 m (Figure 4.11.9). The scan files for the corresponding scan positions are listed in Table 4.11.2.

***Tab. 4.11.2:** List of scan positions for the C-Scat displacement experiment.*

Position	UTC start scanning on 04 May 2020	Files
0 m	07:46	Scan-20200504-074635
		Scan-20200504-074715
		Scan-20200504-075614
4 m	08:02	Scan-20200504-080233
		Scan-20200504-080322
		Scan-20200504-081213
8 m	08:18	Scan-20200504-081903
		Scan-20200504-081949
		Scan-20200504-082841
12 m	08:32	Scan-20200504-083255

		Scan-20200504-083343
		Scan-20200504-084239
16 m	08:46	Scan-20200504-084644
		Scan-20200504-084732
		Scan-20200504-085628

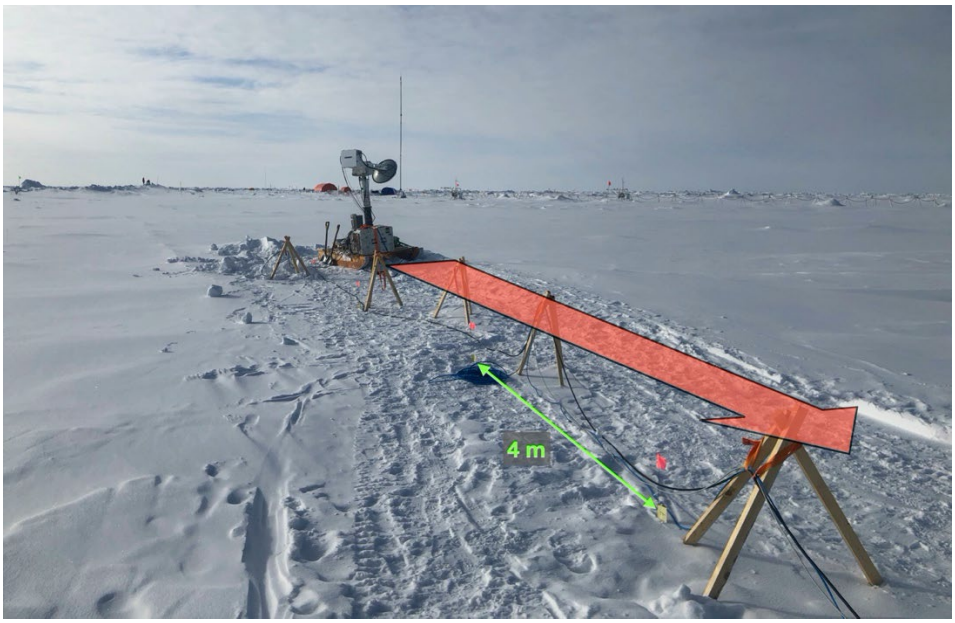

***Fig 4.11.9**.: Displacement experiment with C-Scat along 16m transect with 4m intervals. (photo: Robert Ricker)*

Snow removal experiment

Snow has both an effect on the permittivity and temperature gradient at the sea ice surface. On 2 May we removed the snow from an area of about 5 m x 3 m x 0.22 m in ELBARA's and HUTRAD's field of view, close to the thermistor string installation (DTC Hans) corresponding to flags 12 and 13 as described above. Figure 4.11.10 shows a view of the two radiometers performing measurements over snow-free sea ice.

Fig 4.11.10.: *Displacement experiment at RS 4 with ELBARA (front) and HUTRAD (back) looking at the snow-free sea-ice. (photo: Reza Naderpour)*

The temperature at the snow surface was about -13°C, and -8.5°C the at the snow-ice-interface just after the snow removal on 2 May, 13:15 UTC. The radiometer measurements of the snow-free sea ice surface continued until 5 May, 8:30 UTC. Figure 4.11.11 shows the change of brightness temperature which was caused by the removal of the snow. All brightness temperatures were significantly reduced with an outstanding reduction of about 10 K for the horizontal polarization at 19 GHz.

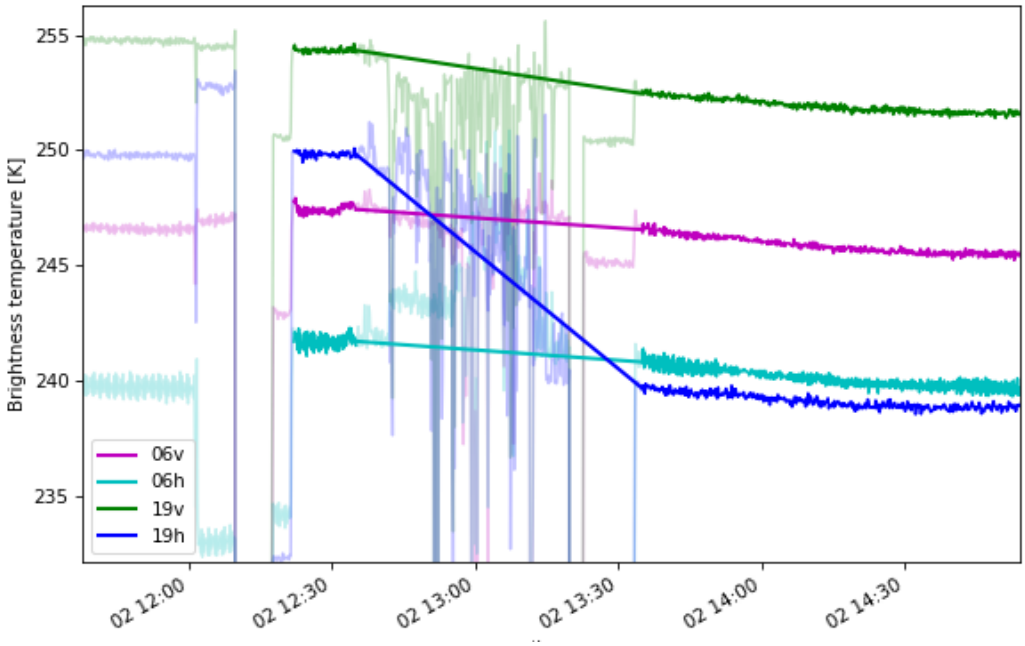

***Fig 4.11.11**.: Brightness temperatures measured with HUTRAD at 45° elevation angle before, during, and after the snow removal experiment. The duration of the snow removal process and elevation angles different from 45° are shown transparent. The solid lines indicate the change of brightness temperature resulting from the removal of snow with the strongest change visible in the 19 GHz horizontal polarization.*

Snow and Ice Complex Permittivity Measurements

Complex permittivity of sea ice and snow is a crucial parameter determining electromagnetic characteristics of these media and link the microwave remote sensing observation to medium properties such as snow density and liquid water content as well as sea ice salinity, density, and microstructure. Therefore, using a Vector Network Analyzer and open-end microwave resonator sensors, the frequency response of sea ice and snow were measured.

Together with electromagnetic simulations, one can retrieve the complex permittivity of ice and snow. Several cores were used for these measurements such that each core was cut in smaller sections (5 to 10 cm long) and the frequency response of each was measured. For these cores, (one at RS 4 and others from various locations of the floe and different types of ice) other parameters such as density, salinity and electrical conductivity were measured too.

4.11.5 Data management

All data are handled, documented, archived and published following the MOSAiC data policy (see APPENDIX). All final data of all on-ice and onboard remote sensing instruments will be stored at the MOSAiC Central Storage (MCS) and at PANGAEA (World Data Center PANGAEA Data Publisher for Earth & Environmental Science (www.pangaea.de)) after post-processing and quality checks. Storage and release of data follow the MOSAiC data policy.

All data are handled, documented, archived and published following the MOSAiC data policy.

4.12 Buoy Deployments in the Distributed Network

Jennifer Hutchings[1], Philipp Anhaus[2], Stefanie Arndt[2], Jari Haapala[3] (not onboard), Ruibo Lei[4] (not onboard), Marcel Nicolaus[2] (not onboard), Dirk Notz[5] (not onboard)

[1]US.Oregon SU
[2]DE.AWI
[3]FI.FMI
[4]CH.PRIC
[5]DE.UHamburg

4.12.1 Objectives

The distributed network (DN) includes an array of GPS positioning buoys and SVPs that are used to monitor sea ice deformation on scales of kilometers to a couple of hundred kilometers. This is embedded in the International Arctic Buoy Program network, which provides regional coverage. October through February this array became skewed with closing and shear on the eastern (upstream) side compared to the western (downstream) side of the array. Our objective for GPS buoy deployments during leg 3 was to fix gaps and skewedness in the DN such that deformation can continue to be monitored through the following three legs.

4.12.2 Work at Sea

With the returning light it was possible to land at sites in the distributed network without landing pads and lights. We took advantage of this to reseed the distributed network P-sites (*figure 1.9*) to maintain a symmetrical array about the Polarstern suitable for monitoring sea ice deformation. There were also deployments of radiation buoys made at some of the L-sites.

Buoy deployments by Helicopter

Flights were made on March 17, March 22 and April 4 to deploy SVP, Universal Tracker and SIMBA buoys throughout the distributed network. On April 24th Philipp Anhaus, Steven Fons, Alexey Niubom deployed an ice-mass-balance buoy (R12) at the L3 site. See Table 4.12.1 and Chapter 4.6 (Optics) for more details.

Buoy deployments by foot and skidoo

Several buoys were deployed in and close to the Central Observatory. This includes two SIMBAs, a snow buoy and 5 radiation buoys. We also deployed four SVP buoys to mark the locations in the Central Observatory so leg 4 can find the site on return. See table 4.12.2.

Buoy maintenance by helicopter

During PS122.3 each of the two ITBOBs (Ice-Tethered-Bio-Optical-Buoy) deployed on the L1 (2019R8 / IMB074) and the L2 (2019R9 / IMB075) site as well as the IMBflex (Ice-Mass-Balance) buoy on L3 (2019M30 / IMB084) required maintenance.
The ITBOBs record incoming, reflected, and through snow and sea ice transmitted irradiance, changes in snow depth, oxygen, conductivity, temperature, CDOM and chlorophyll fluorescence, and scattering in the water column. In addition, a thermistor chain is measuring the temperature of air, snow, ice, and water. Moreover, a camera is installed to observe the sensors and the changes of the environment close by. The main component of the IMBflex is a thermistor string measuring air, snow, ice, and water temperatures. In addition, bio-optical data (Eco Triplet, Optode und CTD) are recorded under the ice and a snow pinger above the surface is monitoring the change in the snow surface. A camera is attached as well.

The buoy 2019R8 / IMB074 on the L1 site needed a system reboot after April 05. This was successfully conducted on April 22 and data were recorded even during the gap. According to

recent photographs recorded from the webcam the metal frame where the RAMSES radiometers are attached is tilted due to the formation of a ridge and subsequently a lead (not shown).

The battery of buoy 2019R9 / IMB075 on the L2 site drained and data stopped being recorded on March 17. The battery was successfully exchanged on April 17. However, since February 06 snow pinger, Eco triplet, Optode, and CTD data are not recorded due unknown reasons. This issue could not be solved during PS122.3. Since April 10 the buoy 2019M30 / IMB084 on L3 stopped recording data. This issue could not be solved during PS122.3. Further, the buoy was (is most likely again) completely buried in snow.

Over the course of Leg 3, all active Snow Buoys in the DN have been visited at least once. Doing so, the actual distances between the sensor and the snow/air interface has been measured as well as partially the actual snow depth. All readings are documented in the LogBook in the subsection “Distributes Network (DN)”.
Snow Buoy 2019S84 at M1 was flipped when it was visited on May 02. As all cables were still connected, the buoy could be set up again and is sending useful data since then.
In contrast, Snow Buoy 2019S87 at M5 died on April 13. During the visit of the site on April 26, the upper part of the mast was completely disconnected. The mast could be recovered and was brought back to the ship, while the deeply frozen-in body was left behind.

Buoy maintenance by foot and skidoo

The two salt harps deployed during PS122.2 at the SYI dark site / LM site on January 15 needed maintenance. This included a battery change of the controller battery and several attempts to filter out broken modules. Currently the modules 1, 2, and 3 are connected which yield reasonable data. However, the aim is to connect at least one more functioning module in order to retrieve a whole profile.

Tab 4.12.1: *Buoys deployed in the distributed network during MOSAiC Leg 3.*

	Buoy Type	IMEI	Site	Time Deployed	Latitude	Longitude	Deployed by	Buoy Owner	Ice Thickness	Freeboard	Snow Depth
2020P210	SVP	300234010082440	P75	3/22/20 10:31	85.8858	17.9916	Hutchings	Haapala			
2020P211	SVP	300234010084660	P76	3/22/20 10:44	86.0572	21.5399	Hutchings	Haapala			
2020P213	SVP	300234010307830	P77	3/22/20 10:58	86.4110	20.4387	Hutchings	Haapala			
2020P214	SVP	300234011097770	P78	3/22/20 10:17	85.8436	14.0495	Hutchings	Haapala			
2020P215	SVP	300234011091780	P79	3/22/20 10:05	85.9451	11.4272	Hutchings	Haapala			
2020P160	ISVP	300234068219470	P80	3/22/20 13:06	86.3047	-5.0542	Hutchings	Ruibo Lei			
2020P216	UT	300234068280900	P70	3/17/20 14:35	86.7512	15.0341	Hutchings	Hutchings			
2020P217	UT	300234068281900	P71	3/17/20 15:25	86.9512	11.0002	Hutchings	Hutchings			
2020P218	UT	300234068283720	P72	3/17/20 15:04	87.0002	12.0138	Hutchings	Hutchings			
2020P219	UT	300234068283890	P73	3/17/20 14:58	86.8016	8.7057	Hutchings	Hutchings			
2020P220	UT	300234068287880	P74	3/17/20 14:24	86.8493	15.9989	Hutchings	Hutchings			
2019P185	UT	300234066412350	P75	3/17/20 14:46	86.7011	11.9561	Hutchings	Hutchings			
2019P186	UT	300234066415350	P76	3/17/20 15:14	86.9514	11.0007	Hutchings	Hutchings			
2020T73	SIMBA	300234068328160	Ak02	4/4/20 11:12	84.5898	12.6661	Hutchings	Ruibo Lei	177	3	17
2020T74	SIMBA	300234068225520	Ak03	4/4/20 11:43	84.6507	13.5380	Hutchings	Ruibo Lei	167	3	17
2020T76	SIMBA	300234068528490	Ak04	4/4/20 14:47	84.6886	12.3006	Hutchings	Ruibo Lei	151	9	13
2020T77	SIMBA	300234068524740	Ak05	4/4/20 11:12	84.5898	12.6661	Hutchings	Ruibo Lei	165	5	15
2020R12	Rad+LC	300025060614630	L3	4/24/20 13:48	83.9267	14.7608	Anhaus	Nicolaus	167.0	7.9	17.2

Tab 4.12.2: *Buoys deployed in the Central Observatory and Dark Site during MOSAiC Leg 3.*

Short ID	Buoy Type	IMEI	Site	Time Deployed	Deployed by	Buoy Owner	Co-Deployments	Ice Thickness	Freeboard	Snow Depth
2020P212	SVP	300234010303850	CO	3/17/20	Hutchings	Haapala	Remote Sensing			
2020P228	SVP	300234010303850	CO	5/12/20	Hutchings	Haapala	Remote Sensing			
2020P227	ISVP	300234068210190	CO	3/12/20	Hutchings	Ruibo Lei	SIMB3,AFOB,DOT, Met City			
2020P226	ISVP	300234068118580	CO	24/04/20	Hutchings	Ruibo Lei	Ocean Cluster			
2020P225	ISVP	300234068210310	CO	23/04/20	Hutchings	Ruibo Lei	ROV / LSO			
2020T75	SIMBA	300234068325170	Old Heli Pad	4/23/20	Hutchings	Ruibo Lei	Stress bouy FMI002	165	6	16
2020T79	SIMBA	300234068527600	CO	4/16/20 10:00	Hutchings	Ruibo Lei	ASFS50, ASFS30, 23m mast	NR	32	NR
2020S97	Snow Buoy	300234066083130	CO	29/4/20 14:03	Anhaus	Nicolaus	R14, DTC27, DTC28, DTC29, DTC08			17, 14, 17.5, 17
2020R10	Rad+LC	300025060612750	CO	3/8/20 14:47	Anhaus	Nicolaus		149.0	6.8	27.8
2020R11	Rad+LC	300025060613750	SYI / LM	3/29/20 14:21	Anhaus	Nicolaus		159.0	17.8	42.8
2020R13	AWI radiation	100000000000020	CO	5/6/20 8:39	Anhaus	Nicolaus	DTC40_512	336	92	32
2020R14	AWI radiation	100000000000030	CO	4/3/20 11:46	Anhaus	Nicolaus	S97, DTC27, DTC28, DTC29, DTC08	313	11.7	57.7
2020R20	Spectral Radiation Station	card	SYI / LM	4/10/20 12:26	Anhaus	Nicolaus		162	17.2	29.2